TECHNISCHE UNIVERSITÄT MÜNCHEN
Fakultät für Medizin

The role of TCR signals and downstream events for NKT and regulatory T cell identity and function in the mouse

Christoph-Maximilian Peter Drees

Vollständiger Abdruck der von der promotionsführenden Einrichtung Fakultät für Medizin der Technischen Universität München zur Erlangung des akademischen Grades eines

Doktors der Medizin

genehmigten Dissertation.

Vorsitzender:	Prof. Dr. Ernst J. Rummeny
Prüfer der Dissertation:	1. Prof. Dr. Marc Schmidt-Supprian
	2. Prof. Dr. Angela Krackhardt
	3. Prof. Dr. Jürgen Ruland

Die Dissertation wurde am 22.08.2016 bei der Technischen Universität München eingereicht und durch die promotionsführende Einrichtung Fakultät für Medizin am 17.05.2017 angenommen.

Eidesstattliche Erklärung

Hiermit versichere ich an Eides statt, dass die vorgelegte Dissertation von mir selbstständig und ohne unerlaubte Hilfe angefertigt ist.

München, den 22.08.2016 ……..

Unterschrift

Für Mama und Papa

Table of Contents

Acknowledgements

First and foremost I want to express my sincere gratitude to Marc Schmidt-Supprian for the opportunity to join his research group. I want to thank Marc for his continuous support during and after my time in his laboratory and for keeping the right balance between supervision and scientific freedom, which enabled me to develop and pursue my own ideas. I also want to acknowledge Ludger Klein, who agreed on mentoring my thesis.

I am indebted to all members of the Schmidt-Supprian laboratory for creating a wonderful working atmosphere and for making it a pleasure to come to the lab everyday. I am especially grateful to Christoph Vahl for teaching me more about Flow Cytometry in two weeks than I have learned the previous two years before we have met. Many thanks to Klaus Heger, not only for helpful discussions and support but also for good company outside the lab. I thank Sabrina Bortolluzi for her enthusiasm and commitment. I am grateful to Julia Knogler for her excellent technical assistance.

Thanks to Konstanze Pechloff, Andreas Gewies, Oliver Gorka and Stefan Wanninger for the bright spots during my time in the Opelhalle. I am thankful to Nathalie Knies for her good advices in the right moments.

I particularly thank Julius C. Fischer for superb collaborations and discussions. I am indebted to Michi Bscheider, who was a great help especially during my first months in the laboratory of Jürgen Ruland.

I am deeply grateful to Diana for her patience and love and to my family for their unconditional support. I owe them everything.

Abbreviations

7-AAD	7-Aminoactinomycin D
APC	antigen-presenting cell
αGalCer	α Galactosyl Ceramide
CCR6	chemokine receptor 6
CD	cluster of differentiation
c-Maf	c-Musculoaponeurotic Fibrosarcoma
DP	double positive
Egr2	early growth response gene 2
Foxp3	forkhead box P3
GF	germ free
ICOS	inducible co-stimulator
IL	interleukin
IFN-γ	interferon-γ
LP	lamina propria
MACS	magnetic activated cell sorting
MALT 1	mucosa associated lymphatic tissue 1
MFI	median fluorescence intensity
MHC	major histocompatibility complex
mLN	mediastinal lymph nodes
mRNA	messenger ribonucleic acid
mTOR	mechanistic target of rapamycin
NKT cell	Natural Killer T cell
NKT_{FH} cell	follicular helper NKT cells
PKCθ	protein kinase C θ
pLN	peripheral lymph node
PLZF	promyelocytic zink finger protein
PMA	Phorbol-12 myristate 13-acetate
RORγt	RAR-related orphan receptor gamma
SAP	SLAM associated protein
SLAMF	signaling lymphocyte activation molecule
STAT3	signal transducer and activator of transcription
T-bet	T-cell-specific T-box transcription factor
TCR	T cell receptor
T_{FH} cell	follicular helper T cell
Th cell	T helper cell
ThPOK	T helper poxviruses and zinc finger and Krüppel family
T_{reg} cell	regulatory T cell

List of Publications

This thesis is based on the following publications and manuscripts:

1. Drees C. [#], Vahl J.C. [#], Bortoluzzi S., Heger K.D., Fischer J.C., Wunderlich F.T., Peschel C., Schmidt-Supprina M. Roquin paralogs differentially regulate functional NKT cell subsets. *Manuscript in preparation*. [#], Equal contribution.

2. Drees C. and Schmidt-Supprian M. Age and location specific distribution of NKT cell subsets in the gut. *Manuscript in preparation*.

3. Vahl J.C. [#], Drees C. [#], Heger K., Heink S., Fischer J.C, Nedjic J., Ohkura N., Morikawa H., Poeck H., Schallenberg S., Rieß D., Hein M.Y., Buch T., Polic B., Schönle A., Zeiser R., Schmitt-Gräff A., Kretschmer K., Klein L., Korn T., Sakaguchi S. and Schmidt-Supprian M. Continuous T cell Receptor Signals Maintain a Functional Regulatory T cell Pool. *Immunity*. 2014 Nov 20;41(5):722-36. doi: 10.1016/j.immuni.2014.10.012. Epub 2014 Nov 6. [#], Equal contribution.

4. Drees C., Vahl J.C and Schmidt-Supprian M. TCR Signals fuel Treg Cells. *Oncotarget*. 2015 Sep 8;6(26):21773-4.

Summary

T cells develop in the thymus from hematopoietic precursor cells. During maturation some T cells receive strong T cell receptor (TCR) stimulation required for the initiation of lineage defining developmental programs, a selection process referred to as *agonist selection*.

This thesis explores the biology of two agonist selected T cell populations namely Natural Killer T (NKT) cells and regulatory T (T_{reg}) cells by means of genetically modified mouse models. NKT cells differentiate in the thymus into NKT1, NKT2 and NKT17 cells. The expression of signature transcription factors orchestrates their cell fates and production of subset specific cytokines. The key molecules however, which regulate the differentiation into these NKT cell lineages, are only incompletely understood. T_{reg} cells are characterized by their ability to suppress overshooting immune reactions. Their dependence on strong TCR stimulation during thymic development is well established, the role of continuous TCR signals for mature peripheral T_{reg} cells however still needed to be thoroughly investigated.

In **Paper 1** we describe Roquin proteins as central suppressors of NKT17 cell polarization in the thymus. TCR signals induce the degradation of Roquin proteins via the paracaspase MALT1. Therefore, we aimed to elucidate the consequences of isolated ablation of Roquin proteins for the NKT cell lineage. Conditional knockout of Roquin 1 and Roquin 2 in T cells leads to a decrease of total NKT cells in the thymus with a selective expansion of NKT17 cells. In addition, the peripheral NKT cell pool is essentially abolished. These changes are mediated through cell intrinsic and extrinsic mechanisms. Interestingly, transgenic expression of the Vα14i TCR at the CD4 CD8 double positive (DP) stage in the thymus restores the development of NKT cells and mitigates the developmental bias towards NKT17 differentiation. Roquin deficient NKT17 cells are characterized by an increased TCR expression and are uniformly positive for all NKT17 specific markers tested. TCR signal transduction and subset specific cytokine production however depend on the expression of Roquin paralogs.

In **Paper 2** we analyze the distribution of functional NKT cell subsets in the thymus and lamina propria of the gut. It is known that RORγt expressing NKT17 cells constitute a main portion of NKT cells in peripheral lymph nodes. Here we show that

NKT17 cells also represent the predominant NKT cell population in the lamina propria (LP) of the large intestine. The distribution of NKT cell subsets in the colon LP and thymus is age dependent with a preponderance of early developmental stages and NKT2 cells soon after birth. By analyzing NKT cells in the gut and thymus of germ free (GF) mice we could show that the distribution of NKT cells in both organs is likewise affected by the microbiota.

In **Paper 3** we study the effects of induced TCR ablation on mature T_{reg} cells. We show that once T_{reg} cell identity, namely expression of the lineage defining transcription factor forkhead box P3 (Foxp3) and hypomethylation of T_{reg} signature genes has been established, it does not depend on continuous signal through the antigen receptor. However, T_{reg} cells lose their activated phenotype after TCR ablation. In addition, the homeostasis, maintenance and suppressive functions of peripheral T_{reg} cells depend on continuous TCR signals.

Paper 4 is a review that gives a summary of the most recent data highlighting the importance of constant recognition of self for the biology and function of T_{reg} cells.

1. Roquin paralogs differentially regulate functional NKT cell subsets

1.1 Introduction

Natural killer T (NKT) cells express an evolutionary conserved semi-invariant T cell receptor (TCR) and are characterized by an activated phenotype and rapid secretion of effector cytokines in response to innate and antigenic stimulation. In the mouse, NKT cells represent 0.2 – 0.5% of lymphocytes in thymus, spleen, bone marrow and around 30% in the liver, whereas in humans the fractions are smaller (<0.1 and 1%, respectively)[1]. Despite their rarity, NKT cell responses can drive inflammation or tolerance, thereby impacting on a wide range of immune cells such as dendritic cells, NK cells, B and T cells[2]. NKT cells protect their host organisms from certain strains of bacteria and sustain anti-viral responses as well as contribute to the suppression of certain types of cancer and immune diseases[1,3-6]. On the other hand, NKT cells are involved in the pathophysiology of allergic responses, ulcerative colitis as well as liver cancer[7-9]. Therefore, NKT cell activation can have dramatically different outcomes, depending on diverse environmental factors.

Rare Vα14-Jα18 (Vα14i) TCRα-chain rearrangements in CD4 CD8 double positive (DP) thymocytes lead, in conjunction with a limited number of TCRβ-chains, to the expression of a glycolipid-recognizing TCR. The overwhelming majority of NKT cells express this Vα14i-containing semi-invariant TCR. They are therefore also referred to as iNKT or Vα14i-NKT cells but for simplicity we will call them NKT cells. Recognition of glycolipid antigens presented by CD1d on DP thymocytes through the semi-invariant TCR expressed by precursor cells (stage 0: $CD24^{high}$, $CD44^{low}$, $NK1.1^{-}$) triggers NKT cell development[10,11]. These TCR signals induce massive proliferative expansion, downregulation of CD24 (stage 1) and expression of the key transcriptional regulator of NKT cell maturation, promyelocytic leukemia zinkfinger (PLZF)[12-15]. Thymic NKT cell maturation is indicated by subsequent upregulation of the memory marker CD44 (stage 2) and expression of natural killer cell markers, most prominently NK1.1 (stage 3)[16,17]. While passing through stages 1 – 3, NKT cells also differentiate into functional subsets termed NKT1 ($PLZF^{low}$, $T\text{-}bet^{+}$), NKT2 ($PLZF^{high}$, $GATA3^{+}$) and NKT17 ($PLZF^{int}$, $ROR\gamma t^{+}$) cells, which are polarized towards

the preferential production of cytokines reminiscent of the respective T helper cell lineages[18,19]. To date, the signals and events that drive the differentiation of these NKT cell subsets are incompletely understood.

Roquin-1 and its mammalian paralog Roquin-2, encoded by *rc3h1* and *rc3h2* respectively, are mRNA-binding proteins which repress immune reactions by redundant and unique post-transcriptional regulation of genes, including costimulatory molecules and proinflammatory cytokines[20-24]. Thereby, these proteins act as safeguards against autoimmunity by preventing the spontaneous generation of follicular T helper (T_{FH}) cells, IL-17-producing Th17 cells and IFNγ-producing short lived effector CD8 T cells[20,22,25]. However, their role for the development of agonist-selected T cell subsets such as NKT cells is unknown.

Here, we report that conditional ablation of both Roquin paralogs in T cells essentially prevents the generation of mature NKT cells in the thymus, with the exception of NKT17 cells, whose production is dramatically increased by cell-intrinsic mechanisms. Roquin-1/2-deficient NKT cells express high amounts of NKT17 associated markers but display a hyporesponsive phenotype as shown by decreased signaling through the TCR and impaired cytokine production. In addition, peripheral NKT cells are essentially absent, mainly due to cell-extrinsic mechanisms.

1.2 Material and Methods

Mice

CD4Cre[26], *Rc3h1*$^{F/F}$[24], *Rc3h2*$^{F/F}$[22], *Vα14i*^{StopF}[27], *IL6Rα*$^{-/-}$ and *IL6Rα*$^{F/F}$[28] mice were kept on a C57BL/6 genetic background. Mice were housed in specific pathogen-free animal facilities of the Max-Planck Institute of Biochemistry and the Technische Universität München. Unless indicated otherwise, age-matched animals were analyzed at 6 - 12 weeks of age. *CD4Cre Rc3h1-2*$^{F/F}$ mice were analyzed before any visible signs of pathology. All experiments were performed in accordance with German Federal Animal Protection Laws and approved by the Regierung of Oberbayern.

Flow Cytometry

Single cell suspensions were stained using commercial antibodies and kits (supplemental methods). mCD1d-PBS57-tetramers were provided by the NIH

tetramer core facility. For enrichment of thymic NKT cells, $CD8^+$ thymocytes were depleted using CD8a Microbeads (Miltenyi Biotec). For intracellular cytokine stainings, cells were stimulated for 4 hours with 100 ng/ml phorbol-12-myristat-13-acetat (PMA, Sigma) and 1000 ng/ml ionomycin (Calbiochem) together with 2 µM monensin (eBioscience). Samples were acquired on a FACSCantoII or LSRFortessa (BD) and analyzed with FlowJo (FlowJo LLC). To analyze the relative expression of extracellular and intracellular proteins, median fluorescent intensities (MFI) were calculated and the mean MFI of mCD1d-PBS57 $tetramer^-$ $TCR\beta^+$ T cells of the respective control mice was set to 1.

Bone marrow chimeras

B6.SJL-Ptprca Pepcb/BoyJ (B6.SJL congenic);C57BL/6 heterozygous recipient mice (CD45.1/2) were lethally irradiated with 2 x 5.5 Gy 4 hours apart and intravenously injected with 4 - 5 x 10^6 bone marrow cells in a B6.SJL (CD45.1) : C57BL/6 (CD45.2) ratio of 1 : 1. Before transplantation, bone marrow was T cell depleted using CD90.2 MicroBeads (Miltenyi Biotec). Two to three days before until two weeks after transplantation recipient mice were treated with Borgal® 24% (Virbac Animal Health) in drinking water at a dose of 0.1 ml per kg body weight per day. Mice were analyzed 7 - 9 weeks after transplantation.

Statistics

Statistical analysis was performed by student t test or as indicated in the figure legends.

1.3 Results

Ablation of Roquin proteins leads to a reduction of thymic and loss of peripheral NKT cells

To assess the role of Roquin proteins in NKT cells, we analyzed mice with T cell-specific ablation of one or both of these proteins. We employed CD4Cre for this purpose, as it efficiently recombines conditional alleles, including *Rc3h1*$^{F/F}$[24] and Rc3h2$^{F/F}$[22] in DP thymocytes. CD4Cre-mediated protein ablation is complete in NKT cell precursors[16,17,29,30], which represent “older” DP thymocytes due to the late timing

of the Vα14-Jα18 rearrangement[16,17,30,31]. Knockout of Roquin-1 and co-ablation of Roquin-1/2 led to a two-fold reduction of NKT cell proportions and numbers in the thymus (Figure 1A-B). Analysis of the thymic developmental stages 1-3 revealed gain of stage 2 and significant loss of stage 3 NKT cells in *CD4Cre Rc3h1*$^{F/F}$ compared to control mice, which was strongly exacerbated when Roquin-2 was co-ablated (Figure 1A, C). Accordingly, the absolute numbers of stage 3 NKT cells were reduced from an average of 32 x 10^4 cells in controls to 16 x 10^4 in *CD4Cre Rc3h1*$^{F/F}$ and 1 x 10^4 in *CD4Cre Rc3h1-2*$^{F/F}$ mice (Figure 1C).

Moreover, loss of Roquin proteins also affected NKT cells in peripheral lymphoid organs. In the spleens of *CD4Cre Rc3h1*$^{F/F}$ mice NKT cell proportions and absolute numbers were reduced by more than 50%, primarily due to a reduction of stage 3 NKT cells (Figure 1D-E; supplemental Figure 1A). Strikingly, NKT cells were virtually absent in the spleens of *CD4Cre Rc3h1-2*$^{F/F}$ mice (Figure 1D-E). A similar picture was observed in the liver, peripheral (pLN), mesenteric lymph nodes (mLN) and lung (Figure 1F; supplemental Figure 1B). Immune cells were dramatically expanded in liver and most prominently in pLNs, but not in mLNs of *CD4Cre Rc3h1-2*$^{F/F}$ compared to control mice. Therefore, absolute NKT cell numbers were reduced in liver and mLN, but not pLN (Figure 1F). In contrast to Roquin-1, loss of Roquin-2 has no discernable effects on NKT cell development and numbers (supplemental Figure 1C-D).

Taken together, ablation of Roquin proteins leads to a dose-dependent decrease in thymic NKT cell generation, with a clear maturation block between stage 2 and 3. In the periphery, NKT cells were only barely detectable in *CD4Cre Rc3h1-2*$^{F/F}$ mice.

Roquin proteins restrict NKT17 cell differentiation.

Given that most NKT17 cells are phenotypically stage 2, we determined the subset composition[32]. We found increased proportions of NKT17 cells in *CD4Cre Rc3h1*$^{F/F}$ mice, while most of the NKT cells in *CD4Cre Rc3h1-2*$^{F/F}$ mice were NKT17 (Figure 2A). Loss of Roquin-2 alone had no effect on NKT subset composition (supplemental Figure 1E). Importantly, also the absolute numbers of NKT17 cells were more than 10 fold increased from an average of 0.5 x 10^4 in controls to 6.5 x 10^4 cells in *CD4Cre Rc3h1-2*$^{F/F}$ mice. We therefore conclude that the increased proportions are due to strongly increased NKT17 cell production in absence of Roquin-mediated regulation

and not merely a consequence of a decreased NKT1 population (Figure 2B). At this point, as we observed more pronounced changes in absence of both Roquin proteins, we focused on the analysis of thymic NKT cells of *CD4Cre Rc3h1-2$^{F/F}$* mice in further experiments.

The inducible costimulator ICOS is the first described target of Roquin's post-transcriptional activities, but ICOS is also differentially expressed between NKT cell subsets. We therefore compared ICOS median fluorescence intensities (MFIs) on NKT1, NKT2 and NKT17 cells. In controls, the highest ICOS expression could be found on NKT17 and NKT2 cells, while NKT1 cells expressed similar amounts as TCRβ$^+$ tetramer$^-$ thymocytes (Figure 2C). Loss of both Roquin paralogs enhanced ICOS expression to a similar extent in all subsets (Figure 2C), indicating that the differential ICOS expression in NKT cell subsets occurs largely independently of Roquin-mediated regulation.

NKT17 cells are characterized by enhanced expression of the chemokine receptor CCR-6, the integrin $\alpha_E\beta7$ (CD103), Syndecan-1 (CD138) and Neuropilin-1 (Nrp-1)[33-35] (Figure 1D). Unlike controls, Roquin-1/2-deficient NKT17 cells were uniformly positive for all of these markers (Figure 2D). Interestingly, a fraction of Roquin-1/2-deficient NKT1 and NKT2 cells expressed CD138, the surface protein most faithfully representing NKT17 lineage commitment. This could indicate a bias towards NKT17 differentiation in these cells.

In summary, we demonstrate that Roquin proteins prevent excessive NKT17 differentiation at the expense of other subsets.

Expression of a knock-in Vα14i-TCR facilitates the development of all NKT cell subsets in absence of Roquin proteins.

Transgenic expression of a Vα14i-TCR has frequently been employed to rescue defects in early NKT cell development due to compromised TCRα rearrangements or thymocyte survival. We recently generated the *Vα14i^{StopF}* allele, which expresses a Vα14i-TCR from within the endogenous TCRα gene locus upon Cre-mediated recombination. In combination with CD4Cre, this leads to massive NKT cell overproduction (Figure 3A)[27]. In *CD4Cre Vα14i^{StopF} Rc3h1-2$^{F/F}$* mice, expression of Cre leads to both, inactivation of the four Roquin alleles and induction of the Vα14i TCRα-chain. Vα14i-TCR expression occurs within 6h (unpublished observations) after Cre expression, while it takes considerably longer before the cells are depleted

of their Roquin mRNA and protein reservoirs. Therefore, in contrast to the situation in *CD4Cre Rc3h1-2$^{F/F}$* mice, in *CD4Cre Vα14i^{StopF} Rc3h1-2$^{F/F}$* mice the induced Vα14i-TCR initially signals to a cell that still contains Roquin proteins, which are then lost during NKT cell development. Vα14i-TCR expression restored the development of NKT cells of all stages in *CD4Cre Vα14i^{StopF} Rc3h1-2$^{F/F}$* mice, although the overall numbers were still significantly reduced compared to controls (Figure 3A-B). In Vα14i knock-in mice, NKT cell development is strongly biased towards cells early in their development (Figure 3B), which is also reflected in the expression of RORγt and PLZF (Figure 3C). We defined NKT0 and NKT0' (Figure 3C) as early progenitor stages (unpublished observations). While there was no difference in NKT0 cells numbers, loss of Roquin led to a reduction in cell numbers of the putative subsequent developmental stage, NKT0'. *CD4Cre Vα14i^{StopF} Rc3h1-2$^{F/F}$* thymi showed an essentially identical distribution of NKT1, NKT2 and NKT17 cells as controls, with the exception of a statistically significant 2.5 fold increase in the proportions of the NKT17 subset (Figure 3C). However, due to the overall decreased NKT cell numbers, the increase in absolute NKT17 cell numbers in absence of Roquin proteins was not significant (Figure 3C). Mature Roquin-1/2-deficient NKT cells of all subsets and stages could be detected in the spleen, although the numbers were reduced compared to controls (Figure 3D-E). Most diminished were PLZF^{high} (NKT2) cells, whereas NKT17 cell numbers were not significantly altered (Figure 3D-E).

In conclusion, we show that transgenic expression of a knock-in Vα14i NKT cell TCR largely overcomes the block in NKT cell development, strongly reduces the bias towards NKT17 cell production in *CD4Cre Vα14i^{StopF} Rc3h1-2$^{F/F}$* mice and allows the accumulation of peripheral mature NKT cells lacking Roquin proteins.

Roquin paralogs cell-intrinsically drive NKT17 differentiation, while the loss of peripheral NKT cells is also due to cell-extrinsic factors.

The results derived from experiments with the Vα14i-TCR indicated that Roquin proteins play decisive roles during the earliest stages of NKT cell development. DP thymocytes are critically important for positive selection of developing NKT cells by presenting antigen and through stimulation via homotypic interactions between signaling lymphocytic activation molecule (SLAM) family members[16,36]. However, the expression of CD1d and of CD150 (SLAMF1) and Ly108 (SLAMF6), which are required for successful NKT cell development[36], were not significantly altered by lack

of Roquin paralogs in DP thymocytes (Figure 4A), arguing against an indirect role of these cells. To directly distinguish between cell-intrinsic or extrinsic mechanisms we created mixed bone-marrow chimeras. We adoptively transferred T cell depleted CD45.1 B6.SJL congenic bone marrow mixed with an equal amount of either CD45.2 control, or CD45.2 *CD4Cre Rc3h1-2*$^{F/F}$ T cell depleted bone marrow into lethally irradiated CD45.1/2 double positive mice (Figure 4B; supplemental Figure 2A). Thymi and spleens of the resulting chimeras were analyzed 7-9 weeks after transplantation. Even after lethal irradiation 20 – 30% of thymic NKT cells were host-derived in the resulting chimeras and similar proportions of radio-resistant CD45.1/2 host T and NKT cells were found in the spleens (supplemental Figure 2B). Further, to account for the engraftment variations typical for these experiments, we normalized the CD45.1 to CD45.2 ratios to the ratios of double negative (DN) thymocytes and B cells, which are Roquin-proficient. This analysis revealed that Roquin-1/2-deficient NKT cells develop in normal proportions from their precursors, similar to other thymic cell lineages and similar to both CD45.1 competitor and CD45.2 control NKT cells. Strikingly, Roquin-1/2-deficient NKT cells could also be detected at nearly normal proportions in the spleen, in striking contrast to the situation in *CD4Cre Rc3h1-2*$^{F/F}$ mice (Figure 1D-E; Figure 4C; supplemental Figure 2B). The proportions of Roquin-1/2-deficient (dKO) CD45.2 NKT17 cells were strongly and significantly increased, in contrast to the CD45.1 competitor and the CD45.1 and CD45.2 cells in the control chimeras (Figure 4D). In the spleen, Roquin-1/2-deficient NKT cells of all subsets could be detected with predominating NKT17 cells (Figure 4C; supplemental Figure 2B-C).

Furthermore, we found that elevated ICOS expression and the spontaneous differentiation of memory/effector-like T cells and follicular helper T (T_{FH}) cells of the Roquin-1/2-deficient T lineage is cell-intrinsic (supplemental Figure 3A-C), similar to the san/san T lineage[37].

Our results thus demonstrate that the massive NKT17 cell production in *CD4Cre Rc3h1-2*$^{F/F}$ mice is mediated through cell-intrinsic mechanisms, while the reduction of mature peripheral NKT cells is largely caused by cell-extrinsic mechanisms.

Evidence for decreased TCR signaling and enhanced apoptosis in Roquin-1/2-deficient NKT cells.

Having demonstrated the cell-intrinsic nature of the NKT17 bias of Roquin-1/2-deficient NKT cells, we embarked on further molecular characterizations. Compared to controls, NKT17 cells lacking Roquin paralogs express higher amounts of TCR on their surface, while NKT1 express lower levels (Figure 5A, supplemental Figure 4A-B). Conventional CD4 T cells upregulate Ly-6C upon deprivation of TCR-mediated self-recognition[38]. Within the NKT lineage, NKT1 cells had the largest proportion of Ly-6C positive cells, while only a few NKT2 and essentially no NKT17 cells were putatively self-deprived, inversely correlating with TCRβ expression. Loss of Roquin-1/2 decreased the percentage of Ly-6C positive cells in all NKT subsets, although the differences were not dramatic (Figure 5B). Next, we assessed the expression of the TCR-induced transcription factor early response gene 2 (Egr2), which was also shown to induce PLZF by binding to its promoter in immature NKT cells[39]. Loss of Roquin-1/2 lead to a significant decrease of Egr2 levels in TCR^+ thymocytes and all NKT subsets, including NKT17 cells which had the highest TCR surface levels (Figure 5C). In NKT17 cells, decreased Egr2 expression was also accompanied by a 50% reduction of PLZF protein (Figure 5C), but PLZF expression was unchanged in the other subsets. PLZF was shown to regulate the expression of c-Maf[40], a transcriptional regulator of cytokine production highly expressed in Th17 cells[41] which contributes to Th17 differentiation through the induction of RORγt[42]. Interestingly, we found significantly increased c-Maf expression in Roquin-1/2-deficient NKT2 and NKT17 cells, independent of PLZF levels (Figure 5C). IL-6 together with TCR signals strongly induces c-Maf expression via STAT3[43]. However, in accordance with previous data[44], we did not detect significant expression of the STAT3-activating IL-6R on bulk NKT cells. Complete or T cell-specific ablation of the IL-6Rα-chain did not affect NKT cell development and subset differentiation in the thymus, but led to increased splenic NKT cell numbers (supplemental Figure 5A-C). Nevertheless, STAT3 phosphorylation was increased in NKT2 and NKT17 compared to NKT1 cells (Figure 5C), indicating that another receptor might activate STAT3. However, this receptor or downstream signals do not appear to be regulated by Roquin proteins, as Roquin-1/2-deficient NKT1 and NKT17 cells showed slightly reduced STAT3 phosphorylation compared to controls (Figure 5C). Fate decisions between NKT1 and NKT17 cells are controlled by the transcription factor T helper poxviruses and

zinc finger and Krüppel family (ThPOK), whose expression is strongly reduced in NKT17 cells[33,45]. ThPOK levels were elevated in the absence of Roquin-1/2 in all subsets, except for NKT17, where they were reduced (Figure 5C), possibly reflecting their strong polarization into this lineage.

In order to address the loss of NKT1 and NKT2 cells we monitored cell death, which revealed significantly increased apoptosis in both Roquin-1/2-deficient and control NKT cells at stage 2 (Figure 5D; supplemental Figure 6A) harboring over 90% of NKT17 cells. NKT[46], and especially NKT17 cells depend on interleukin-7 (IL-7) for their generation, homeostasis and survival[47]. Accordingly, NKT17 cells expressed 3 times more IL-7 receptor α-chain (CD127) than NKT1 and NKT2 cells. Loss of Roquin-1/2 led to a selective increase in CD127 expression in NKT17 cells (Figure 5E), suggesting that decreased IL-7 signaling does not underlie their enhanced propensity to die.

Together, our data indicate that in Roquin-1/2-deficient NKT cells TCR signals and STAT3 activating signals are diminished. Mechanisms including enhanced c-Maf expression appear to drive them into the NKT17 lineage, where they are more prone to die.

Roquin paralog-deficient NKT cells are compromised in their cytokine secretion abilities.

The differentiation of NKT cell subsets and cytokine production also depends on signaling through the mechanistic Target of Rapamycin (mTOR) protein complexes[48] and ablation of the negative regulator tuberous sclerosis 1 (TSC1) leads to phenotypes strikingly resembling those of loss of Roquin-1/2[49]. However, we did not find evidence for increased mTOR signaling in Roquin-1/2-deficient NKT cells compared to controls. There was no difference in phosphorylation of either mTOR or downstream proteins such as 4-EBP1 (mTORC1) and AKT (mTORC2) (Figure 6A). Roquin-deficiency not only controls the differentiation of pro-inflammatory T lymphocytes, but also their effector functions (supplemental Figure 6B)[25,50] To our surprise, PMA/ionomycin stimulation induced significantly lower proportions of cytokine-producing cells in all Roquin-1/2-deficient NKT cell subsets compared to controls (Figure 6B). Furthermore, cytokine production per cell appeared to be lower in the absence of Roquin-1/2 (Figure 6C).

Therefore, in contrast to the increased expression NKT17 specific markers, Roquin-1/2-deficient NKT cells showed a hyporesponsive phenotype characterized by overall defective cytokine production.

1.4 Discussion

During their development in the thymus NKT cells pass sequential stages and mature into functionally different subsets. Here, we show that the RNA-binding Roquin-1 and -2 proteins prevent excessive differentiation into the NKT17 lineage. The numbers of NKT17 cells deficient for the Roquin paralogs exceeded their controls over 10-fold and showed strongly enhanced lineage commitment. Mixed bone marrow chimeras demonstrated that NKT17 polarization is cell-intrinsic and conditional expression of a Vα14i-TCR, concomitantly with Roquin-1/2 ablation, suggested that signals early during NKT cell development play decisive roles.

To date, it remains unclear when and how the NKT17 fate is initiated during NKT cell development. We detected selective PLZF downregulation in Roquin-1/2-deficient NKT17 cells and normal levels in the other subsets. This argues against a causal role for PLZF regulation, as enhanced PLZF levels, as seen in Lethal-7 miRNA-deficiency, shift the balance from NKT1 to NKT2/17[51]. Ablation or loss of function mutations of ThPOK result in the production of CD8 and DN NKT cells, characterized by low NK1.1 expression[33,52,53]. This goes hand in hand with a dramatic polarization towards NKT17 differentiation, which is also observed, although to a much lesser extent, in haploinsufficiency[33,45]. The elevated ThPOK levels in Roquin-1/2-deficient thymocytes and NKT1/2 cells indicate that lower ThPOK levels in NKT17 cells are rather consequence than cause for exaggerated NKT17 differentiation in absence of Roquin-1/2.

Significant reduction of ThPOK mRNA was also detected in NKT cells deficient for the mTOR negative regulator TSC1[49], which show similar phenotypes, including a dramatic NKT17 bias and the reduction of mature thymic and peripheral NKT cells. This phenotype was attributed and functionally linked to elevated mTORC1 activity, reduced expression of Tbet and ICOS-dependent signals[49]. In our studies, we did not detect significant differences in mTORC1 or mTORC2 pathway activation in Roquin-1/2-deficient NKT17 compared to control cells. Furthermore, at least in the CD8 T cell

lineage, loss of Roquin activity strongly enhances the acquisition of an effector state characterized by high Tbet expression[24,50]. In TSC1-deficient NKT cells, reduced Tbet levels might facilitate the transcriptional acquisition of high ICOS expression, which contributes to NKT17 polarization[49]. A similar outcome with respect to elevated ICOS and NKT17 differentiation could independently be achieved through enhanced translation of ICOS mRNA in a Roquin-1/2-deficient situation.

ICOS is implicated in the regulation of c-Maf expression, in addition to IL-6 in conjunction with TCR-induced Ca^{2+} signals[43] or TGFβ[54] as well as IL-27[55]. C-Maf is characteristically overexpressed in Th17, T_{FH}[41] and, as we show here, NKT17 cells. Reduced TCR signal strength in NKT cells argues against a role for TCR signaling in enhancing c-Maf expression in the absence of Roquin-1/2. As we and others[44] showed that IL-6R signals are dispensable for NKT17 development, it seems more likely that cytokines such as IL-27 trigger c-Maf expression in developing NKT17 cells. IL-27 also induces the Roquin target ICOS, which in turn amplifies expression of c-Maf[55]. C-Maf induces an IL-17 producing cell fate together with its binding partner Sox5t by directly enhancing RORγt expression and by binding to various additional gene loci implicated in Th17 differentiation[42], including the Roquin targets Irf4, and Nfkbiz[25]. Further transcriptional activation of these and other target genes during initial NKT17 differentiation could then be potentiated by the absence of Roquin-1/2-mediated post-transcriptional control, resulting in the production of NKT17 cells at the expense of other subsets.

Stage 2 NKT cells are highly proliferative and display high apoptosis rates. In the absence of Roquin-1/2 there is a tendency for further enhanced NKT cell death. The general inflammatory environment caused by loss of Roquin paralogs in T cells could compound the pro-apoptotic tendencies of Roquin-1/2-deficient NKT cells, explaining their absence in the periphery. Both, the expression of a Vα14i-TCR and the presence of a majority of wild-type T cells in our mixed bone marrow chimeras substantially reduce general inflammation. This could explain why in both models mature Roquin-1/2-deficient NKT cells can be maintained in the periphery.

Loss of Roquin functionality in conventional T cells leads to disease-causing effector T cell polarization and excessive cytokine production[20,22,25,37]. In striking contrast, after ablation of Roquin-1/2, all NKT cell subsets showed a decreased production of subset specific cytokines, which in the case of NKT17 correlates with reduced STAT3 phosphorylation. NKT cells acquire features of memory T cells and

innate-like cytokine production capabilities during their development and it appears that they become desensitized towards autoantigen recognition during their development[27]. At present, we do not know whether loss of Roquin proteins dampens cytokine production by NKT cells through direct or indirect means. Upregulation of c-Maf is a consistent feature of Roquin-1/2-deficient thymic NKT cells. In addition to promoting the differentiation of IL-17-producing T cell subsets, c-Maf is highly expressed in exhausted CD4 and CD8 T cells. Overexpression of c-Maf was sufficient to inhibit CD8 T cell cytokine production and anti-tumor responses[56]. Therefore, high c-Maf levels could contribute to the blunted cytokine responses of Roquin-1/2-deficient NKT cells.

NKT cells are a small TCR repertoire-restricted glycolipid-recognizing subset implicated in a large spectrum of human diseases, including infection, autoimmunity and malignancy. During their development, they mature into functionally different subsets. Here, we show that the post-transcriptional regulators Roquin-1 and -2 play key cell-intrinsic roles in restricting the excessive developmental generation of NKT17 cells at the expense of other NKT cell subsets.

1.5 References

1. Berzins SP, Smyth MJ, Baxter AG. Presumed guilty: natural killer T cell defects and human disease. *Nature Reviews Immunology*. 2011;11(2):131–142.
2. Juno JA, Keynan Y, Fowke KR. Invariant NKT cells: regulation and function during viral infection. *PLoS Pathog.* 2012;8(8):e1002838.
3. Haeryfar SMM, Mallevaey T. Editorial: CD1- and MR1-Restricted T Cells in Antimicrobial Immunity. *Front Immunol*. 2015;6(5450):701–5.
4. Salio M, Silk JD, Yvonne Jones E, Cerundolo V. Biology of CD1- and MR1-Restricted T Cells. *Annu. Rev. Immunol.* 2014;32(1):323–366.
5. Vivier E, Ugolini S, Blaise D, Chabannon C, Brossay L. Targeting natural killer cells and natural killer T cells in cancer. *Nature Reviews Immunology*. 2012;12(4):239–252.
6. Mori L, Lepore M, De Libero G. The Immunology of CD1- and MR1-Restricted T Cells. *Annu. Rev. Immunol.* 2016;34(1):479–510.
7. Heller F, Fuss IJ, Nieuwenhuis EE, Blumberg RS, Strober W. Oxazolone colitis, a Th2 colitis model resembling ulcerative colitis, is mediated by IL-13-producing NK-T cells. *Immunity*. 2002;17(5):629–638.
8. Wingender G, Rogers P, Batzer G, et al. Invariant NKT cells are required for airway inflammation induced by environmental antigens. *J. Exp. Med.* 2011;208(6):1151–1162.

9. Wolf MJ, Adili A, Piotrowitz K, et al. Metabolic Activation of Intrahepatic CD8+ T Cells and NKT Cells Causes Nonalcoholic Steatohepatitis and Liver Cancer via Cross-Talk with Hepatocytes. *Cancer Cell*. 2014;26(4):549–564.
10. Bendelac A, Savage PB, Teyton L. The Biology of NKT Cells. *Annu. Rev. Immunol.* 2007;25(1):297–336.
11. Matsuda JL, Mallevaey T, Scott-Browne J, Gapin L. CD1d-restricted iNKT cells, the "Swiss-Army knife" of the immune system. *Current Opinion in Immunology*. 2008;20(3):358–368.
12. Savage AK, Constantinides MG, Han J, et al. The Transcription Factor PLZF Directs the Effector Program of the NKT Cell Lineage. *Immunity*. 2008;29(3):391–403.
13. Kovalovsky D, Uche UO, Eladad S, et al. The BTB–zinc finger transcriptional regulator PLZF controls the development of invariant natural killer T cell effector functions. *Nature Immunology*. 2008;1–10.
14. Raberger J, Schebesta A, Sakaguchi S, et al. The transcriptional regulator PLZF induces the development of CD44 high memory phenotype T cells. *PNAS*. 2008;105(46):17919–17924.
15. Kovalovsky D, Alonzo ES, Uche OU, et al. PLZF Induces the Spontaneous Acquisition of Memory/Effector Functions in T Cells Independently of NKT Cell-Related Signals. *J. Immunol.* 2010;184(12):6746–6755.
16. Godfrey DI, Stankovic S, Baxter AG. Raising the NKT cell family. *Nature Immunology*. 2010;11(3):197–206.
17. Benlagha K, Wei DG, Veiga J, Teyton L, Bendelac A. Characterization of the early stages of thymic NKT cell development. *J. Exp. Med.* 2005;202(4):485–492.
18. Gapin L. ScienceDirect Development of invariant natural killer T cells. *Current Opinion in Immunology*. 2016;39:68–74.
19. Engel I, Seumois GEG, Chavez L, et al. Innate-like functions of natural killer T cell subsets result from highly divergent gene programs. *Nature Immunology*. 2016;1–15.
20. Di Yu, Tan AH-M, Hu X, et al. Roquin represses autoimmunity by limiting inducible T-cell co-stimulator messenger RNA. *Nature*. 2007;450(7167):299–303.
21. Glasmacher E, Hoefig KP, Vogel KU, et al. Roquin binds inducible costimulator mRNA and effectors of mRNA decay to induce microRNA-independent post-transcriptional repression. *Nature Immunology*. 2010;1–10.
22. Vogel KU, Edelmann SL, Jeltsch KM, et al. Roquin Paralogs 1 and 2 Redundantly Repress the Icos and Ox40 Costimulator mRNAsand Control Follicular Helper T Cell Differentiation. *Immunity*. 2013;1–14.
23. Pratama A, Ramiscal RR, Silva DG, et al. Roquin-2 Shares Functions with Its Paralog Roquin-1 in the Repression of mRNAs Controlling T Follicular Helper Cells and Systemic Inflammation. *Immunity*. 2013;38(4):669–680.
24. Bertossi A, Aichinger M, Sansonetti P, et al. Loss of Roquin induces early death and immune deregulation but not autoimmunity. *Journal of Experimental Medicine*. 2011;208(9):1749–1756.
25. Jeltsch KM, Hu D, Brenner S, et al. Cleavage of roquin and regnase-1 by the paracaspase MALT1 releases their cooperatively repressed targets to

promote TH17 differentiation. *Nature Immunology*. 2014;1–13.
26. Lee PP, Fitzpatrick DR, Beard C, et al. A critical role for Dnmt1 and DNA methylation in T cell development, function, and survival. *Immunity*. 2001;15(5):763–774.
27. Vahl JC, Heger K, Knies N, et al. NKT Cell-TCR Expression Activates Conventional T Cells in Vivo, but Is Largely Dispensable for Mature NKT Cell Biology. *PLoS Biol*. 2013;11(6):e1001589.
28. Wunderlich FT, Ströhle P, Könner AC, et al. Interleukin-6 Signaling in Liver-Parenchymal Cells Suppresses Hepatic Inflammation and Improves Systemic Insulin Action. *Cell Metabolism*. 2010;12(3):237–249.
29. Schmidt-Supprian M, Tian J, Grant EP, et al. Differential dependence of CD4+CD25+ regulatory and natural killer-like T cells on signals leading to NF-kappaB activation. *Proc. Natl. Acad. Sci. U.S.A.* 2004;101(13):4566–4571.
30. Egawa T, Eberl G, Taniuchi I, et al. Genetic Evidence Supporting Selection of the Vα14i NKT Cell Lineage from Double-Positive Thymocyte Precursors. *Immunity*. 2005;22(6):705–716.
31. Sun Z, Unutmaz D, Zou YR, et al. Requirement for RORgamma in thymocyte survival and lymphoid organ development. *Science*. 2000;288(5475):2369–2373.
32. Lee YJ, Holzapfel KL, Zhu J, Jameson SC, Hogquist KA. Steady-state production of IL-4 modulates immunity in mouse strains and is determined by lineage diversity of iNKT cells. *Nature Immunology*. 2013;1–10.
33. Engel I, Zhao M, Kappes D, Taniuchi I, Kronenberg M. The transcription factor Th-POK negatively regulates Th17 differentiation in Va14i NKT cells. *Blood*. 2012;120(23):4524–4532.
34. Dai H, Rahman A, Saxena A, et al. Syndecan-1 identifies and controls the frequency of IL-17-producing naïve natural killer T (NKT17) cells in mice. *Eur. J. Immunol.* 2015;n/a–n/a.
35. Milpied P, Massot B, Renand A, et al. IL-17-producing invariant NKT cells in lymphoid organs are recent thymic emigrants identified by neuropilin-1 expression. *Blood*. 2011;118(11):2993–3002.
36. Griewank K, Borowski C, Rietdijk S, et al. Homotypic interactions mediated by Slamf1 and Slamf6 receptors control NKT cell lineage development. *Immunity*. 2007;27(5):751–762.
37. Vinuesa CG, Cook MC, Angelucci C, et al. A RING-type ubiquitin ligase family member required to repress follicular helper T cells and autoimmunity. *Nature*. 2005;435(7041):452–458.
38. Martin B, Auffray CED, Delpoux A, et al. Highly self-reactive naive CD4 T cells are prone to differentiate into regulatory T cells. *Nature Communications*. 2013;4:1–12.
39. Lazarevic V, Zullo AJ, Schweitzer MN, et al. The gene encoding early growth response 2, a target of the transcription factor NFAT, is required for the development and maturation of natural killer T cells. *Nature Immunology*. 2009;10(3):306–313.
40. Gleimer M, Boehmer von H, Kreslavsky T. PLZF Controls the Expression of a Limited Number of Genes Essential for NKT Cell Function. *Front Immunol*. 2012;3:374.
41. Bauquet AT, Jin H, Paterson AM, et al. The costimulatory molecule ICOS regulates the expression of c-Maf and IL-21 in the development of follicular T helper cells and TH-17 cells. *Nature Immunology*.

2008;10(2):167–175.
42. Tanaka S, Suto A, Iwamoto T, et al. Sox5 and c-Maf cooperatively induce Th17 cell differentiation via RORγt induction as downstream targets of Stat3. *Journal of Experimental Medicine*. 2014;211(9):1857–1874.
43. Yang Y, Ochando J, Yopp A, Bromberg JS, Ding Y. IL-6 plays a unique role in initiating c-Maf expression during early stage of CD4 T cell activation. *J. Immunol.* 2005;174(5):2720–2729.
44. Rachitskaya AV, Hansen AM, Horai R, et al. Cutting edge: NKT cells constitutively express IL-23 receptor and RORgammat and rapidly produce IL-17 upon receptor ligation in an IL-6-independent fashion. *J. Immunol.* 2008;180(8):5167–5171.
45. Enders A, Stankovic S, Teh C, et al. ZBTB7B (Th-POK) Regulates the Development of IL-17-Producing CD1d-Restricted Mouse NKT Cells. *J. Immunol.* 2012;189(11):5240–5249.
46. Tani-ichi S, Shimba A, Wagatsuma K, et al. Interleukin-7 receptor controls development and maturation of late stages of thymocyte subpopulations. *PNAS*. 2013;110(2):612–617.
47. Webster KE, Kim H-O, Kyparissoudis K, et al. IL-17-producing NKT cells depend exclusively on IL-7 for homeostasis and survival. *Mucosal Immunology*. 2014;7(5):1058–1067.
48. Yang W, Gorentla B, Zhong X-P, Shin J. mTOR and its tight regulation for iNKT cell development and effector function. *Molecular Immunology*. 2015;1–10.
49. Wu J, Yang J, Yang K, et al. iNKT cells require TSC1 for terminal maturation and effector lineage fate decisions. *J. Clin. Invest.* 2014;124(4):1685–1698.
50. Chang P-P, Lee SK, Hu X, et al. Breakdown in repression of IFN-γ mRNA leads to accumulation of self-reactive effector CD8+ T cells. *The Journal of Immunology*. 2012;189(2):701–710.
51. Pobezinsky LA, Etzensperger R, Jeurling S, et al. Let-7 microRNAs target the lineage-specific transcription factor PLZF to regulate terminal NKT cell differentiation and effector function. *Nature Immunology*. 2015;1–9.
52. Engel I, Hammond K, Sullivan BA, et al. Co-receptor choice by Vα14 iNKT cells is driven by Th-POK expression rather than avoidance of CD8-mediated negative selection. *J. Exp. Med.* 2010;207(5):1015–1029.
53. Wang L, Carr T, Xiong Y, et al. The sequential activity of Gata3 and Thpok is required for the differentiation of CD1d-restricted CD4+ NKT cells. *Eur. J. Immunol.* 2010;40(9):2385–2390.
54. Rutz S, Noubade R, Eidenschenk C, et al. Transcription factor c-Maf mediates the TGF-β-dependent suppression of IL-22 production in TH17 cells. *Nature Immunology*. 2011;12(12):1238–1245.
55. Pot C, Jin H, Awasthi A, et al. Cutting edge: IL-27 induces the transcription factor c-Maf, cytokine IL-21, and the costimulatory receptor ICOS that coordinately act together to promote differentiation of IL-10-producing Tr1 cells. *The Journal of Immunology*. 2009;183(2):797–801.
56. Giordano M, Henin C, Maurizio J, et al. Molecular profiling of CD8 T cells in autochthonous melanoma identifies Maf as driver of exhaustion. *EMBO J.* 2015;34(15):2042–2058.

1.6 Figures

Figure 1

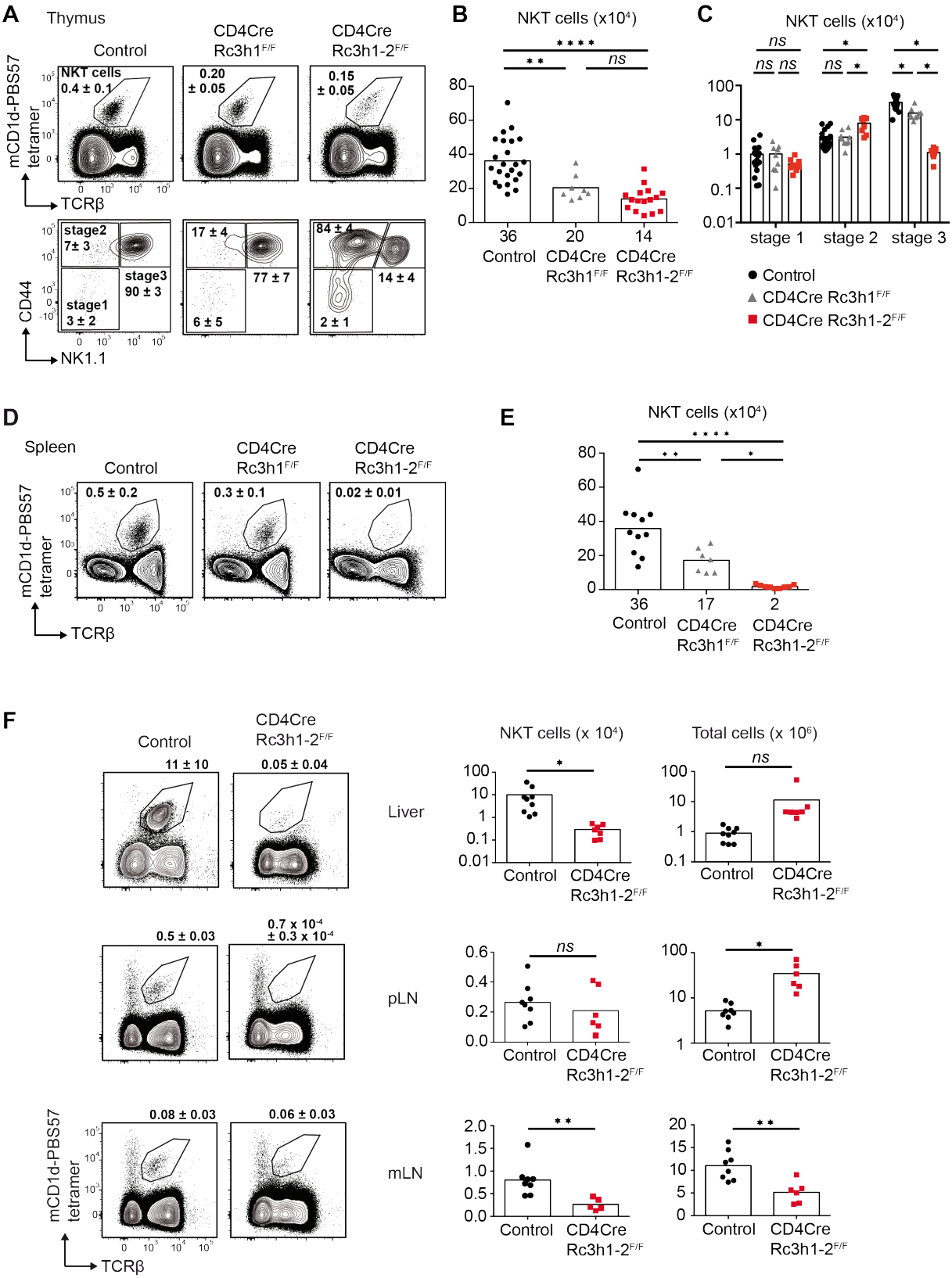

Figure 1. Ablation of Roquin paralogs leads to an expansion of stage 2 NKT cells and reduction of NKT cells in the periphery. (A) Percentage of thymic mCD1d-PBS57 tetramer^{+} NKT cells and NKT

cell stages in control, *CD4Cre Rc3h1*$^{F/F}$ and *CD4Cre Rc3h1-2*$^{F/F}$ mice. Numbers in representative plots indicate mean percentage ± SD calculated from at least 8 mice per genotype pooled from at least three independent experiments. (B) Absolute cell numbers (x 10^4) of thymic NKT cells of the indicated genotypes. Each dot represents one mouse and bars indicate the mean cell number, which is also depicted below the graph. Graph shows pooled data from at least three independent experiments. **, P < 0.01; ****, P < 0.0001; *ns,* not significant; one-way ANOVA. (C) Absolute cell numbers (x 10^4) of thymic NKT cell stages of the indicated genotypes. Bars show the mean numbers. Each dot represents one mouse of the indicated genotype of at least three independent experiments. Statistical significance was determined by multiple t-tests using the Holm-Sidak method. *, P < 0.05; *ns*, not significant. (D) Spleens of controls, *CD4Cre Rc3h1*$^{F/F}$ and *CD4Cre Rc3h1-2*$^{F/F}$ mice were analyzed for the presence of NKT cells. Shown are representative contour plots of each genotype gated on total lymphocytes. Numbers indicate mean percentage ± SD calculated from a total of at least seven mice per genotype pooled from at least two independent experiments. (E) Total cell numbers (x 10^4) of NKT cells in the spleens of controls, *CD4Cre Rc3h1*$^{F/F}$ and *CD4Cre Rc3h1-2*$^{F/F}$ mice. Bars represent the mean cell number (also depicted below the graph) with each dot representing one analyzed mouse pooled from at least two independent experiments. *, P < 0.05; **, P < 0.01; ****, P < 0.0001; one-way ANOVA. (F) Total cell numbers (x 10^4) of lymphocytes and NKT cells in the liver, pLN and mLN of control and *CD4Cre Rc3h1-2*$^{F/F}$ mice. Bars indicate the mean cell number with each dot representing one mouse. Data is pooled from at least 6 mice per genotype from at least two independent experiments. Statistical significance was determined by unpaired t-test with *, P < 0.05; **, P < 0.005; *ns,* not significant.

Figure 2

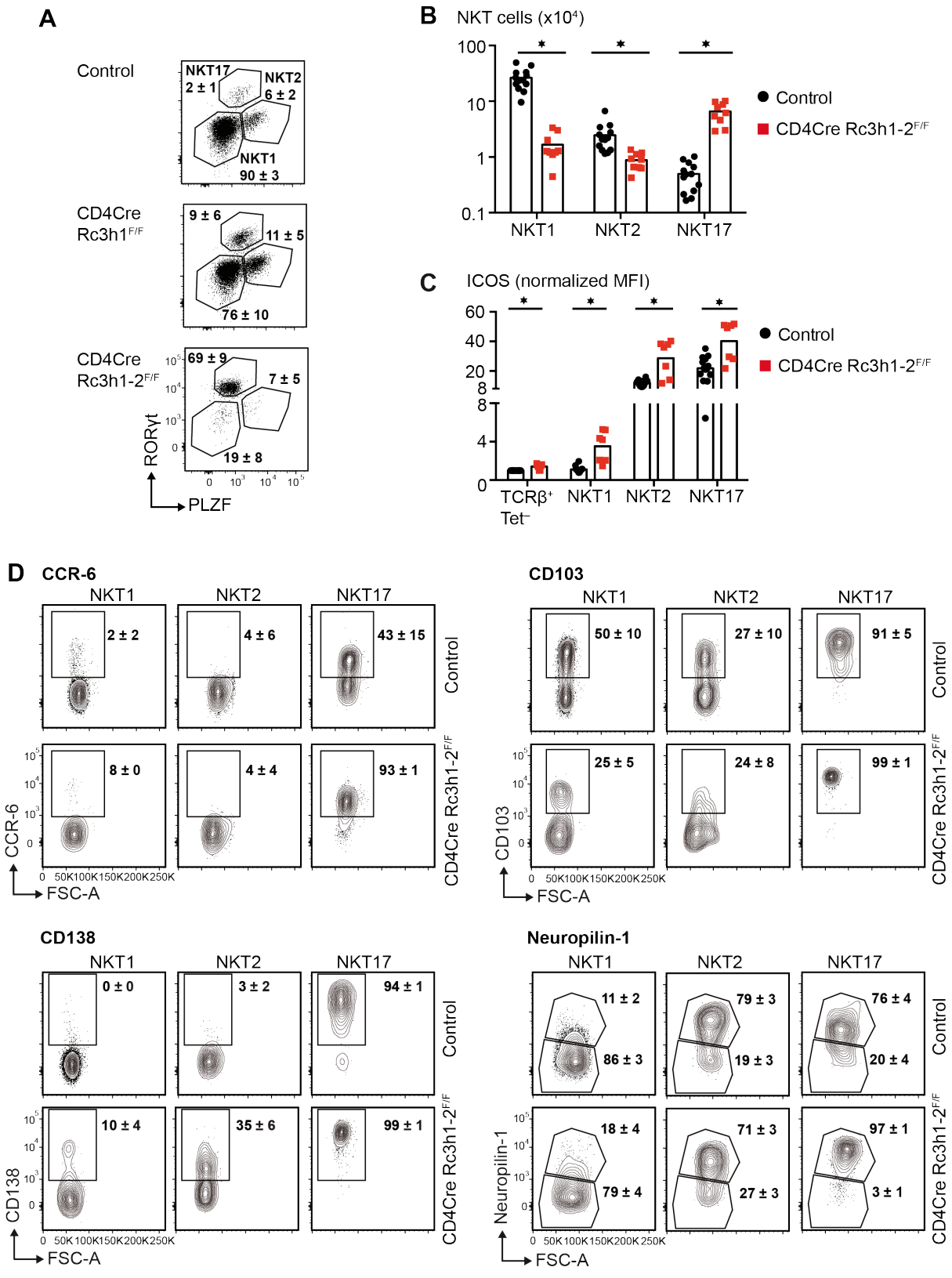

Figure 2. Ablation of Roquin promotes polarization into the NKT17 lineage. (A) Percentage of NKT1, NKT2 and NKT17 cells in the thymi of control, *CD4Cre Rc3h1$^{F/F}$* and *CD4Cre Rc3h1-2$^{F/F}$* mice. Depicted numbers in representative contour plots indicate mean percentage ± SD calculated from at least 8 mice per genotype of at least three independent experiments. Cells were acquired after

depletion of $CD8^+$ thymocytes by MACS. (B) Absolute cell numbers (x 10^4) of thymic NKT cell subsets of the indicated genotypes. Columns show the mean cell number with each dot representing one mouse. Shown data is pooled from at least three independent experiments. Statistical significance was determined by multiple t-tests using the Holm-Sidak method. *, $P < 0.05$. (C) ICOS median fluorescent intensity (MFI) on thymic $tetramer^-$ $TCR\beta^+$ thymocytes and NKT1, NKT2 and NKT17 cells of the indicated genotypes. Bars indicate mean MFI and each dot represents one mouse. MFI was normalized to the mean MFI of control $TCR\beta^+$ $tetramer^-$ thymocytes, which was set to 1. Shown data is pooled from at least three independent experiments. Statistical significance was determined by multiple t-tests using the Holm-Sidak method. *, $P < 0.05$. (D) CCR-6, CD103, CD138 and Neuropilin-1 expression on thymic NKT1, NKT2 and NKT17 cells of control and *CD4Cre Rc3h1-2*$^{F/F}$ mice. Numbers in representative contour plots show the mean percentage ± SD calculated from at least three mice per marker pooled from at least two independent experiments. Before acquisition, thymi were CD8 depleted by MACS (A, C-D).

Figure 3

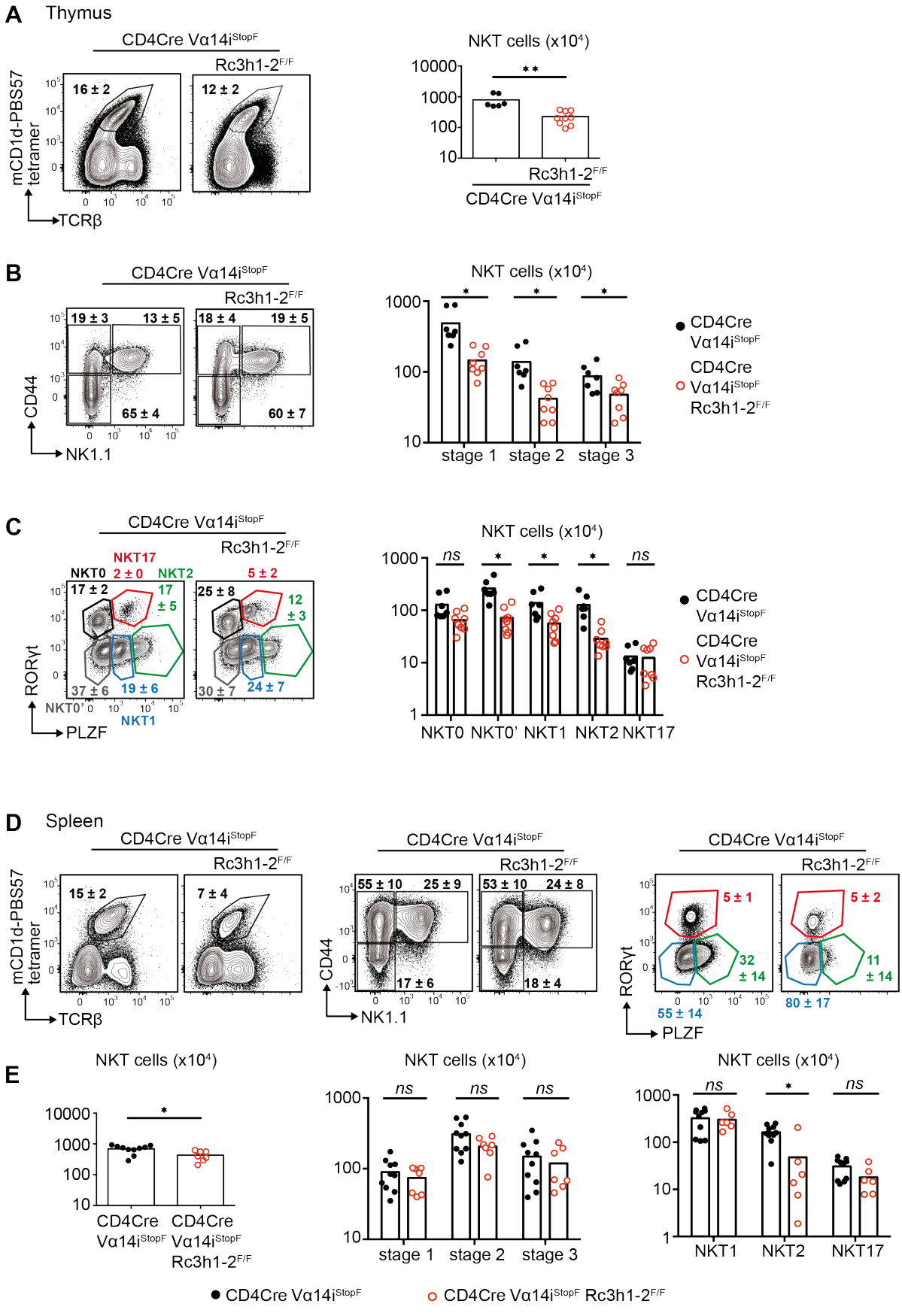
A
Thymus
CD4Cre Vα14i^StopF
Rc3h1-2^F/F
mCD1d-PBS57 tetramer
TCRβ
16 ± 2
12 ± 2
NKT cells (x10⁴)
10000
1000
100
10
**
Rc3h1-2^F/F
CD4Cre Vα14i^StopF
B
CD4Cre Vα14i^StopF
Rc3h1-2^F/F
CD44
NK1.1
19 ± 3
13 ± 5
65 ± 4
18 ± 4
19 ± 5
60 ± 7
NKT cells (x10⁴)
1000
100
10
stage 1
stage 2
stage 3
CD4Cre Vα14i^StopF
CD4Cre Vα14i^StopF Rc3h1-2^F/F
C
CD4Cre Vα14i^StopF
Rc3h1-2^F/F
NKT17
NKT0
2 ± 0
NKT2
5 ± 2
17 ± 2
17 ± 5
37 ± 6
19 ± 6
25 ± 8
12 ± 3
30 ± 7
24 ± 7
RORγt
PLZF
NKT0'
NKT1
NKT cells (x10⁴)
1000
100
10
1
ns
NKT0
NKT0'
NKT1
NKT2
NKT17
CD4Cre Vα14i^StopF
CD4Cre Vα14i^StopF Rc3h1-2^F/F
D
Spleen
CD4Cre Vα14i^StopF
Rc3h1-2^F/F
mCD1d-PBS57 tetramer
TCRβ
15 ± 2
7 ± 4
CD44
NK1.1
55 ± 10
25 ± 9
17 ± 6
53 ± 10
24 ± 8
18 ± 4
RORγt
PLZF
5 ± 1
32 ± 14
55 ± 14
5 ± 2
11 ± 14
80 ± 17
E
NKT cells (x10⁴)
10000
1000
100
10
*
CD4Cre Vα14i^StopF
CD4Cre Vα14i^StopF Rc3h1-2^F/F
NKT cells (x10⁴)
1000
100
10
ns
stage 1
stage 2
stage 3
NKT cells (x10⁴)
1000
100
10
1
ns
*
NKT1
NKT2
NKT17
CD4Cre Vα14i^StopF
CD4Cre Vα14i^StopF Rc3h1-2^F/F

Figure 3. Transgenic expression of the Vα14i TCR at the DP stage enables the development of thymic NKT1 and NKT2 cells as well as peripheral NKT cells in *CD4Cre Rc3h1-2$^{F/F}$* mice. Representative contour plots show the mean percentage ± SD of thymic NKT cells (A), NKT cell stages (B) and NKT cell subsets (C) in mice of the indicated genotype. Bar charts show the total cell numbers (x 10^4) of thymic NKT cells (A), NKT cell stages (B) and NKT cell subsets (C) in *CD4Cre Vα14i^{StopF}* and *CD4Cre Vα14i^{StopF} Rc3h1-2$^{F/F}$* mice. Bars indicate the mean cell number with each dot representing one analyzed mouse pooled from at least three independent experiments. (D) Representative contour plots show the mean percentage ± SD of splenic NKT cells (left), NKT cell stages 1 – 3 (middle) and NKT1, NKT2 and NKT17 cells (right) in *CD4Cre Vα14i^{StopF}* compared to *CD4Cre Vα14i^{StopF} Rc3h1-2$^{F/F}$* mice (E) Bar charts show the mean cell number (bars) of splenic NKT cells (left), NKT stages 1 – 3 and NKT1, NKT2 and NKT17 cells (right) gated as shown in (D) and isolated from spleens of the indicated genotypes. Each symbol represents one analyzed mouse and shown data was pooled from three independent experiments (D-E). Statistical significance was determined by multiple t-tests using the Holm-Sidak method. *, $P < 0.05$; *ns,* not significant.

Figure 4

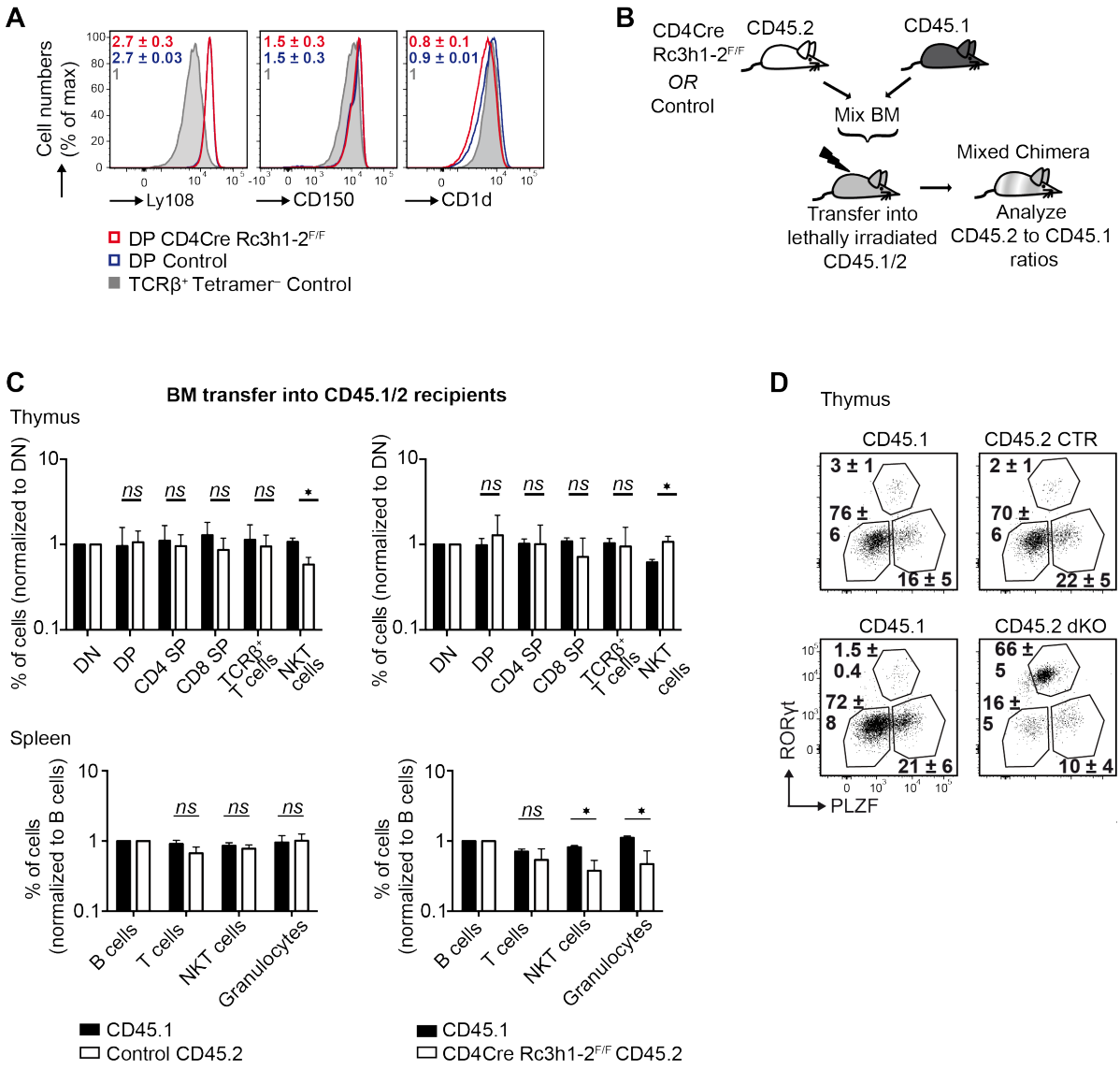

Figure 4. The expansion of NKT17 cells after Roquin ablation is cell intrinsically regulated, NKT cell extrinsic mechanisms however contribute to the reduction of peripheral NKT cells. (A) Representative histograms show the expression of Ly108 (SLAMF6), CD150 (SLAMF1) and CD1d on DP thymocytes of the indicated genotypes normalized to TCRβ$^+$ tetramer$^-$ cells of control mice. Data indicates mean normalized MFI ± SD of 4 mice pooled from three independent experiments. For normalization MFI of TCRβ$^+$ tetramer$^-$ cells was set to one. (B) Experimental setup of the bone marrow chimeras experiment: CD45.1/2 double positive recipient mice were transplanted with a 1 / 1 mixture of CD45.1 B6.SJL bone marrow together with either CD45.2 control or CD45.2 *CD4Cre Rc3h1-2$^{F/F}$* bone marrow. Bone marrow was T cell depleted by MACS using CD90.2 beads. Mice were sacrificed 7-9 weeks after transplantation and NKT cells in thymi and spleens were analyzed. (C) The indicated thymic (upper row) or splenic (lower row) immune cell populations of both groups were analyzed for the expression CD45.1 and CD45.2. Data represents mean percentage ± SD of 7 experimental and 4 control mice from one out of two independent experiments and is normalized to the engraftment of DN thymocytes (thymus) or B cells (spleen). Statistical significance was determined by multiple t-tests using the Holm-Sidak method. *, P < 0.05; *ns,* not significant. (D) Representative dot plots show the distribution of NKT1, NKT2 and NKT17 cells in the thymi of the indicated bone marrow chimeras. Cells were acquired after MACS depletion of CD8$^+$ thymocytes. Numbers indicate mean percentages ± SD calculated from 4 controls and 7 experimental mice of one out of two independent experiments.

Figure 5

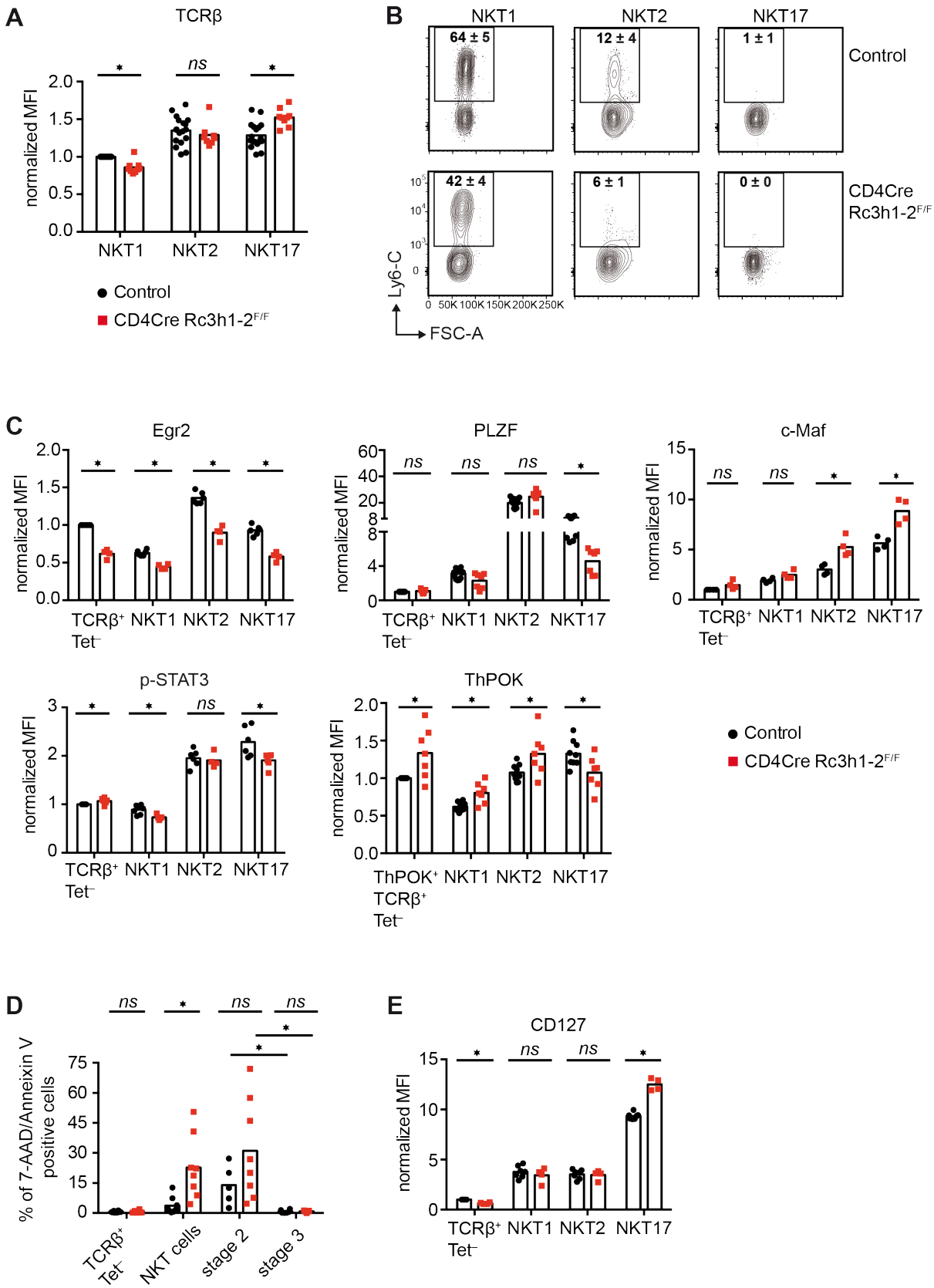
A
TCRβ
normalized MFI
NKT1
NKT2
NKT17
Control
CD4Cre Rc3h1-2F/F
B
NKT1
NKT2
NKT17
64 ± 5
12 ± 4
1 ± 1
42 ± 4
6 ± 1
0 ± 0
Control
CD4Cre Rc3h1-2F/F
Ly6-C
FSC-A
C
Egr2
PLZF
c-Maf
p-STAT3
ThPOK
TCRβ+ Tet−
ThPOK+ TCRβ+ Tet−
D
% of 7-AAD/Anneixin V positive cells
TCRβ+ Tet−
NKT cells
stage 2
stage 3
E
CD127

Figure 5. Evidence for decreased TCR signaling and enhanced apoptosis in Roquin 1/2-deficient NKT cells. (A) Bars show mean normalized TCRβ MFI ± SD of the indicated thymic NKT cell populations of either control or *CD4Cre Rc3h1-2*$^{F/F}$ mice. MFI was normalized to TCRβ MFI of NKT1 cells of control mice, which was set to one. Each dot represents one mouse and the shown data was pooled from at least three independent experiments. Statistical analysis was determined by multiple t-tests using the Holm-Sidak method with *, $P < 0.05$; *ns,* not significant. (B) Representative contour plots show Ly6C expression on NKT1, NKT2 and NKT17 cells of the indicated genotypes. Shown data was pooled from two independent experiments and numbers indicate the mean percentage ± SD of Ly6C$^+$ cells of at least four mice per genotype. (C) Thymic NKT cells of control and *CD4Cre Rc3h1-2*$^{F/F}$ mice were analyzed for expression of the intracellular transcription factors Egr2, PLZF, c-Maf, ThPOK as wells as for STAT3 phosphorylation. Bars indicate mean MFI of the indicated cell population. MFI was normalized to the MFI of TCRβ$^+$ tetramer$^-$ cells, which was set to one. Each dot represents one mouse pooled from at least three independent experiments (PLZF, ThPOK p-STAT3) or one experiment (Egr2, c-Maf). Cells were acquired after depletion of CD8$^+$ thymocytes by MACS. Statistical significance was determined by multiple t-tests using the Holm-Sidak method. *, $P < 0.05$; *ns*, not significant. (D) Thymic NKT cells were isolated from either control or *CD4Cre Rc3h1-2*$^{F/F}$ mice and analyzed for cell death by 7-AAD and Annexin V stainings. Bars indicate the mean percentage of 7-AAD$^+$ Annexin V$^+$ double positive cells. Each dot represents one mouse pooled from three independent experiments. Statistical significance was determined by unpaired t-test with welch correction. *, $P < 0.05$. *ns*, not significant. (E) Roquin deficient NKT cells were analyzed for the expression of the IL-7 receptor α-chain (CD127). Bars indicated mean MFI ± SD normalized to TCRβ$^+$ tetramer$^-$ cells, which was set to one. Each dot represents one mouse pooled from two independent experiments. Before acquisition, thymi were CD8 depleted by MACS (A – C, E). Statistical significance was determined by multiple t-tests using the Holm-Sidak method. *, $P < 0.05$; *ns,* not significant.

Figure 6

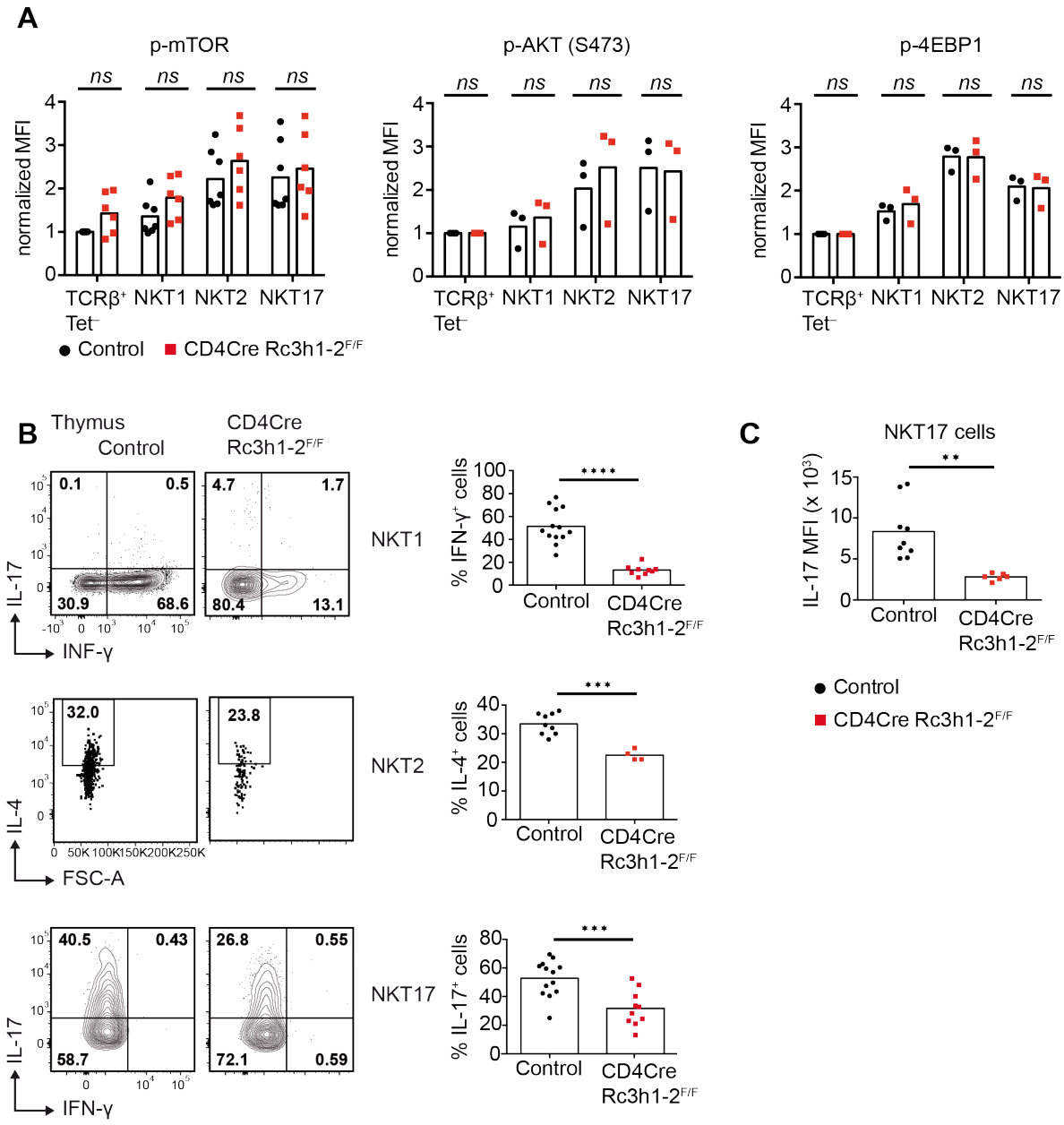

Figure 6. Signaling through mTOR does not contribute to the decreased production of subset specific cytokines of Roquin1/2 deficient NKT cells. (A) Thymic NKT cells were analyzed for the presence of intracellular p-mTOR, p-AKT (S473) and p-4EBP1 proteins by flow cytometry. Cells were acquired after depletion of $CD8^+$ thymocytes by MACS. Bars indicate mean normalized MFIs pooled from two independent experiments (p-mTOR) or from one experiment (p-AKT, p-4EBP1) with each dot representing one analyzed mouse. Statistical significance was determined by by multiple t-tests using the Holm-Sidak method. *ns,* not significant. (B) Representative contour plots show the cytokine production thymic NKT1, NKT2 and NKT17 cells of the indicated genotypes. $CD8^+$ MACS depleted thymocytes were stimulated for four hours with PMA and Ionomycin in the presence of monensin in complete RPMI Medium with 10% FCS. Bar graphs show mean % of IFN-γ^+ NKT1, IL-4^+ NKT2 and IL-17^+ NKT17 cells with each dot representing one mouse pooled from a total of three independent experiments. Statistical significance was determined by unpaired t tests. ***, P < 0,001; ****, P < 0,0001. (C) Data shows mean IL-17 MFI of IL-17^+ thymic NKT17 cells of the indicated genotypes after restimulation with PMA and ionomycin for 4 hours in the presence of monensin. Each data point represents one mouse and data was pooled from three independent experiments. Statistical analysis was determined by students t-test. **, P < 0.005.

1.7 Supplemental Information

Flow cytometry antibodies and kits

Commercial antibodies used in our study: Bcl-6 (K112-91), B220 (RA3-6B2), CCR-6 (29-2L17), CD4 (GK1-5, RM4-5), CD8a (53-6.7), CD11b (M1/70), CD44 (IM7), CD45.1 (A20), CD45.2 (104), CD62L (MEL-14), CD90.2 (53-2.1), CD127 (A7R34), CD138 (281-2), c-MAF (sym-0F1), CXCR5 (2G8), Egr2 (erongr2), Foxp3 (FJK-16s), Gr-1 (RB6-8C5), IL-17 (eBio17B7), IL-4, (11B11), IL6Rα (D7715A7), INF-γ (XMG1.2), Ly-6C (HK1.4), Neuropilin-1 (JE12), NK1.1 (PK136), PD-1 (J43), PLZF (9E12), RORγt (AFKJS-9, Q31-387), TCRβ (H57-597), T-bet (4B10), ThPOK (2POK). For intracellular transcription factor stainings, cells were fixed and permeabilized with the Foxp3 transcription factor staining kit (eBioscience). For intracellular cytokine stainings cells were fixed and permeabilized with the Cytofix/Cytoperm kit (BD) or Foxp3 transcription factor staining kit (eBioscience). For analysis of intracellular phosphorylated proteins, single cell suspensions were prepared using serum free buffer. Cells were processed using the Transcription Factor Phospho Buffer set (BD) or fixed with Phosflow Lyse/Fix buffer (BD) and permeabilized with Perm buffer III (BD). Cells were stained overnight using commercially available monoclonal antibodies against: p-STAT3 (pS727), p-mTOR (MRRBY), p-4EBP1 (236B4) and p-AKT (S473) (M89-61) from BD. For detection of Apoptosis cells were stained with Annexin V (eBioscience) and 7-AAD (eBioscience) using the Annexin V detection kit (eBioscience).

Isolation of lamina propria and lung lymphocytes

For isolation of lamina propria lymphocytes, Peyer's patches and fat tissue were removed and intestines flushed with ice cold PBS. Intestines were then longitudinally opened and cut into 1-1,5 cm pieces. After vigorously vortexing in PBS, samples were incubated two times for 15-20 min at 37°C in HBSS buffer containing 5% FCS and 5 mM EDTA, 1 mM DTT and 10 mM HEPES. Then, cells were washed in PBS and intestines digested for 45min at 37°C in $PBS^{+Ca/+Mg}$ containing 5% FCS, 1 mg/ml collagenase, Type 2 (cellsystems) and 0,1 mg/ml DNase I (Roche). Lymphocytes were then purified by a 40/80% Percoll (Biochrom) gradient.

To prepare lung single-cell suspensions, lungs were digested using RPMI containing 0.02 mg/mL Liberase TM and 10 U DNase (both Roche Diagnostics).

Suppl. Figure 1

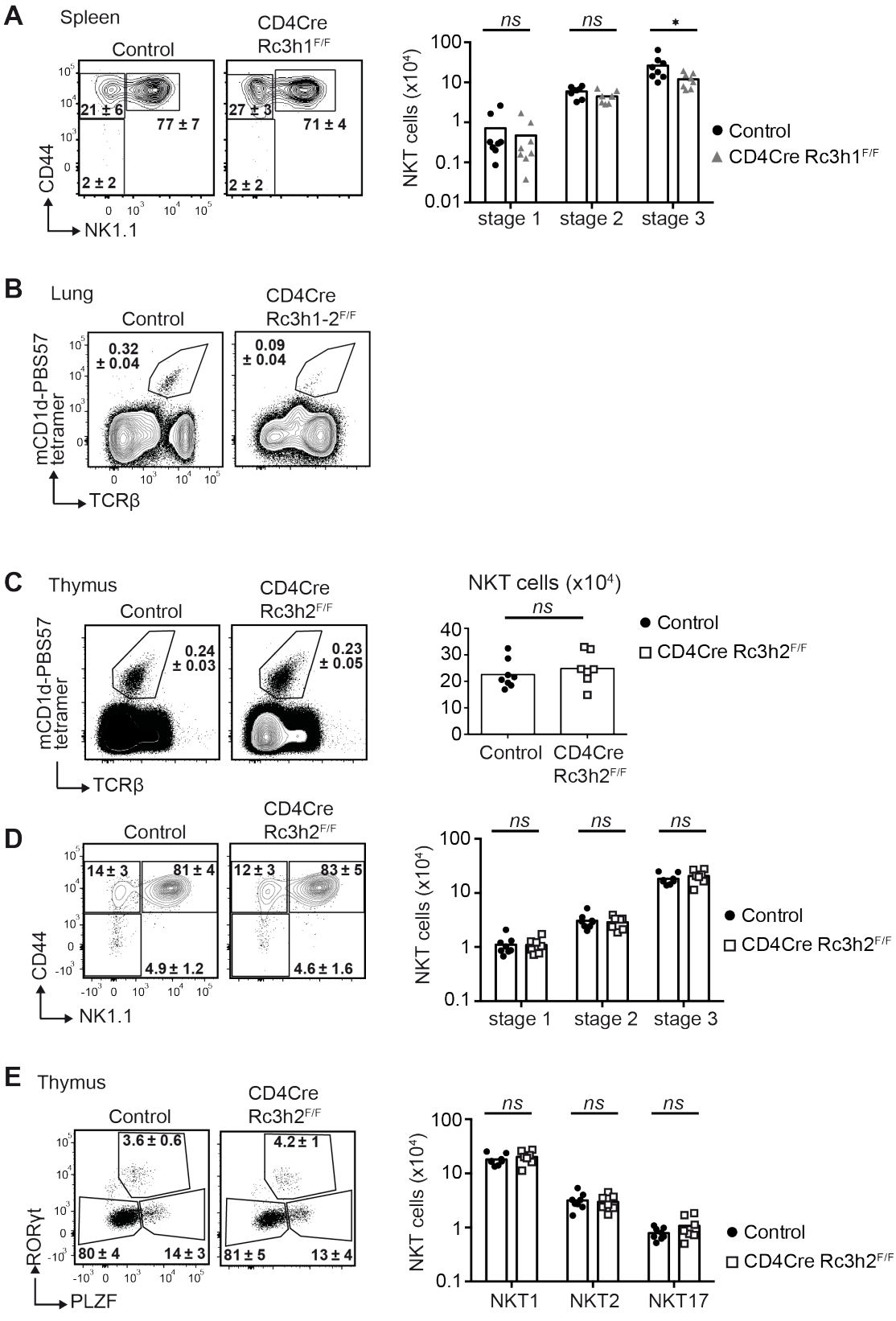

Supplemental Figure 1. Conditional deletion of Roquin 2 in T cells does not affect NKT cell development. (A) Contour plots show the distribution of NKT cell stages in the spleens of control and *CD4Cre Rc3h1$^{F/F}$* mice. Numbers indicate the mean percentage ± SD of NKT cell stages 1 – 3. Bar chart shows the mean cell numbers (x 10^4) of splenic NKT cell stages 1 – 3 NKT of the indicated

genotypes. Each data point represents one analyzed mouse pooled from at least two independent experiments. (B) Representative contour plots show mean percentages ± SD of tetramer$^+$ NKT in the lungs of 3 control and 3 *CD4Cre Rc3h1-2*$^{F/F}$ mice. (C, D) Representative contour plots show mean percentages ± SD of tetramer$^+$ NKT cells (B) and NKT cell stages 1 – 3 (C) in the thymi of control and *CD4Cre Rc3h2*$^{F/F}$ mice. Bar charts show the mean absolute cell numbers (x 10^4) of NKT cells (B) and NKT cell stages 1 – 3 (C). Each data point represents one mouse pooled from two independent experiments. (E) Contour plots show the relative distribution of thymic NKT1, NKT2 and NKT17 cells ± SD of control and *CD4Cre Rc3h2*$^{F/F}$ mice. Bar charts show the corresponding mean cell numbers (x 10^4) with each point indicating one mouse. Data is pooled from at least 7 mice per genotype of at least two independent experiments. Statistical significance was determined multiple t-tests using the Holm-Sidak method. *, $P < 0.05$; *ns*, not significant.

Suppl. Figure 2

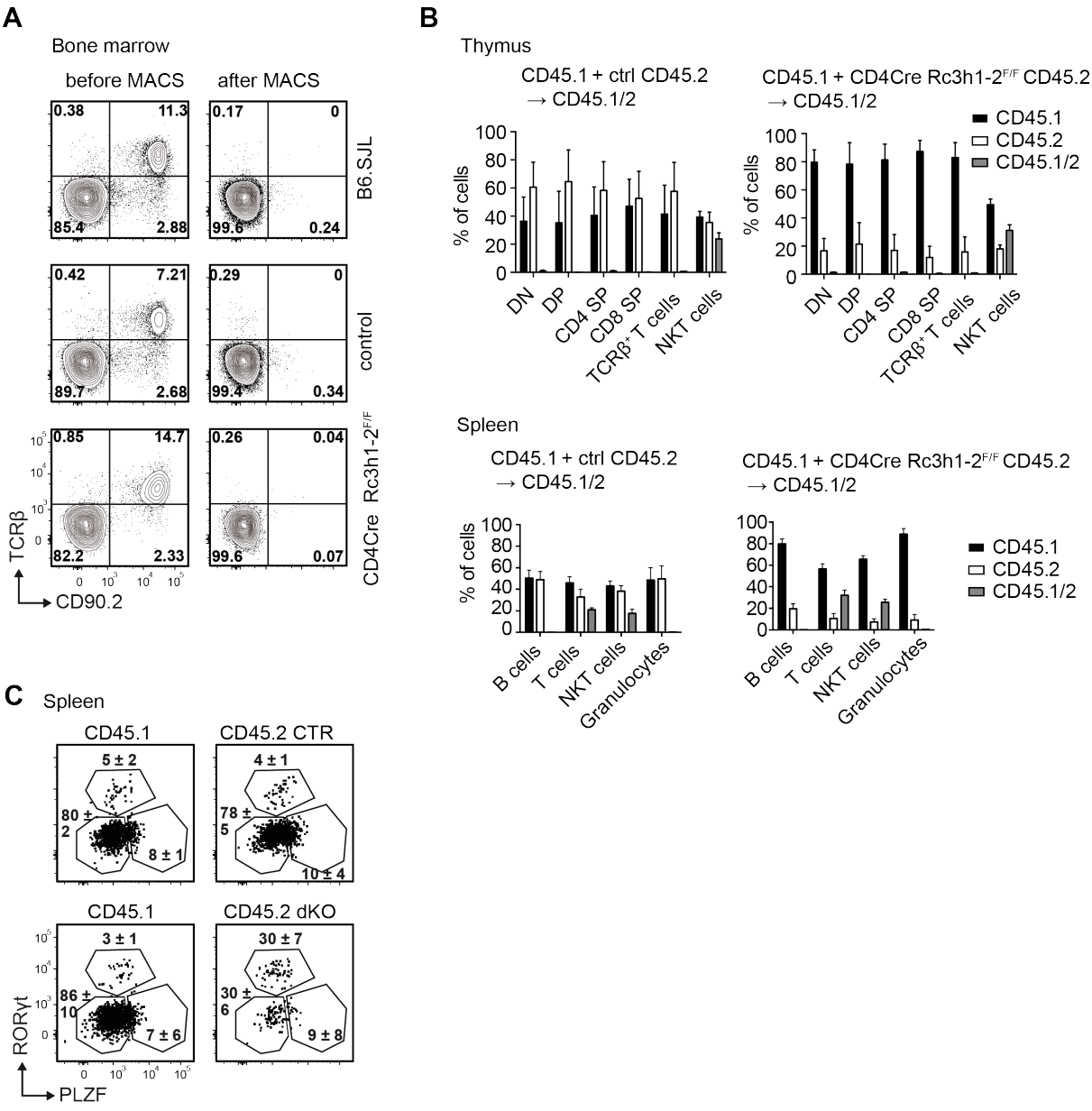

Supplemental Figure 2. Roquin paralogs control NKT cell development by cell intrinsic and extrinsic mechanisms. (A) Representative contour plots show the expression of CD90.2 and TCRβ on bone marrow cells isolated from CD45.1 B6.SJL, CD45.2 control and CD45.2 *CD4Cre Rc3h1-2*$^{F/F}$ mice before and after depletion of T cells by CD90.2 beads. (B) Analysis of CD45.1 and CD45.2 expression on the indicated thymic T cell populations (upper graphs) and splenic immune cell populations (lower graph) of bone marrow chimeras transplanted with B6.SJL and either control (left) or *CD4Cre Rc3h1-2*$^{F/F}$ (right) bone marrow. Bar charts indicate mean percentages ± SD calculated from 4 (control) or 7 (experimental) mice from one out of two independent experiments. (C) Representative contour plots show splenic NKT cell subsets (NKT1, NKT2 and NKT17 cells) gated on either CD45.1 or CD45.2 NKT cells of the indicated bone marrow chimeras. Numbers represent mean percentages of NKT1, NKT2 and NKT17 cells ± SD calculated from 4 (control) or 7 (experimental) of one out of two independent experiments.

Suppl. Figure 3

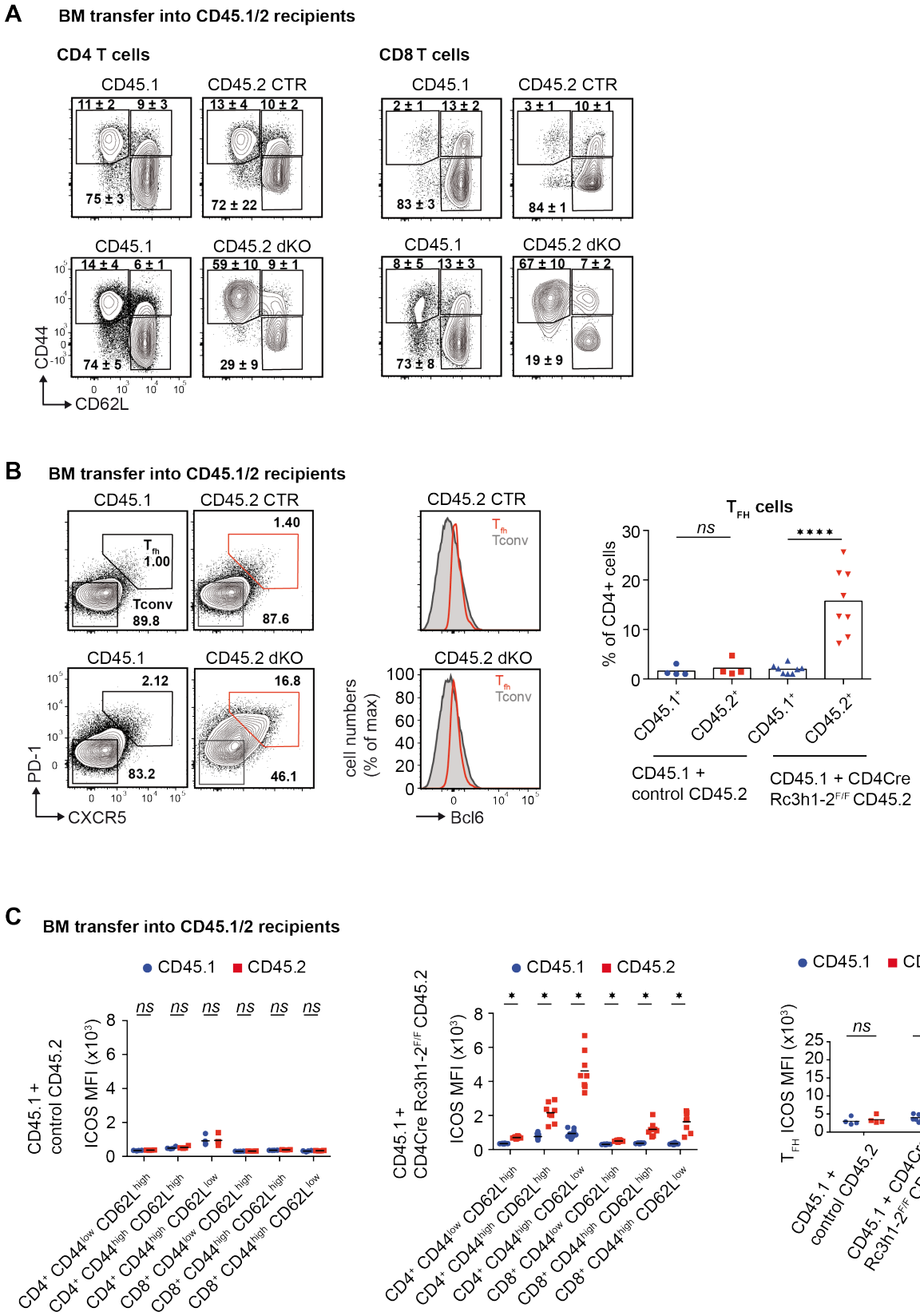

Supplemental Figure 3. The expansion of T follicular helper T_{FH} cells and differentiation of naïve T cells into effector and memory T cells in *CD4Cre Rc3h1-2$^{F/F}$* mice is cell intrinsically regulated. (A) Representative contour plots show the frequencies (mean ± SD) of splenic CD44^{low} CD62L^{high}, CD44^{high} CD62L^{high}, and CD44^{high} CD62L^{low} CD4 (left) and CD8 (right) T cells in bone

marrow chimeras as outlined in Figure 5. Cells were gated on either CD45.1$^+$ or CD45.2$^+$ cells. (B) Left: representative contour plots show the frequencies of splenic T_{FH} cells gated on either CD45.1 or CD45.2 T cells. The respective expression of Bcl-6 is shown for CD45.2 T_{FH} cells and PD-1$^-$ CXCR5$^-$ conventional T cells. Right: each data point represents one mouse and bars show the mean percentage of splenic T_{FH} cells of the indicated populations. Cells were gated as shown on the left. (C) Mean ICOS MFI of the indicated splenic CD45.1 (blue) or CD45.2 (red) T cell populations of the indicated bone marrow chimeras. MIF was normalized to ICOS MIF of CD45.1$^+$ CD4$^+$ CD44^{low} CD62L^{high} T cells, which set to 1. Left graph represents the analysis of bone marrow chimeras with B6.SJL + control CD45.2 cells; middle graph represents data from bone marrow chimeras transplanted with B6.SJL + CD45.2 *CD4Cre Rc3h1-2$^{F/F}$* bone marrow. Right graph shows ICOS expression per cell of T_{FH} cells of the indicated experimental group and gated as shown in (B). Each dot represents one mouse. Data was calculated from one out of two independent experiments with 4 control and 7 experimental mice. Statistical significance was determined by multiple t-tests using the Holm-Sidak method. *, P < 0.05; ****, P < 0.0001; *ns*, not significant.

Suppl. Figure 4

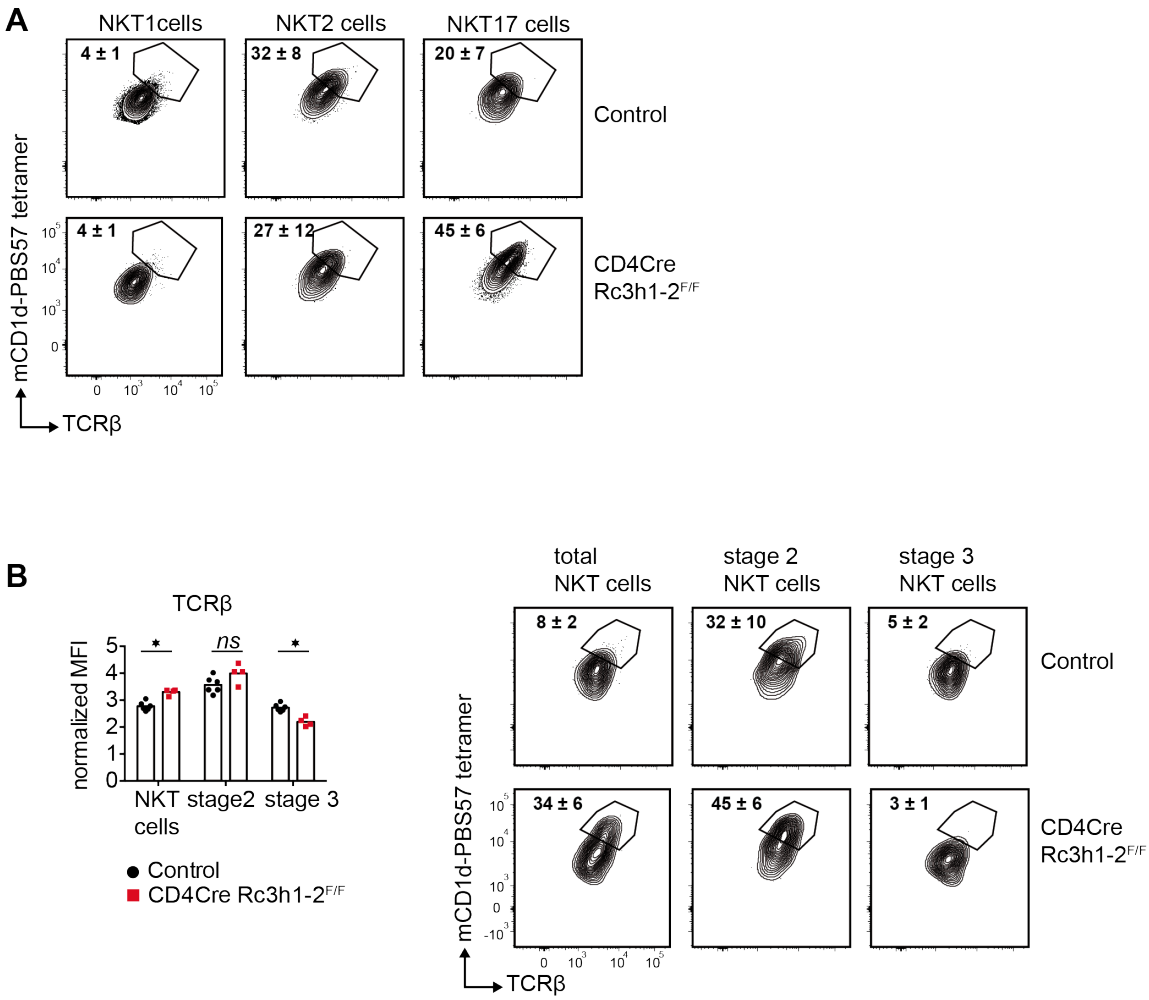

Supplemental Figure 4. Increased TCR expression after Roquin ablation. (A) Representative contour plots show the mean percentage ± SD of thymic TCRβ^{high} NKT1, NKT2 and NKT17 cells of either control or *CD4CreRc3h1-2$^{F/F}$* mice. Gates were set so that < 5% of NTK1 cells are within the TCRβ^{high} gate. Data was calculated from 8 – 17 mice per genotype pooled from at least three independent experiments. Before analysis, thymi were CD8 depleted by MACS. (B) Left: bar chart indicates mean normalized TCRβ MFI ± SD of the indicated thymic NKT cells populations of either control or *CD4Cre Rc3h1-2$^{F/F}$* mice with each dot representing one analyzed mouse. Cells were normalized to TCRβ MFI of DP thymocytes, which was set to one. Right: representative contour plots show the mean percentage ± SD of total thymic NKT cells, stage 2 and stage 3 NKT cells of the indicated genotypes. Shown data was calculated from 4 *CD4Cre Rc3h1-2$^{F/F}$* and 6 control mice. Statistical analysis was determined by multiple t-tests with *, P < 0.05; *ns*, not significant.

Suppl. Figure 5

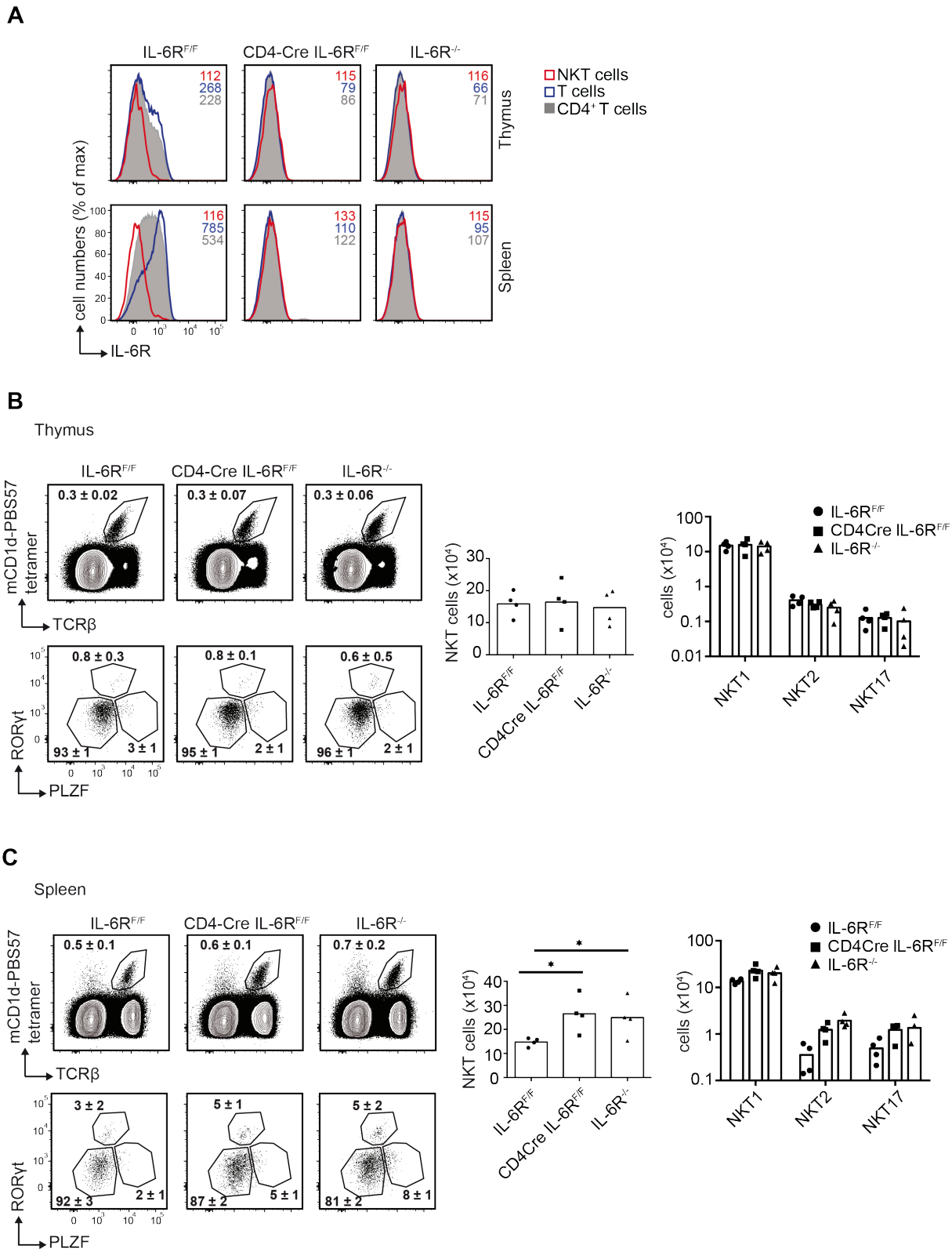

Supplemental Figure 5. Signaling through the interleukin-6 receptor is dispensable for NKT cell development. (A) Representative histograms including MFIs show IL-6Rα expression on mCD1d-PBS57 tetramer$^+$ NKT cells, tetramer$^-$ TCRβ$^+$ T cells and tetramer$^-$ TCRβ$^+$ CD4$^+$ T cells isolated from the indicated organs. Representative contour plots show the mean percentage ± SD of total NKT cells and NKT subsets in the thymus (B) and spleen (C) of the indicated genotypes. Bar charts show the respective mean cell numbers (x10^4) of total NKT cells and NKT cell subsets in the thymus (B) and

spleen (C) of the indicated genotypes. Each data point represents one mouse and shown data was calculated from 4 mice per genotype of one experiment. Statistical significance was determined by students t-test. *, $P < 0.05$.

Suppl. Figure 6

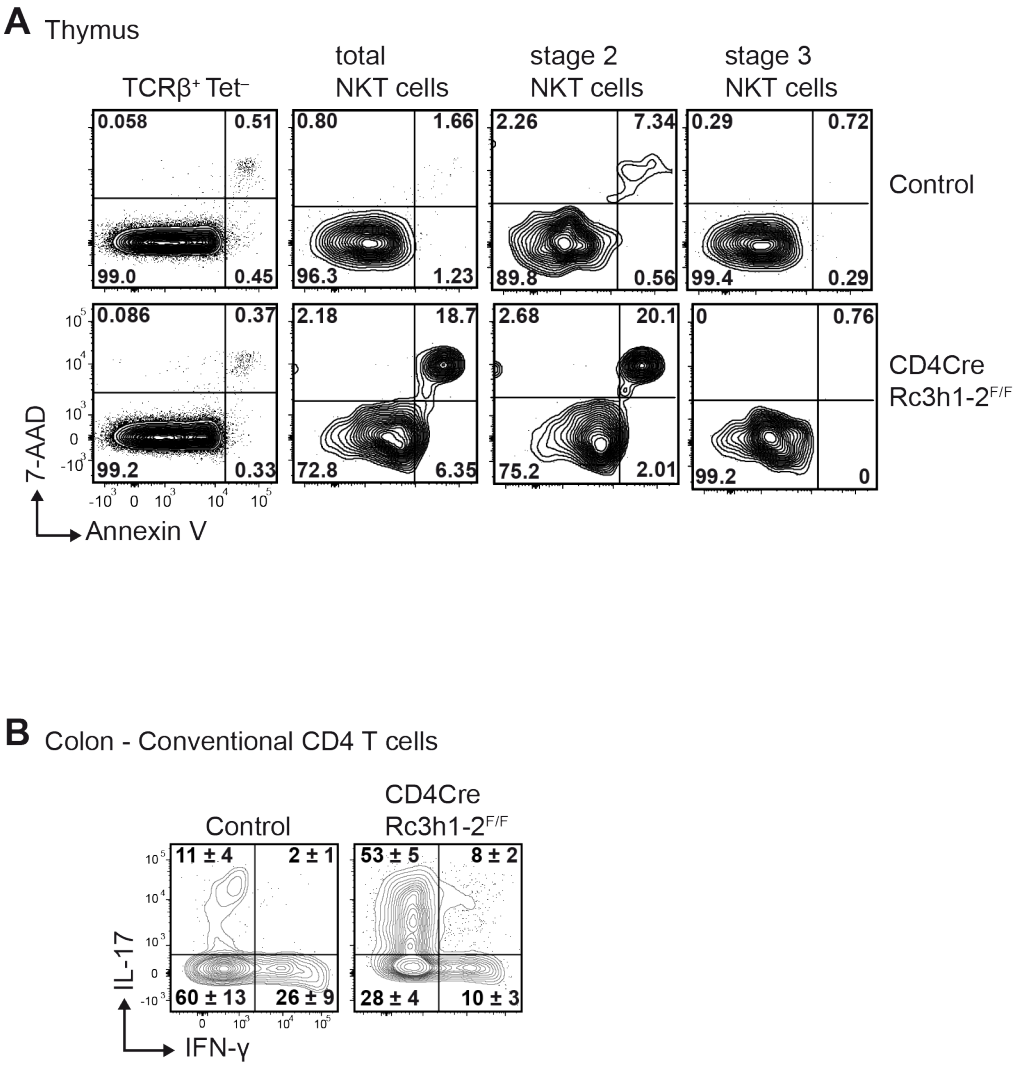

Supplemental Figure 6. Roquin ablation leads to increased apoptosis of thymic NKT cells and enhances IL-17 production of colon LP Th17 cells. (A) Representative contour plots show 7-AAD and Annexin V stainings of the indicated thymic T cell populations. Cells were isolated from either control or *CD4Cre Rc3h1-2$^{F/F}$* mice and are representative for at least 5 mice per genotype pooled from three independent experiments. (B) Representative contour plots show IFN-γ and IL-17 production of CD4^{+} Foxp3^{-} RORγt^{+} colon lamina propria (LP) lymphocytes of the indicated genotypes. Numbers indicate mean ± SD calculated from three mice of one experiment.

2. Age and location specific distribution of NKT cell subsets in the gut

2.1 Introduction

Naïve T cells emigrating from the thymus spread throughout the body via blood and lymphatic vessels. When their T cell receptor (TCR) successfully recognizes a protein epitope presented by major histocompatibility complex (MHC) class II molecules on antigen presenting cells (APCs) several signaling cascades downstream of the TCR/CD3 complex are initiated. Together with additional co-stimulatory signals through CD28 and cytokines secreted by APCs, naïve T cells differentiate into diverse T helper (Th) subsets characterized by specific transcription factor expression and secretion of subset specific cytokines. In contrast, NKT cell subsets namely NKT1, NKT2 and NKT17 cells acquire their subset specific attributes in the thymus and then colonize secondary lymphoid organs after emigration. During their maturation differential PLZF expression coincides with the expression of transcription factors such as T-bet (NKT1 cells), GATA3 (NKT2 cells) and RORγt (NKT17 cells) for the development of mature NKT cell subsets with specific cytokine profiles[1]. NKT cells are often referred to as innate-like T cells since they express a restricted TCR repertoire recognizing glycolipids and have a pre-activated phenotype allowing immediate immune response after activation[2]. It is not well understood whether in addition there are non committed NKT cell precursors in the periphery, which express the NKT cell specific Vα14-Jα18 TCR α-chain but have not yet fully matured into one of the above mentioned NKT cell subsets. In the periphery, additional NKT cell subpopulations were described: follicular helper NKT cells (NKT_{FH}) were shown to support B cell responses in an interleukin-21 (IL-21) dependent mechanism and $PLZF^-$ NKT cells (NKT10) in adipose tissue control regulatory T cell (T_{reg} cell) function by secretion of interleukin-2. Both NKT cell populations could not be detected in the thymus which points towards a certain plasticity in NKT cell differentiation[3-5].

The distribution of NKT1, NKT2 and NKT17 cells is organ specific and additionally depends on the genetic background. In C57BL/6 mice most NKT cells belong to the T-bet expressing NKT1 lineage characterized by the capability of

producing large amounts of interferon-γ (IFN-γ) after stimulation[6,7]. IL-17 producing NKT17 cells are very rare in C57BL/6 mice, where they are most abundant in peripheral lymph nodes[7,8]. Interestingly, also on barrier surfaces such as the lung a high percentage of IL-17 producing NKT cells can be found[9]. The distribution of the NKT cell subsets in the gut however is less clear. Here, a complex interaction network of host immune cells and symbiotic microorganisms shapes different types of immune responses[10]. It has been described that colonic NKT cells are crucial for the induction of oxazolone-induced colitis, a Th2 cytokine driven model for ulcerative colitis[11]. On the other hand, interactions with commensals such as *Bacteroides fragilis* glycolipids were shown to inhibit NKT cell proliferation early in life and therefore protect from autoimmune colitis[12]. Germfree mice have increased total NKT cell numbers in the colon and lungs and are prone to organ specific pathology in *in vivo* models of asthma and the aforementioned ulcerative colitis model. However, with respect to the functional and phenotypical diversity of NKT cells it is not clear whether different NKT cell subsets may also exert different roles (protective or harmful) in these models[13]. Lipids from several bacterial strains, both commensals and pathogenic bacteria, have been shown to interact with the NKT cell TCR. This results in an ambivalent function for NKT cells. On the one hand, NKT cells support clearance of pathogens, on the other hand, NKT cell interactions with commensal are important for immune homeostasis in the gut[14,15].

Here we show that NKT17 cells are enriched in the colon lamina propria in an age dependent manner. In addition, we demonstrate that the microbial flora affects the distribution of NKT cell subsets in the gut and thymus.

2.2 Results

Distribution of NKT cell subsets in the intestinal lamina propria.

NKT17 cells are overall very rare in C57BL/6 mice. However, since it was shown that this subset is enriched at barrier surfaces such as the lung, we isolated NKT cells from the lamina propria (LP) of the gut and compared the distribution of NKT cell subsets to the thymus by analyzing intracellular PLZF and RORγt expression.

In the thymi of 6 weeks old C57BL/6 mice 0.19 ± 0.03% stained positively for mCD1d-PBS57 tetramers. This was similar to the colon LP (0.18 ± 0.04%) whereas

in the small intestine (ileum) the percentage of NKT cells was increased (0.5 ± 0.18%) (Figure 1A). In the thymus most of NKT cells were $PLZF^{low}$ NKT1 cells. Around 10% of total NKT cells expressed high amounts of PLZF (NKT2 cells) and only 2% stained positively for RORγt and $PLZF^{int}$ (NKT17 cells). In the colon LP however, 44 ± 5% of NKT cells belonged to the NKT17 subset. 53 ± 5% were NKT1 cells and there were no $PLZF^{high}$ NKT2 cells detectable. In the ileum the percentage of NKT17 cells (8 ± 5%) was also higher compared to the thymus, but still was significantly smaller compared to the colon LP. In addition, in the ileum there were also some NKT2 cells detectable (2 ± 1%) (Figure 1A). Most of NKT17 cells do not express CD4, but we found around 15% of colon LP NKT17 cells to be $CD4^+$ at the age of 6 weeks (Figure 1B). Notably, to a similar extent $CD4^+$ NKT17 cells could be also detected in the thymus (data not shown). It is also worth mentioning that when the distribution of NKT1, NKT2 and NKT17 cells differed in the thymi of C57BL/6 and BALB/c mice (with an increased percentage and absolute number of NKT2 and NKT17 cells in BALB/c mice), the distribution of NKT1 and NKT17 cells in the colon was very similar between these two different genetic backgrounds (Suppl. Figure 1B).

Taken together we show that in the gut NKT17 cells predominantly reside in the LP of the large intestine.

Age dependent distribution of NKT cell subsets.

Since the percentage of RORγt expressing NKT17 cells were specifically increased in the colon, we analyzed NKT cell subsets in mice of different ages ranging from 12 days to 1,5 years. The colonization of the gut with diverse bacterial strains starts after weaning from the mother and therefore very young animals serve as a surrogate model for analyzing the impact of commensals on the distribution of NKT cells subsets in the gut.

In the colon of 12 days old C57BL/6 mice the percentage of total NKT cells was 0.5 ± 0.1% and steadily increased from 6 weeks (0.3 ± 0.1%) to 1.5 years (2.2 ± 0.5%) (Figure 1C; Suppl. Figure 1A). Notably, in the thymus of 12 days old mice only 0.08 ± 0.02% of thymocytes stained positively for mCD1d-PBS75 tetramers but with age NKT cell proportions of total thymocytes remained constant at around 0.3 – 0.4% (Suppl. Figure 2A, B). Due to thymic involution however the absolute NKT cell number decreased from a maximum mean number at around 12 weeks (38.0×10^4

cells) to only 5,0 x 10^4 at the age of 1,5 years (Suppl. Figure 2B). The distribution of NKT cell subsets was also age dependent in the colon. At 12 days, the percentage of NKT17 cells was the smallest with a mean of only 17%. However, the NKT17 cell population increased with age and constituted the majority of NKT cells (> 50%) from the age of 12 weeks onwards, at the expense of the NKT1 cell population (Figure 1C). This also represented an increase of $CD44^+$ $NK1.1^-$ NKT cells from 62 ± 5% at 12 days to 84 ± 2%, even though this increase of stage 2 NKT cells was not as pronounced as the increase of NKT17 cells. The aforementioned $CD4^+$ NKT17 cell subset diminished in size with age (Figure 1C). Finally, $PLZF^{high}$ NKT2 cells could only be detected at the age of 12 days (19 ± 3%), but were not present in older mice (Figure 1B; Suppl. Figure 1A).

The distribution of thymic NKT cell subsets was only markedly different at the age of 12 days. Here, the percentage of $CD44^-$ $NK1.1^-$ stage 1 and $CD44^+$ $NK1.1^-$ stage 2 NKT cells was increased which also reflected a marked increase in NKT2 cells (48 ± 3%) but only a somewhat larger NKT17 cell pool (4 ± 1%). With increasing age, the percentages of NKT2 and NKT17 cells continuously decreased and $PLZF^{low}$ NKT1 cells became the main NKT cell population in the thymus (69 ± 7% at 6 weeks and 92 ± 3% at 1.5 years). Since in the thymus NKT1 cells also express NK1.1 and CD44, it was not surprising that also the percentage of stage 3 NKT cell increased with age (73 ± 8% at 6 weeks and 94 ± 1% at 1.5 years) (Suppl. Figure 2A, C, D). The absolute cell numbers correlated with the relative distribution of NKT cell stages and NKT cell subsets but again the different populations became smaller with age due to the decreasing number of total thymocytes (Suppl. Figure 2B, C).

In summary we could demonstrate that the distribution of mature NKT cell subsets in the thymus and colon LP is age dependent.

NKT cells in germ free mice.

To study the role of commensal bacteria for the induction of NKT17 cells in the gut, we next analyzed NKT cell subsets in 6 weeks old C57BL/6 germ free (GF) mice and compared them to 6 weeks old C57BL/6 mice purchased from Janvier.

While the percentage of total NKT cells in the colon LP was similar compared to controls, the proportion of NKT17 cells was actually somewhat increased in germ free mice (Figure 1D). Notably, this was also the case in the thymus, where the percentage of NKT17 cells was around twice as high as in control mice (13 ± 1%

compared to 5 ± 1%). This also reflected an increase in NKT17 cell numbers (3.5 x 10^4 compared to 1.9 x 10^4). In contrast, the NKT2 cell population was decreased both in percentage and absolute cell numbers (Suppl. Figure 3A). Finally, NKT17 cells were also increased in the lungs of germ free mice (34 ± 4% compared to 19 ± 5%).

The presence of microbial antigens therefore reduces the numbers of NKT17 cells in the thymus, colon LP and lungs.

2.3 Discussion

There is increasing evidence that NKT cells fulfill very specific tasks at lymphoid and non-lymphoid tissues depending on their transcription factor profile. For example, administration of an NKT cell agonist through oral gavage, led to NKT2 cell activation in the mediastinal lymph nodes (mLN) and the initiation of a local immune response mediated by IL-4. On the other hand, intravenous injection lead to systemic INF-γ and IL-4 release driven by NKT1 cell located near vascular structures in the spleen and liver[7]. The role of IL-17 secreting NKT17 cells, however, has not been sufficiently addressed so far. Here we show that in C57BL/6 mice NKT17 cells are specifically enriched in the colon LP. With increasing age the proportion of colon LP NKT17 cells expanded at the expense of NKT1 cells. In addition, we show that a portion of NKT17 cells, in general known to be exclusively $CD4^-$, actually do express CD4. At the age of 12 days $CD4^+$ NKT17 cells make up 30 - 40% of the total NKT17 cell population in the gut but with age these cells disappear.

The hygiene hypothesis states that exposure to environmental factors such as dust and bacteria early in life can bias otherwise pro-inflammatory and pro-allergic Th2 immune responses into predominantly Th1 cytokine responses. Fittingly, NKT2 cells in the colon LP were only present at the age of 12 days. At later time points, NKT1 and then NKT17 cells became the predominant NKT cell subset in the colon. This could either mean that NKT17 cells are actively induced in the colon LP from NKT cell precursors (for instance within the NKT1/NKT2 subsets) or that NKT17 cell proliferation surpasses proliferation of the other subsets present in the colon LP or a combination of both. NKT2 cells are present only very early in life in the colon LP and it has been shown that a portion of NKT2 cells expresses T-bet mRNA and protein, is capable of IFN-γ production and could therefore function as precursors for quiescent

NKT1 cells[5,16]. In addition, lack of let-7 miRNA targeting Zbtb16 mRNA leads to an increase PLZF^{high} NKT2 cells in the thymus at the expense of PLZF^{low} NKT1 cells[17]. Fittingly, with age NKT1 cells become the predominant population in the thymus and NKT2 cells, very abundant early after birth, vanish over time. Altogether this data indicates that NKT1 cells can at least to some extent emerge from the NKT2 subset supporting the above mentioned hygiene hypothesis since in the colon LP NKT2 cells disappear soon after birth. However, this plasticity could not be clearly demonstrated for NKT17 cells so far and it's currently unknown whether this subset can also develop from NKT2 cells. Several questions still need to be addressed: it is not clear why NKT17 cells are specifically enriched in the colon LP and are much less abundant in the small intestine. Given the role of the microbiota for the induction of other T cell subsets such as regulatory T (T_{reg}) cells and Th17 cells, it is possible that certain bacterial strains also affect NKT cell differentiation (especially considering their specificity for glycolipid antigens)[18-20]. In this context, also the described CD4$^+$ NKT17 cell subsets needs to be further investigated. Even though it is unlikely that CD4 expression itself has a functional consequence for CD1d recognizing NKT cells, it still could serve as a surrogate marker for NKT17 cells with specific properties. Next, it has been shown that germ free mice have a worse outcome in an (Th2 cytokine driven) ulcerative colitis model. However, it is still not clear, whether IL-4 and IL-13 producing NKT2 cells are the main pathogenic NKT cell subset during the course of the disease. In the steady state, NKT17 cells and not NKT2 cells were increased in germ free mice (even though not to a great extent), but it is not known whether the distribution of the NKT cell subsets changes over the course of disease.

Especially in the context of recently published work, which report a diverse role of T helper 17 (Th17) cells capable of inducing either pro-inflammatory or regulatory immune responses, it should be informative to decipher the exact role of colon LP NKT17 cells[21,22]. In addition, further investigation needs to be done to more precisely analyze cytokine secretion patterns and global gene expression of colon LP NKT17 (germ free vs. wild-type) and thymic NKT17 cells.

2.4 Materials and Methods

Mice

C57BL/6 and BALB/c mice were purchased from Janvier and were analyzed at the age of 6 weeks if not otherwise indicated. Germ free mice were kindly provided by Dirk Haller, Technische Universität München. All experiments were performed in accordance with German Federal Animal Protection Laws and approved by the Regierung of Oberbayern.

Flow Cytometry

Single cell suspensions were prepared from indicated organs and stained with commercially available antibodies: CD4 (GK1-5, RM4-5), CD44 (IM7), NK1.1 (PK136), PLZF (9E12), RORγt (AFKJS-9, Q31-387), TCRβ (H57-597), T-bet (4B10). For the staining of intracellular proteins cells were fixed and permeabilized using the Foxp3 / Transcription Factor Staining Buffer Set (eBioscience). For the detection of intracellular cytokines, cells were stimulated for 4 hours with 100 ng/ml phorbol-12-myristat-13-acetat (PMA, Sigma) and 1000 ng/ml ionomycin (Calbiochem) in the presence of Monensin and stained with antibodies against IL-17 (eBio17B7), IL-4, (11B11) and IFN-γ (XMG1.2). mCD1d-tetramers were kindly provided by the NIH tetramer core facility. For isolation of lamina propria lymphocytes, longitudinally opened 1-1,5cm bowel pieces were first incubated in HBSS buffer containing 5% FCS and 5mM EDTA, 1mM DTT and 10mM HEPES for 2 x 15 – 20min and after washing with ice cold PBS. Then bowel pieces were digested in $PBS^{+Ca/+Mg}$ containing 5% FCS, 1mg/ml collagenase (CellSystems) and 0,1mg/ml DNase I (Roche) for 45min at 37°, and lymphocytes were purified by a 40/80% Percoll (Biochrom) gradient. Mononuclear cells from the lungs were isolated by mashing them through 100µm cell strainer (Falcon®). Cells were then purified by a 40/80% Percoll (Biochrom) gradient.

2.5 References

1. Gapin L. ScienceDirect Development of invariant natural killer T cells. *Current Opinion in Immunology*. 2016;39:68–74.
2. Salio M, Silk JD, Yvonne Jones E, Cerundolo V. Biology of CD1- and MR1-Restricted T Cells. *Annu. Rev. Immunol.* 2014;32(1):323–366.

3. Chang P-P, Barral P, Fitch J, et al. Identification of Bcl-6-dependent follicular helper NKT cells that provide cognate help for B cell responses. *Nature Immunology*. 2011;13(1):35–43.
4. Michelet X, Zhang S, Brennan PJ, et al. Regulatory iNKT cells lack expression of the transcription factor PLZF and control the homeostasis of Treg cells and macrophages in adipose tissue. *Nature Immunology*. 2014;1–12.
5. Engel I, Seumois GEG, Chavez L, et al. Innate-like functions of natural killer T cell subsets result from highly divergent gene programs. *Nature Immunology*. 2016;1–15.
6. Lee YJ, Holzapfel KL, Zhu J, Jameson SC, Hogquist KA. Steady-state production of IL-4 modulates immunity in mouse strains and is determined by lineage diversity of iNKT cells. *Nature Immunology*. 2013;1–10.
7. Lee YJ, Wang H, Starrett GJ, et al. Tissue-Specific Distribution of iNKT Cells Impacts Their Cytokine Response. *Immunity*. 2015;1–23.
8. Doisne J-M, Becourt C, Amniai L, et al. Skin and peripheral lymph node invariant NKT cells are mainly retinoic acid receptor-related orphan receptor (gamma)t+ and respond preferentially under inflammatory conditions. *The Journal of Immunology*. 2009;183(3):2142–2149.
9. Michel M-L, Keller AC, Paget C, et al. Identification of an IL-17-producing NK1.1(neg) iNKT cell population involved in airway neutrophilia. *J. Exp. Med.* 2007;204(5):995–1001.
10. Belkaid Y, Hand TW. Role of the Microbiota in Immunity and Inflammation. *Cell*. 2014;157(1):121–141.
11. Heller F, Fuss IJ, Nieuwenhuis EE, Blumberg RS, Strober W. Oxazolone colitis, a Th2 colitis model resembling ulcerative colitis, is mediated by IL-13-producing NK-T cells. *Immunity*. 2002;17(5):629–638.
12. An D, Oh SF, Olszak T, et al. Sphingolipids from a Symbiotic Microbe Regulate Homeostasis of Host Intestinal Natural Killer T Cells. *Cell*. 2014;156(1-2):123–133.
13. Olszak T, An D, Zeissig S, et al. Microbial Exposure During Early Life Has Persistent Effects on Natural Killer T Cell Function. *Science*. 2012;336(6080):489–493.
14. McEwen-Smith RM, Salio M, Cerundolo V. CD1d-dependent endogenous and exogenous lipid antigen presentation. *Current Opinion in Immunology*. 2015;34:116–125.
15. Brennan PJ, Brigl M, Brenner MB. Invariant natural killer T cells:an innate activation scheme linkedto diverse effector functions. *Nature Reviews Immunology*. 2013;1–17.
16. Benlagha K. A Thymic Precursor to the NK T Cell Lineage. *Science*. 2002;296(5567):553–555.
17. Pobezinsky LA, Etzensperger R, Jeurling S, et al. Let-7 microRNAs target the lineage-specific transcription factor PLZF to regulate terminal NKT cell differentiation and effector function. *Nature Immunology*. 2015;1–9.
18. Atarashi K, Tanoue T, Shima T, et al. Induction of Colonic Regulatory T Cells by Indigenous Clostridium Species. *Science*. 2011;331(6015):337–341.
19. Ivanov II, Atarashi K, Manel N, et al. Induction of Intestinal Th17 Cells by Segmented Filamentous Bacteria. *Cell*. 2009;139(3):485–498.
20. Surana NK, Kasper DL. Deciphering the tête-à-tête between the microbiota and the immune system. *J. Clin. Invest.* 2014;124(10):1–7.
21. Gaublomme JT, Yosef N, Lee Y, et al. Single-Cell Genomics Unveils Critical Regulators of Th17 Cell Pathogenicity. *Cell*. 2015;163(6):1400–1412.

22. Wang C, Yosef N, Gaublomme J, et al. CD5L/AIM Regulates Lipid Biosynthesis and Restrains Th17 Cell Pathogenicity. *Cell*. 2015;163(6):1413–1427.

2.6 Figures

Figure 1

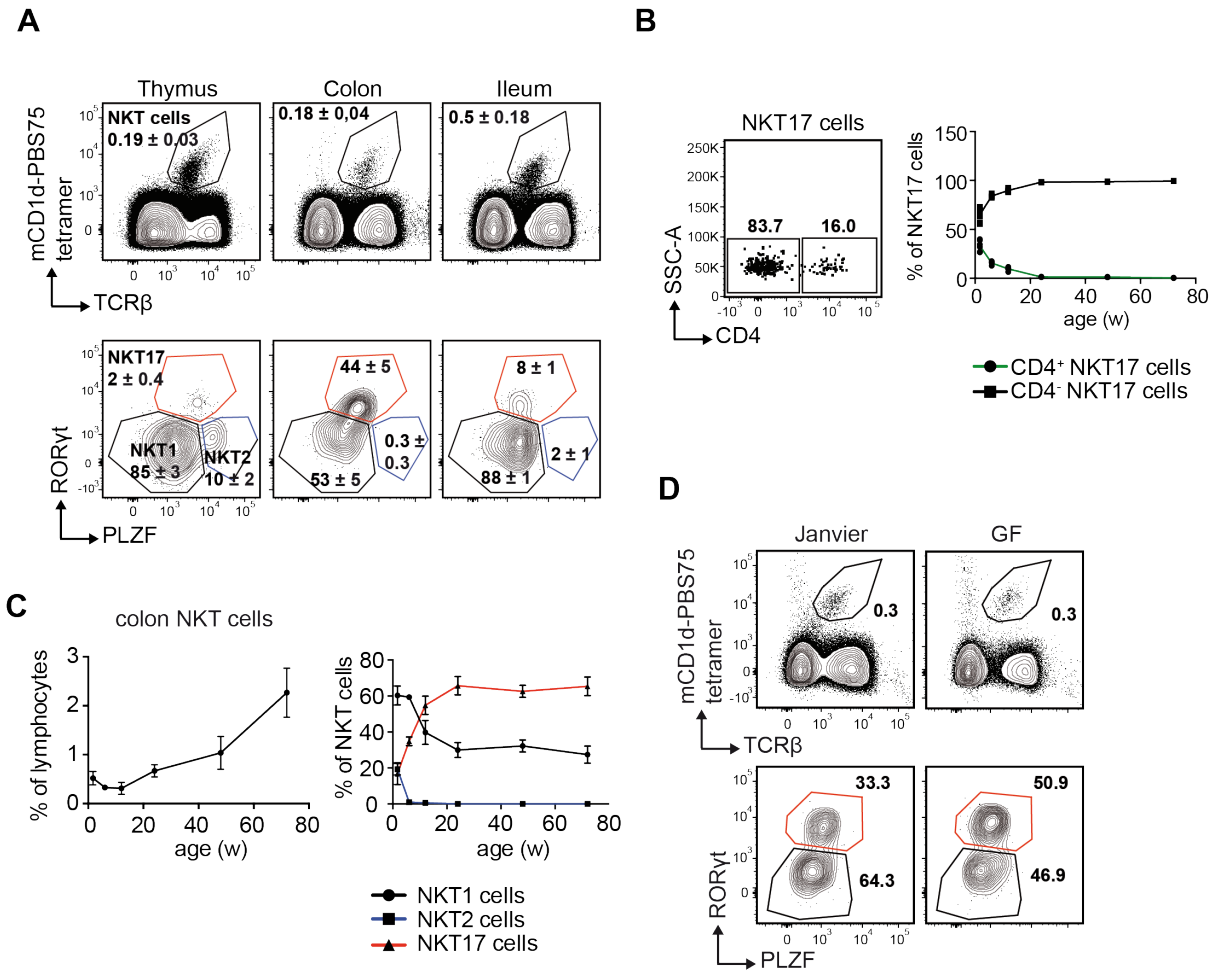

Figure 1. RORγt expressing NKT17 cells are enriched in the colon lamina in an age dependent manner. (A) Representative contour plots show the mean percentage ± SD of mCD1d-PBS57 tetramer$^+$ NKT cells (upper row) and NKT1, NKT2 and NKT17 cells (lower row) isolated from the indicated organs of 6 week old C57BL/6 mice. (B) Representative dot plot shows the percentage of CD4$^-$ and CD4$^+$ NKT17 cells isolated from the colon LP and gated as shown in (A). On the right, the mean percentage of CD4$^-$ and CD4$^+$ NKT17 cells, isolated from the colon LP of C57BL/6 mice at different ages is shown. Each data point represents one mouse. (C) Left: shown is the mean percentage ± SD of mCD1d-PBS57 tetramer$^+$ NKT cells isolated from the colon LP of C57BL/6 mice at different ages. Right: shown is the mean percentage of NKT1, NKT2 and NKT17 cells of the same mice as shown on the left. (D) Representative contour plots show the percentage of total NKT cells (upper row) and NKT1 and NKT17 cells (lower row) isolated from the colon LP of 6 weeks old C57BL/6 mice ordered from Janvier (left) and GF C57BL/6 mice of the same age. Data was calculated from 8 mice of one experiment (A), 2 – 6 mice per age group pooled from two independent experiments (B, C) or 1 -2 mice from one experiment (D).

2.7 Supplemental Information

Suppl. Figure 1

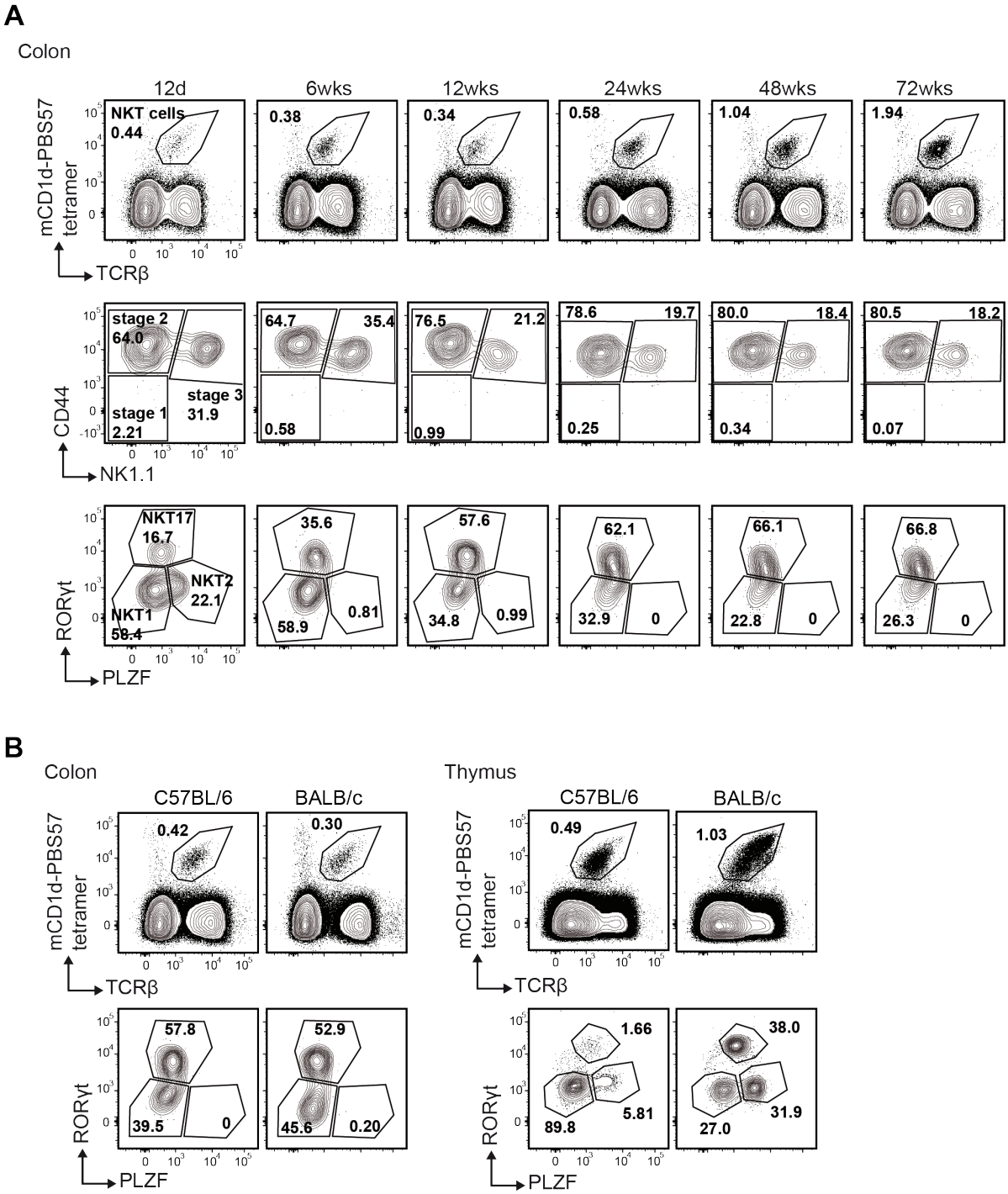

Supplementary Figure 1. Age dependent distribution of NKT cell subsets in the colon lamina propria. (A) Contour plots show the percentage of total NKT cells (upper row), NKT cell stages 1 – 3 (middle row) and NKT1, NKT2 and NKT17 cells (lower row). Cells were isolated from the colon LP of C57BL/6 mice at the indicated ages. Plots are representative of 2 – 6 mice per group pooled from two independent experiments. (B) Contour plots show the percentage of total NKT cells (upper row) and NKT1 and NKT17 cells (lower row) isolated from the colon LP (left) or thymus (right) of 12 weeks old

mice of the indicated genetic background. Plots are representative of 4 mice per group from one experiment.

Suppl. Figure 2

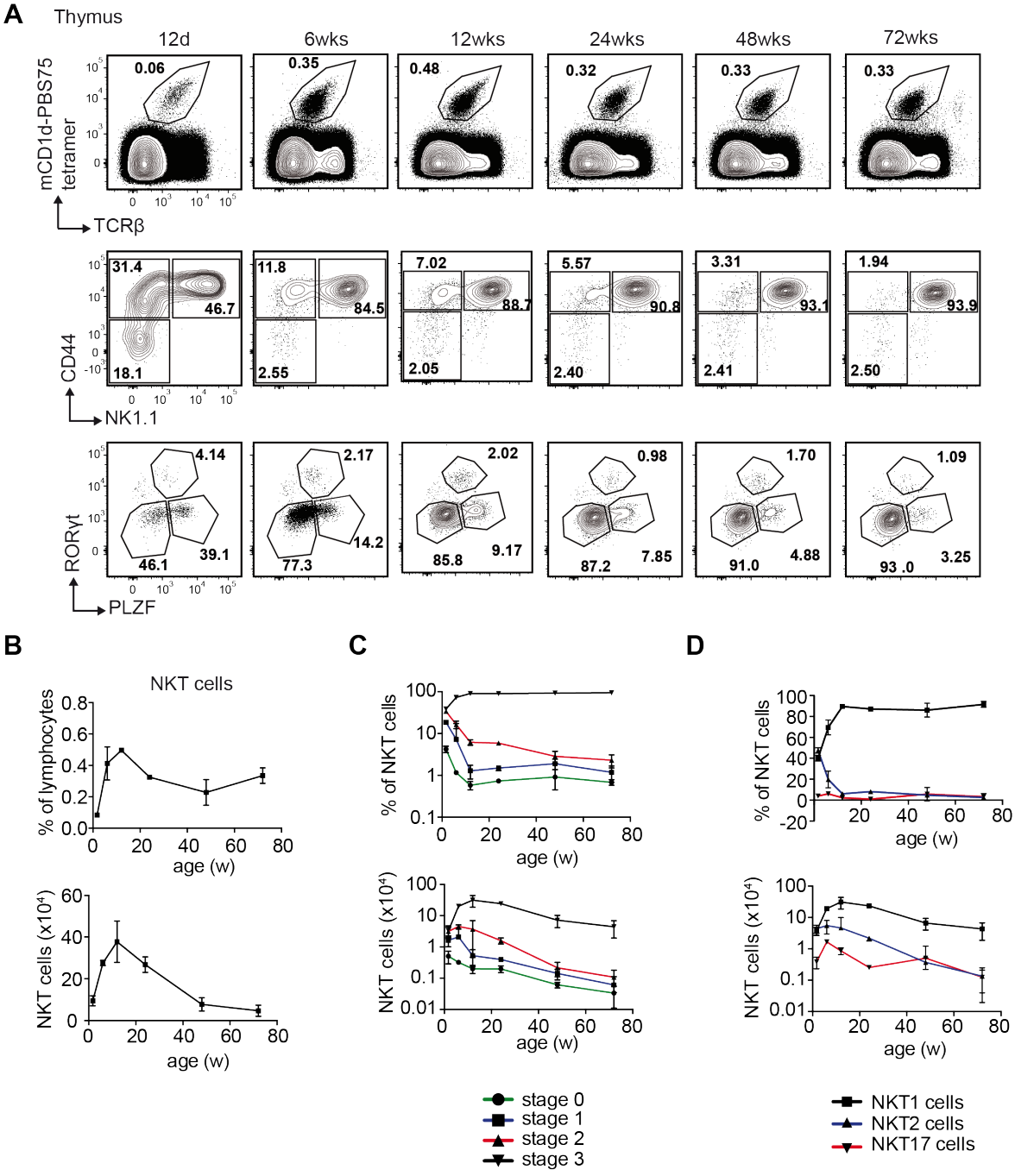

Supplementary Figure 2. Age dependent distribution of thymic NKT cell subsets. (A) Contour plots show the percentage of total NKT cells (upper row), NKT cell stages 1 – 3 (middle row) and NKT1, NKT2 and NKT17 cells (lower row). Cells were isolated from the thymus of C57BL/6 mice at the indicated ages. Plots are representative of 2 – 6 mice per age group pooled from two independent experiments. (B) Graphs show the mean percentage (upper graph) and mean cell number (lower graph) ± SD of thymic NKT cells, gated as indicated in (A) and isolated from C57BL/6 mice at indicated ages. (C) Graphs show the mean percentage (upper graph) and mean cell number (lower graph) ± SD of thymic NKT cell stages 1 – 3, gated as indicated in (A) and isolated from C57BL/6 mice at indicated ages. (D) Graphs show the mean percentage (upper graph) and mean cell number (lower graph) ± SD of thymic NKT1, NKT2 and NKT17 cells, gated as indicated in (A) and isolated from C57BL/6 mice at indicated ages. Data is pooled from 2 – 6 mice per age group from two independent experiments (B – D).

Suppl. Figure 3

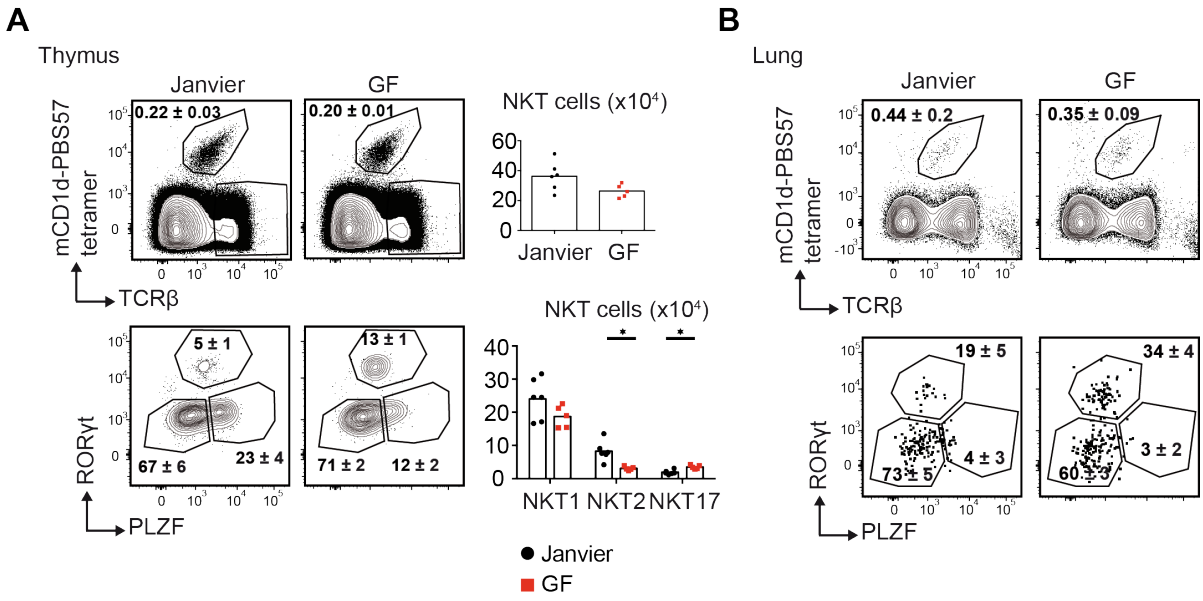

Supplementary Figure 3. Distribution of NKT cell subsets in the thymi and lungs of germ free mice. (A) Representative contour plots show the mean percentage ± SD of total NKT cells (upper row) and NKT1, NKT2 and NKT17 cells (lower row) isolated from the thymi of C57BL/6 mice from Janvier or germ free mice of the same genetic background. Bar charts show the mean cell number of NKT cells (upper graph) and NKT cell subsets (lower graph) with each data point representing one mouse. Data was calculated from 6 control mice and 5 germ free mice of one experiment. Statistical significance determined by multiple t-tests using the Holm-Sidak method. *, P < 0,05. (B) Representative contour plots show the mean percentage ± SD of total NKT cells (upper row) and NKT1, NKT2 and NKT17 cells (lower row) isolated from the lungs of C57BL/6 mice from Janvier or germ free mice of the same genetic background. Data was calculated from 6 control mice and 5 germ free mice of one experiment.

3. The role of continuous TCR signals for mature T_{reg} cell biology

Please cite this article in press as: Vahl et al., Continuous T Cell Receptor Signals Maintain a Functional Regulatory T Cell Pool, Immunity (2014), http://dx.doi.org/10.1016/j.immuni.2014.10.012

Immunity
Article

Continuous T Cell Receptor Signals Maintain a Functional Regulatory T Cell Pool

J. Christoph Vahl,[1,11,13] Christoph Drees,[2,13] Klaus Heger,[1,2] Sylvia Heink,[3] Julius C. Fischer,[2] Jelena Nedjic,[4] Naganari Ohkura,[5] Hiromasa Morikawa,[5] Hendrik Poeck,[2] Sonja Schallenberg,[6] David Rieß,[1,2] Marco Y. Hein,[1,12] Thorsten Buch,[7] Bojan Polic,[8] Anne Schönle,[9] Robert Zeiser,[9] Annette Schmitt-Gräff,[10] Karsten Kretschmer,[6] Ludger Klein,[4] Thomas Korn,[3] Shimon Sakaguchi,[5] and Marc Schmidt-Supprian[1,2,*]

[1]Max Planck Institute of Biochemistry, Am Klopferspitz 18, 82152 Martinsried, Germany
[2]Department of Hematology, Oncology, Klinikum rechts der Isar, Technische Universität München, Ismaninger Straße 15, 81675 Munich, Germany
[3]Department of Neurology, Klinikum rechts der Isar, Technische Universität München, Ismaninger Straße 15, 81675 Munich, Germany
[4]Institute for Immunology, Ludwig-Maximilians University, Goethestraße 31, 80336 Munich, Germany
[5]Department of Experimental Immunology, World Premier International Immunology Frontier Research Center, Osaka University, Suita 565-0871, Japan
[6]Molecular and Cellular Immunology/Immune Regulation, DFG-Center for Regenerative Therapies Dresden (CRTD), Technische Universität Dresden, Fetscherstraße 105, 01307 Dresden, Germany
[7]Institute for Medical Microbiology, Immunology & Hygiene, Trogerstraße 30, Technische Universität München, 81675 Munich, Germany and Institute of Laboratory Animal Sciences, University of Zurich, Winterthurer Straße 190, 8057 Zurich, Switzerland
[8]University of Rijeka School of Medicine, B. Branchetta 20, HR-51000 Rijeka, Croatia
[9]Department of Hematology, Oncology and Stem Cell Transplantation, University of Freiburg, Hugstetter Straße 55, 79106 Freiburg, Germany
[10]Department of Pathology, University Hospital Freiburg, Breisacher Straße 115a, 79106 Freiburg Germany
[11]Present address: Merck Serono, Merck KGaA, Frankfurter Straße 250, 64293 Darmstadt, Germany
[12]Present address: Proteomics and Signal Transduction, Max Planck Institute of Biochemistry, Am Klopferspitz 18, 82152 Martinsried, Germany
[13]Co-first author
*Correspondence: supprian@lrz.tum.de
http://dx.doi.org/10.1016/j.immuni.2014.10.012

SUMMARY

Regulatory T (Treg) cells maintain immune homeostasis and prevent inflammatory and autoimmune responses. During development, thymocytes bearing a moderately self-reactive T cell receptor (TCR) can be selected to become Treg cells. Several observations suggest that also in the periphery mature Treg cells continuously receive self-reactive TCR signals. However, the importance of this inherent autoreactivity for Treg cell biology remains poorly defined. To address this open question, we genetically ablated the TCR of mature Treg cells in vivo. These experiments revealed that TCR-induced Treg lineage-defining Foxp3 expression and gene hypomethylation were uncoupled from TCR input in mature Treg cells. However, Treg cell homeostasis, cell-type-specific gene expression and suppressive function critically depend on continuous triggering of their TCR.

INTRODUCTION

The generation of a peripheral T cell pool with a broad diversity of T cell receptors (TCRs) is critical for a functional immune system. The random nature of somatic TCR gene assembly ensures that a large number of foreign antigens can be recognized. However, this process bears the inherent problem that self-reactive TCRs are also generated. Central and peripheral tolerance mechanisms delete autoreactive T cells or render them ineffective (Xing and Hogquist, 2012). During thymic T cell development, most T cells with a strong self-reactivity to peptide-major histocompatibility complex (MHC) complexes are deleted. Some cells showing intermediate self-reactivity are instructed to develop into regulatory T (Treg) cells, a process known as agonist selection (Josefowicz et al., 2012; Xing and Hogquist, 2012). Treg cells suppress the expansion and function of (autoreactive) effector T cells and their absence or dysfunction leads to severe T cell-mediated pathologies in man and mouse (Josefowicz et al., 2012; Sakaguchi et al., 2008). Treg cells act mostly by suppressing the expansion and function of effector T cells, through various direct and indirect mechanisms.

The key lineage-defining transcription factor Forkhead Box P3 (Foxp3), together with other transcriptional regulators, controls the expression of gene programs necessary to induce and maintain Treg cell identity and function. Foxp3 regulates gene expression mostly in conjunction with other transcriptional regulators, depending on the type of the immune response and the tissue where this response takes place (Fu et al., 2012; Rudra et al., 2012; Stephens et al., 2007). In addition, the establishment of a Treg cell-specific hypomethylation pattern ensures a transcriptionally poised state in a set of Treg cell core genes (Ohkura et al., 2012).

Importantly, these two lineage-defining characteristics of Treg cells, namely Foxp3 expression and the specific hypomethylated state, are induced by rather strong, and in the latter case long-lasting, TCR signals in developing Treg cells. Interruption of

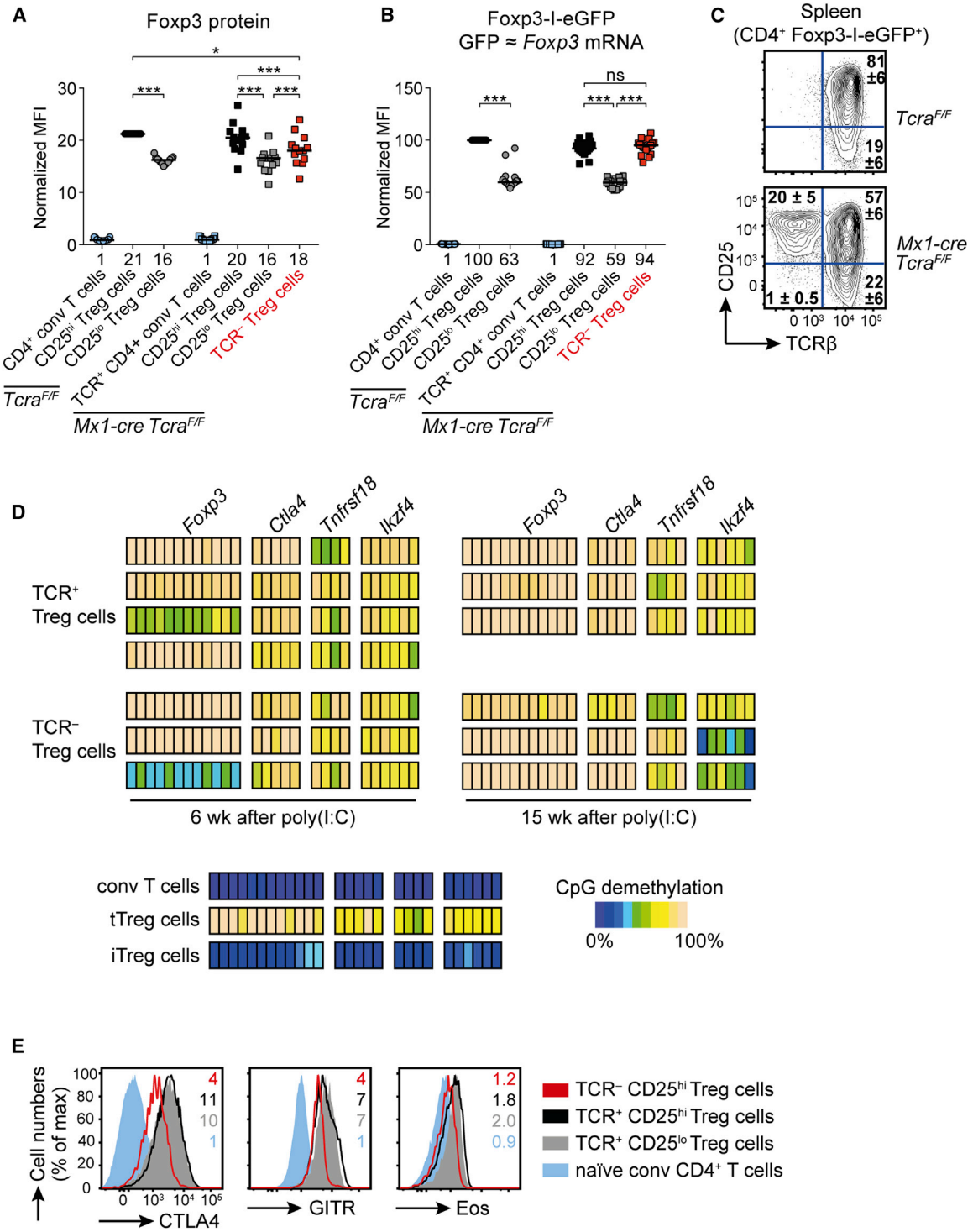

Figure 1. Foxp3 Protein Expression and Treg Cell-Specific Methylation Pattern Remain in Absence of TCR Signals

(A and B) Intracellular Foxp3 expression (A) and Foxp3-I-eGFP expression (B) 6 weeks after poly(I:C) injection. Median fluorescence intensities (MFI) were normalized to CD25^{hi} Treg cells of *Tcra*$^{F/F}$ animals, then set to 1 for CD4^{+} conventional T cells (A), or normalized to CD25^{hi} Treg cells of *Tcra*$^{F/F}$ animals in percentage (B). Numbers below the plot indicate means of the normalized MFIs and were calculated from 10 mice per genotype from 4 independent experiments (A) and from 16 mice per genotype from 5 independent experiments (B). ***$p < 0.001$; *$p < 0.05$; ns, not significant; one-way ANOVA.

(C) Surface CD25 and TCRβ expression on Foxp3-I-eGFP^{+} Treg cells 6 weeks after poly(I:C) injection. Numbers indicate mean percentage ± SD of ≥ 14 mice per genotype from ≥ 4 independent experiments.

(legend continued on next page)

TCR signaling in developing thymic Treg cells by ablation of Lck leads to reduced splenic, but increased lymph node Foxp3$^+$ Treg cell numbers. These Lck-deficient Treg cells display deficiencies in Treg cell signature genes (Kim et al., 2009). Furthermore, a mutation in LAT abolishing its ability to bind to PLCγ1 severely interferes with Treg cell, but not conventional T cell, development (Koonpaew et al., 2006).

Peripheral Treg cell identity depends on continued Foxp3 expression, underscoring its critical importance. Furthermore, the majority of Treg cells express high amounts of CD25, the α chain of the high-affinity IL-2 receptor, and their survival and full Foxp3 expression depends on IL-2 (Josefowicz et al., 2012). The importance of TCR signals for the maintenance of mature Treg cell pool size and lineage identity is less well understood. A reporter mouse for TCR signal strength reveals that Treg cells continuously receive stronger TCR signals than conventional T cells not only during thymic development, but also in the periphery (Moran et al., 2011). However, mice expressing major histocompatibility complex class II (MHCII) glycoproteins only on cortical thymic epithelial cells show normal proportions of CD4$^+$ CD25$^+$ T cells in peripheral lymph nodes (Bensinger et al., 2001), suggesting that homeostasis of mature Treg cells is to a large degree MHCII independent. Furthermore, graded interference in TCR signaling strength by ZAP mutations leads to a reduced number of Treg cells in the thymus, but not in the spleen (Siggs et al., 2007). In contrast, ablation of MHCII expression specifically on CD11c^{hi} dendritic cells significantly reduces proportions and the absolute number of Treg cells in lymph nodes and spleen (Darrasse-Jèze et al., 2009).

To directly address the importance of tonic TCR signaling for peripheral Treg cell homeostasis and lineage identity, we monitored the consequences of induced TCR ablation on mature Treg cells. Our results show that although TCR-deficient Treg cells maintain Foxp3 expression and their lineage-specific hypomethylation pattern, continuous TCR signals are required to maintain their activated phenotype, homeostasis, and their immunosuppressive properties. Therefore, we propose that TCR-derived signals are not only critical during thymic development, but also for the maintenance and function of peripheral Treg cells.

RESULTS

Foxp3 Expression Is Independent of Continuous TCR Signals in Mature Peripheral Treg Cells

In order to study the importance of TCR signaling for Treg cells in vivo, we ablated the TCRα chain by poly(I:C) injection of *Mx1-cre Tcra*$^{F/F}$ mice. This leads to downregulation of TCRβ-chain and CD3 surface expression after 5 days and nearly complete surface absence of both molecules after 10 days (Polic et al., 2001). Two weeks after poly(I:C) treatment, around 25% of the Foxp3$^+$ Treg cells had lost TCR surface expression (see Figure S1A available online). To facilitate the identification of Treg cells, *Mx1-cre Tcra*$^{F/F}$ mice were bred to the Foxp3-I-eGFP reporter strain (Bettelli et al., 2006), in which GFP expression reports *Foxp3* mRNA amounts (*Tcra*$^{F/F}$ stands for *Tcra*$^{F/F}$ and *Tcra*$^{F/F}$ Foxp3-I-eGFP throughout the manuscript). We analyzed Treg cells 6 weeks after induced TCR ablation unless otherwise indicated, so that they lacked TCR signals for at least 1 month. Our analyses were conducted mostly with thymus-derived Treg cells, because we detected only very low numbers of Nrp1^{lo} peripherally derived pTreg cells in the spleen (Figure S1B). Importantly, 6 weeks after TCR loss, TCR-deficient Treg cells still expressed high Foxp3 amounts and were exclusively CD25^{hi} (Figures 1A–1C and S1C and S1D). Analyses of *Mx1-cre* mT/mG reporter mice (Muzumdar et al., 2007) revealed equal Cre-mediated recombination efficiencies in various Treg cell subsets, including CD25^{lo} Treg cells, at this time point (Figure S1E). This indicates that CD25^{lo} Treg cells were either lost or upregulated CD25 after TCR ablation. Because CD25^{hi} and CD25^{lo} Treg cells differ in their gene expression and proliferation (Fontenot et al., 2005), we compared CD25^{hi} TCR-deficient to TCR-expressing CD25^{hi} Treg cells unless stated otherwise. Foxp3 protein levels of TCR$^-$ (CD25^{hi}) Treg cells were slightly reduced (10%) in comparison to TCR$^+$ CD25^{hi} Treg cells, but still significantly higher than those of TCR$^+$ CD25^{lo} Treg cells (Figures 1A and S1C). GFP amounts reporting *Foxp3* mRNA were virtually identical between TCR$^+$ CD25^{hi} and TCR$^-$ Treg cells (Figures 1B and S1D). This indicates that TCR signals induce posttranslational stabilization of the Foxp3 protein. GFP-expression and hence *Foxp3* mRNA amounts remain stable in all TCR$^-$ Treg cells at 4, 8, or 12 days after induced TCR ablation while Foxp3 protein amounts decrease to their final levels within 8 days (Figures S1F and S1G).

Together, these experiments demonstrate that continuous TCR signals are largely dispensable for the maintenance of Foxp3 expression of mature Treg cells.

The Treg Cell-Specific Epigenetic Pattern Is Not Affected by TCR Ablation

Besides Foxp3 expression, the establishment of a specific hypomethylation pattern (nTreg-Me), especially within the gene loci of *Foxp3*, *Gitr*, *Ctla4*, and *Ikzf4 (*Eos), is of critical importance during thymic Treg cell development (Ohkura et al., 2012). Long-lasting TCR stimulation of developing thymocytes is shown to induce nTreg-Me whereas Foxp3 expression is a consequence of strong TCR activation (Ohkura et al., 2012). Bisulfite sequencing of purified TCR-deficient and proficient Treg cells 6 and 15 weeks after poly(I:C)-induced TCR ablation did not reveal changes in the Treg cell-specific methylation pattern (Figure 1D). In line with this finding, the protein amounts of genes that contain hypomethylated regulatory regions were, albeit reduced, still significantly higher in TCR-deficient Treg cells than in naive conventional T cells (Figures 1A, 1E, and 2D). Furthermore, we also did not detect major differences in the mRNA expression levels of several additional genes

(D) CpG methylation status of splenic CD25^{hi} TCR$^+$ and TCR$^-$ Foxp3$^+$ Treg cells, 6 weeks or 15 weeks after poly(I:C) injection. tTreg = thymus-derived Treg; iTreg = in vitro-induced Treg.

(E) Intracellular (CTLA4, Eos) or extracellular (GITR) expression of the indicated splenic T cell subsets (Treg = Foxp3$^+$), all from *Mx1-cre Tcra*$^{F/F}$ mice 6 weeks after poly(I:C) injection. Numbers in representative histograms indicate means of the MFIs, normalized to Foxp3$^-$ CD4$^+$ CD44^{lo} naive T cells of *Tcra*$^{F/F}$ mice. Means were calculated from $\geq$ 5 mice per genotype from $\geq$ 2 independent experiments. See also Figure S1.

Please cite this article in press as: Vahl et al., Continuous T Cell Receptor Signals Maintain a Functional Regulatory T Cell Pool, Immunity (2014), http://dx.doi.org/10.1016/j.immuni.2014.10.012

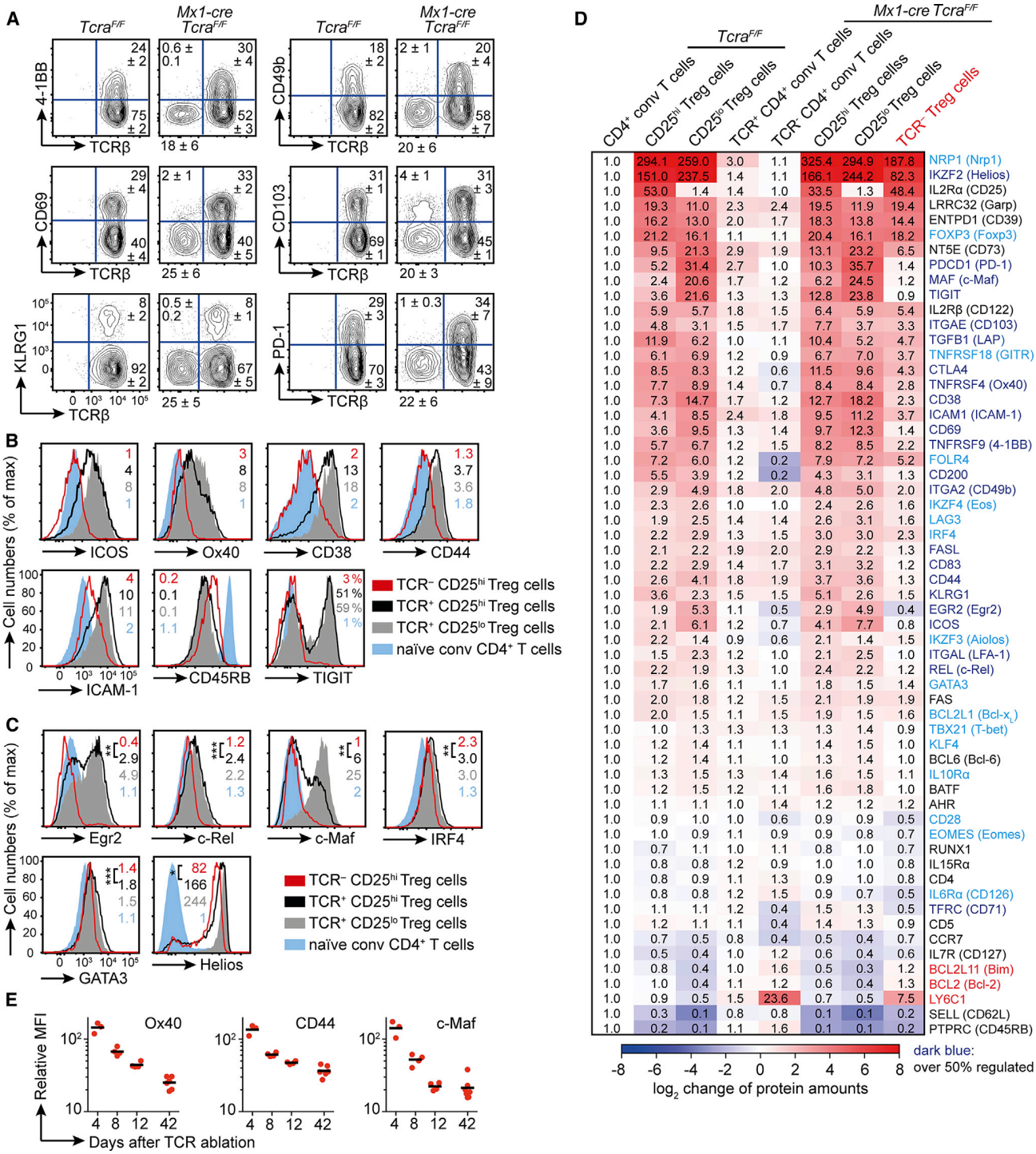

Figure 2. TCR-Deficient Regulatory T Cells Lose Their Activated Phenotype

(A) Extracellular expression of the depicted markers on splenic Foxp3-I-eGFP^{+} CD25^{hi} Treg cells, 6 weeks after poly(I:C) injection. Numbers in representative plots indicate mean percentage ± SD of 6–13 mice per genotype from ≥ 2 independent experiments.

(B and C) Extracellular (B) or intracellular (C) expression of the depicted markers of the indicated splenic T cell subsets (Treg = Foxp3^{+}), all from *Mx1-cre Tcra*$^{F/F}$ mice 6 weeks after poly(I:C) injection. Numbers in representative histograms indicate means of the MFIs, normalized to Foxp3^{-} CD4^{+} CD44^{lo} naive T cells of *Tcra*$^{F/F}$ mice. For TIGIT, percentage of positive cells are shown. Means were calculated from ≥ 5 mice per genotype from ≥ 2 independent experiments. ***p < 0.001; **p < 0.01; *p < 0.05; one-way ANOVA.

(D) Flow cytometric protein level analysis of extra- and intracellular markers of splenic T cell subsets (Treg = Foxp3^{+}) 6 weeks after poly(I:C) injection. MFIs of ≥ 3 mice per analyzed protein were normalized to the expression on or in conventional CD4^{+} T cells to account for interexperimental variations. Data are shown as

(legend continued on next page)

containing Treg cell-specific DNA demethylated regions (Morikawa et al., 2014) (Figure S1H).

These results demonstrate that maintenance of the Treg cell-specific methylation pattern is completely independent of continuous TCR signals. Hypomethylation therefore uncouples the expression of key Treg cell genes from obligate TCR signals to a large extent.

TCR Signals Continuously Activate Peripheral Treg Cells

The peripheral Treg cell pool contains naive and effector or tissue-homing subsets (Campbell and Koch, 2011; Fisson et al., 2003). Naive Treg cells are quiescent and express CD62L and the chemokine receptor CCR7, enabling them to enter secondary lymphoid organs (Campbell and Koch, 2011). In contrast, effector Treg cells are cycling and show increased expression of CD5, CD38, CD44, Ox40, GITR, CD69, and ICAM-1 (Campbell and Koch, 2011; Feuerer et al., 2009; Fisson et al., 2003; Fontenot et al., 2005; Huehn et al., 2004; Stephens et al., 2007). A direct comparison of the $CD25^{hi}$ to the $CD25^{lo}$ Treg cell subsets reveals that the $CD25^{lo}$ subset is enriched for proliferating cells expressing effector markers (Fontenot et al., 2005). It was proposed that the effector Treg cell subset is comprised of short-lived cells that were recently activated by (self-)antigens (Campbell and Koch, 2011; Fisson et al., 2003).

TCR ablation did not reduce the proportions of Treg cells expressing CCR7 and CD62L, suggesting that TCR-deficient Treg cells can recirculate efficiently between secondary lymphoid organs (Figure S2A). In contrast, we observed that activation and/or effector markers such as 4-1BB, CD49b, CD69, PD-1, and KLRG1 were virtually absent on TCR-deficient Treg cells (Figure 2A).

To further elucidate the impact of TCR signals for Treg cell identity, we monitored the protein amounts of well-described Treg cell markers after TCR ablation. Our analysis revealed that surface amounts of the costimulatory molecules ICOS, CD28, and Ox40, as well as of CD38, CD44, CD5, ICAM-1, and TIGIT, were significantly decreased, whereas CD45RB was upregulated (Figures 2B and S2B). Fittingly, relative quantification of intracellular transcription factor protein amounts showed that Egr2, c-Rel, and c-Maf, which have been linked to TCR activation, were dramatically downregulated (Figures 2C and 2D). The expression of several other important transcription factors connected to Treg cell function (Fu et al., 2012; Rudra et al., 2012) such as IRF4, Helios, GATA3, KLF4, T-bet, and Aiolos, but not Runx1 and Bcl-6, was significantly reduced in the TCR-deficient cells, although not to the amounts found in naive $CD4^+$ T cells (Figures 2C, 2D, and S2C). A comprehensive overview of surface-marker proteins and transcription factors analyzed by flow cytometry is shown in Figure 2D.

We then assessed the dynamic changes in protein levels of selected markers 4, 8, and 12 days after TCR ablation. At day 4 TCR downregulation was similar in all tested Treg cell subsets, including $CD25^{lo}$, $CD69^{hi}$, and $CD103^+$ (Figure S2D), confirming equal TCR ablation efficiencies between different Treg cell subsets. The TCR-deficient effector Treg cell subsets slowly shrank in size, with the exception of the $CD103^+$ subset (Figures S2E and S2F). Over time, TCR-deficient Treg cells gradually lost TCR-dependent surface marker and transcription factor expression (Figures 2E and S2G–S2I). This occurred on $CD25^{hi}$ and as long as they persisted also on $CD25^{lo}$ subsets (Figure S2H) and on individual effector subset defined by high-marker protein expression (Figure S2I). We did not detect increased proportions of dead or dying Treg cells at any time point after TCR ablation by propidium iodide and Annexin V staining (Figure S2J). Therefore, individual Treg cell effector subsets are slowly disappearing in response to TCR ablation, and this goes hand-in-hand with loss of typical gene expression.

We conclude that de novo differentiation and maintenance of effector Treg cell subset phenotypes cannot occur in absence of TCR signals. Furthermore, our analysis of effector-type and "naive" $CD25^{hi}$ TCR-deficient Treg cells showed a substantial loss of lineage-defining protein expression. However, although in absence of TCR signals the protein amounts of some activation markers and transcription factors were reduced to amounts found on naive conventional $CD4^+$ T cells, the majority of proteins were present at amounts in between conventional $CD4^+$ T and Treg cells.

TCR-Dependent Gene Expression in Treg Cells Is Dominated by TCR-Induced Transcription Factors and IRF4

To examine the consequences of the loss of TCR signals globally, we analyzed gene-expression changes through Affymetrix microarrays. In total, loss of the TCR affected the expression of 327 genes at least 2-fold and of 65 genes at least 3-fold in $CD25^{hi}$ Treg cells. The majority of these genes were downregulated (71% of the 2-fold regulated genes and 68% of the 3-fold regulated genes); this included genes encoding for cell surface molecules such as 4-1BB (encoded by *Tnfrsf9*), CD38, ICOS, and PD-1 (encoded by *Pdcd1*) as already observed by flow cytometry (Figures 2A–2D and Table S1).

TCR ablation affected various gene subsets (defined in Table S2): Of Treg cell signature genes, 15 (4%) were significantly reduced to less than $^1/_3$ and 135 (30%) were reduced to less than $^2/_3$ of their expression in TCR^+ Treg cells, while only a minor fraction was upregulated (Figure 3A). This indicates that while a proportion of the characteristic Treg cell gene expression relies at least partially on TCR-derived signals, overall TCR-deficient Treg cells maintain their cellular identity.

In agreement with the persistent Foxp3 protein amounts in TCR-deficient Treg cells, Foxp3-regulated genes were not strongly affected. Nevertheless, over 30% of the Foxp3-activated genes in TCR-deficient Treg cells were reduced to less than $^2/_3$ of their expression in TCR^+ Treg cells (Figure 3B), defining a candidate set of Foxp3-activated genes that require TCR signals for full expression. Consistent with the dramatic loss of Egr2 expression upon TCR ablation, we detected a significant reduction in Egr2-dependent gene expression (Figure 3C).

heatmap (Perseus software). Blue letters, significantly ($p < 0.05$) reduced on or in TCR^- Treg cells in comparison to TCR^+ $CD25^{hi}$ Treg cells from both $Tcra^{F/F}$ control, as well as *Mx1-cre* $Tcra^{F/F}$ mice. Red letters, significantly increased ($p < 0.05$); analyzed by one-way ANOVA.

(E) Decay of the indicated proteins after TCR ablation. Shown are MFIs of TCR-deficient relative to MFI of TCR^+ $Foxp3^+$ Treg cells. Depicted are values for individual mice and means. See also Figure S2.

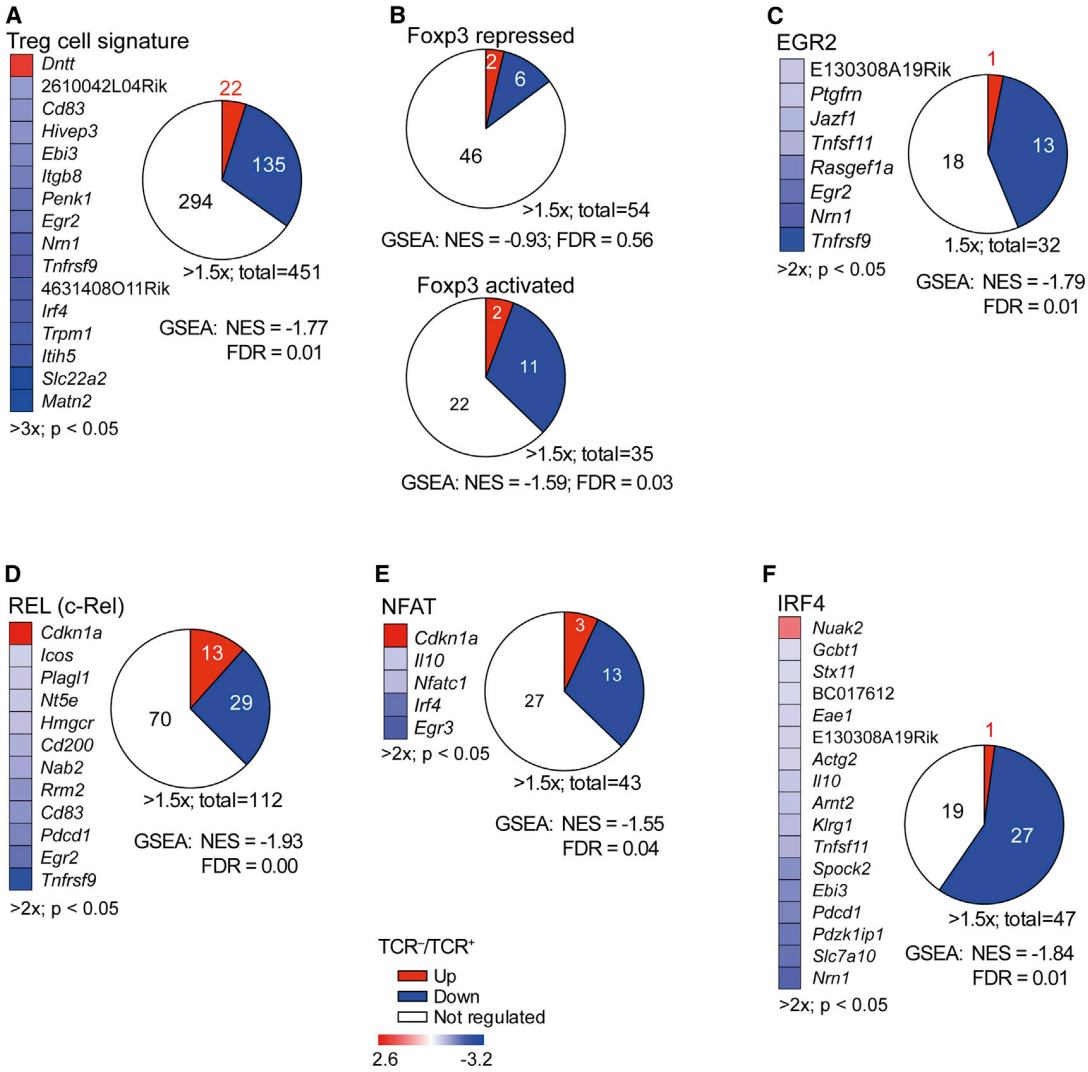

Figure 3. Treg Cell mRNA Expression Is Severely Changed upon TCR Ablation

(A–F) The mRNA expression of splenic Foxp3-I-eGFP^{+} TCR^{+} CD25^{hi} Treg cells from 4 *Tcra*$^{F/F}$ control samples (WT) and Foxp3-I-eGFP^{+} TCR^{-} CD25^{hi} Treg cells from 5 *Mx1-cre Tcra*$^{F/F}$ samples (KO), 6 weeks after poly(I:C) injection, was compared by Affymetrix microarray. Each sample contained pooled Treg cells from 3-5 mice. Normalized enrichment scores (NES) were calculated at the indicated false discovery rate (FDR) at the GSEA server of the Broad Institute. Changes in the expression of (A) Treg cell signature genes and (B) direct Foxp3 target genes that are either repressed (top; less than ½ of expression in TCR^{+} Treg cells: *Tbc1d4*) or activated (bottom; less than ½ of expression in TCR^{+} Treg cells: *Icos*) upon Foxp3 promoter occupancy. Changes in putative target gene expression of (C) Egr2, (D) REL (c-Rel), (E) NFAT transcription factors, and (F) IRF4 are shown. Pie charts show the number of detected genes within the respective category (white, not regulated; red, ≥ 1.5-fold upregulated; blue, $^{2}/_{3}$ of the expression in TCR^{+} Treg cells) in KO relative to WT Treg cells. Heatmaps depict knockout (KO) to WT fold-change values (Log2-transformed; A, ≥ 3-fold; B–F, ≥ 2-fold) of significantly regulated genes ($p < 0.05$; t test). See also Figure S3 and Tables S1 and S2.

A set of general NF-κB target genes was equally up- and downregulated (Figure S3A). However, genes whose expression was reduced in c-Rel-deficient activated T cells were mostly downregulated upon TCR ablation (Figure 3D), underscoring the unique role of c-Rel among the NF-κB transcription factors in Treg cells. GATA3- or Runx1-controlled gene expression remained stable in TCR-deficient Treg cells, as none of them were significantly regulated more than 2-fold (data not shown). An analysis of putative NFAT target genes revealed that 30% depend to some extent on TCR signals in Treg cells (Figure 3E). Among the significantly downregulated NFAT and c-Rel target genes were Egr2, Egr3, and IRF4 (Figures 3D, 3E, and S3B), suggesting a TCR-dependent transcription-factor network. Although IRF4 protein amounts were only reduced by around 20%, TCR ablation had the largest effect on IRF4-controlled gene expression: 57% of the 47 IRF4 target genes were downregulated to less than 2/3 of their expression in TCR^{+} Treg cells, 16 (34%) of which statistically significantly to less than ½ (Figure 3F). Gene-set enrichment analysis (GSEA) confirmed significant (FDR ≤ 0.05) loss of Treg signature genes and Foxp3 activated, Egr2, c-Rel, NFAT, and IRF4 target genes in TCR-deficient Treg cells (Figure 3 and Table S2). Unbiased analysis of the gene-expression data

from TCR-deficient and control Treg cells against publicly available gene sets suggested loss of Egr3 and Egr2 target genes, loss of Foxp3 amplified genes, and a shift toward gene expression of conventional T cells (Figure S3C).

The overwhelming majority of differentially expressed mRNAs were downregulated in TCR-deficient Treg cells, indicating that a large part of the Treg cell-specific gene-expression pattern depends on autoreactive TCR signals. This TCR-dependent gene expression appears to depend on Egr2, Egr3, c-Rel, and most prominently, IRF4. However, TCR-deficient Treg cells globally maintain their transcriptional identity.

The Peripheral Homeostasis of Treg Cells Requires TCR Signals

Having established that TCR signals are indispensable for the differentiation and maintenance of effector Treg cells and critical for the expression of many Treg lineage-defining genes, we wanted to assess the role of TCR signals for "naive" $CD25^{hi}$ Treg cell maintenance. Upon poly(I:C) treatment, T cell development is blocked in *Mx1-cre* $Tcra^{F/F}$ mice, due to complete TCRα inactivation in lymphoid progenitors (Figure 4A). Therefore, we employed these mice to study the homeostasis of peripheral Treg cells in the absence of cellular efflux from the thymus. The population of TCR^{-} Treg cells decayed (Figure 4B), similar to TCR-deficient naive $CD4^{+}$ cells, but in stark contrast to $CD4^{+}$ $CD44^{hi}$ memory and effector T cells and $CD4^{+}$ natural killer T (NKT) cells, which rely on cytokines but not on TCR stimulation (Polic et al., 2001; Vahl et al., 2013). The total number of peripheral Treg cells was not changed significantly 6 weeks and 15 weeks after induced TCR ablation, unlike the number of naive $CD4^{+}$ and $CD8^{+}$ T cells (Figures 4B and S4A). Thus, the peripheral Treg cell pool size is kept stable in the absence of thymic output.

The decrease of peripheral TCR-deficient Treg cells (Figure 4B) could be a consequence of impaired survival and/or proliferation. The proliferation marker Ki-67 was not expressed by TCR-deficient Treg cells (Figure 4C). In order to directly monitor the proliferation of Treg cells in the absence of TCR signals, mice containing TCR-deficient and -proficient Treg cells received BrdU-containing water for 4 weeks. Over 80% of $CD25^{lo}$ Treg cells, as well as 40%–50% of TCR^{+} $CD25^{hi}$ Treg cells incorporated BrdU during this time (Figure 4D). The BrdU-incorporation of TCR-deficient Treg cells was negligible, demonstrating that homeostatic Treg cell proliferation absolutely requires tonic TCR signals (Figure 4D).

Direct ex vivo analyses suggested that loss of the TCR has no major impact on the survival of Treg cells (Figure S2J). However, a significantly higher percentage of TCR-deficient Treg cells contained activated caspases (Figure 4E) after 1 hr in cell culture, indicating that in vitro, TCR-deficient Treg cells have an increased tendency to undergo apoptosis.

Cytokines, most importantly IL-2 and IL-7, influence the homeostasis of Treg cells (Setoguchi et al., 2005). While all TCR-deficient Treg cells expressed high amounts of CD25 (Figure 1C), expression of CD122 (IL-2R and IL-15R β chain), CD127 (IL-7Rα chain), and the IL-15Rα chain were not significantly altered upon TCR ablation (Figures 2D and S4B). Importantly, TCR-deficient Treg cells were competent in cytokine signaling as evidenced by robust phosphorylation of STAT5 and STAT3 transcription factors in response to IL-2 and IL-6 stimulation (Figure 4F). In addition, the homeostatic defects of TCR-deficient Treg cells appeared unrelated to endoplasmic reticulum (ER) stress caused by an unpaired TCRβ chain because we did not detect major alterations in the expression of genes implicated in the endoplasmic reticulum associated degradation (ERAD) and in the unfolded protein response pathways (Table S2).

Together, these results demonstrate that the absence of TCR signals effectively abrogates Treg cell homeostasis, due to essentially abolished proliferation.

Elevated mTOR Signaling in Treg Cells Is TCR Mediated

Signals derived from antigen recognition, costimulation, cytokines, growth hormones, and nutrients converge on the mechanistic target of rapamycin (mTOR) pathway. Signaling through its two multiprotein complexes, mTORC1 and mTORC2, and the upstream kinase AKT regulates cellular growth, protein translation, and survival in many cell types, including T cells (Chi, 2012). Importantly, Treg cells contain and depend on enhanced mTORC1 signaling for their homeostasis and function (Zeng et al., 2013).

We detected lower phosphorylation of mTOR and its targets ribosomal protein S6, kinase p70 S6, the translational inhibitor 4E-BP1, and reduced expression of the mTORC1 target CD71 in TCR^{-} Treg cells (Figures 5A, 5B, and S5A–S5C). We also detected a trend toward downregulation of mTORC1 target genes controlling the cholesterol biosynthesis pathway (Figures 5C and S5D), which has a central role in Treg cells (Zeng et al., 2013). In contrast, we did not observe differences in mTORC1-controlled mitochondrial parameters including their reactive oxygen production, membrane potential, and mass (Figure S5E) (Zeng et al., 2013).

mTORC2 plays an important role in the inhibition of apoptosis by directly phosphorylating the kinase AKT at serine 473, enabling it to phosphorylate and thereby inhibit constitutively active FoxO transcription factors. TCR-deficient Treg cells contained strongly reduced AKT-S473 phosphorylation (Figure 5D) and correspondingly reduced FoxO1 phosphorylation at the AKT target site serine 256, but not protein amounts (Figures 5E and S5F). The proapoptotic BH3-only protein Bim, a FoxO target in T cells (Hedrick et al., 2012), was significantly increased upon TCR ablation (Figures 2B and 5F). Moreover, we observed decreased amounts of the antiapoptotic protein Bcl-xL in TCR-deficient Treg cells. On the other hand, the amounts of the antiapoptotic protein Bcl-2 were significantly elevated, possibly due to mutual posttranslational control with Bim (Jorgensen et al., 2007) (Figures 2B and 5F). Finally, inhibitory phosphorylation of the proapoptotic Bcl-2 family member Bad, an AKT target (del Peso et al., 1997), was reduced (Figure 5F). However, globally we did not observe enhanced FoxO1-dependent gene expression in TCR^{-} Treg cells (Figure S5G). Therefore, it is also possible that the observed Bim/Bcl-2 balance is caused by absent repression of Bcl-2 through complexes containing c-Maf and c-Myb (Peng et al., 2007), as both are strongly reduced after TCR ablation (Figures 2C and S3A).

Our results provide correlative evidence that in the absence of continuous TCR stimulation, signaling through the mTORC1 and mTORC2 pathways is attenuated in Treg cells. Although we detected only minor effects in downstream gene expression,

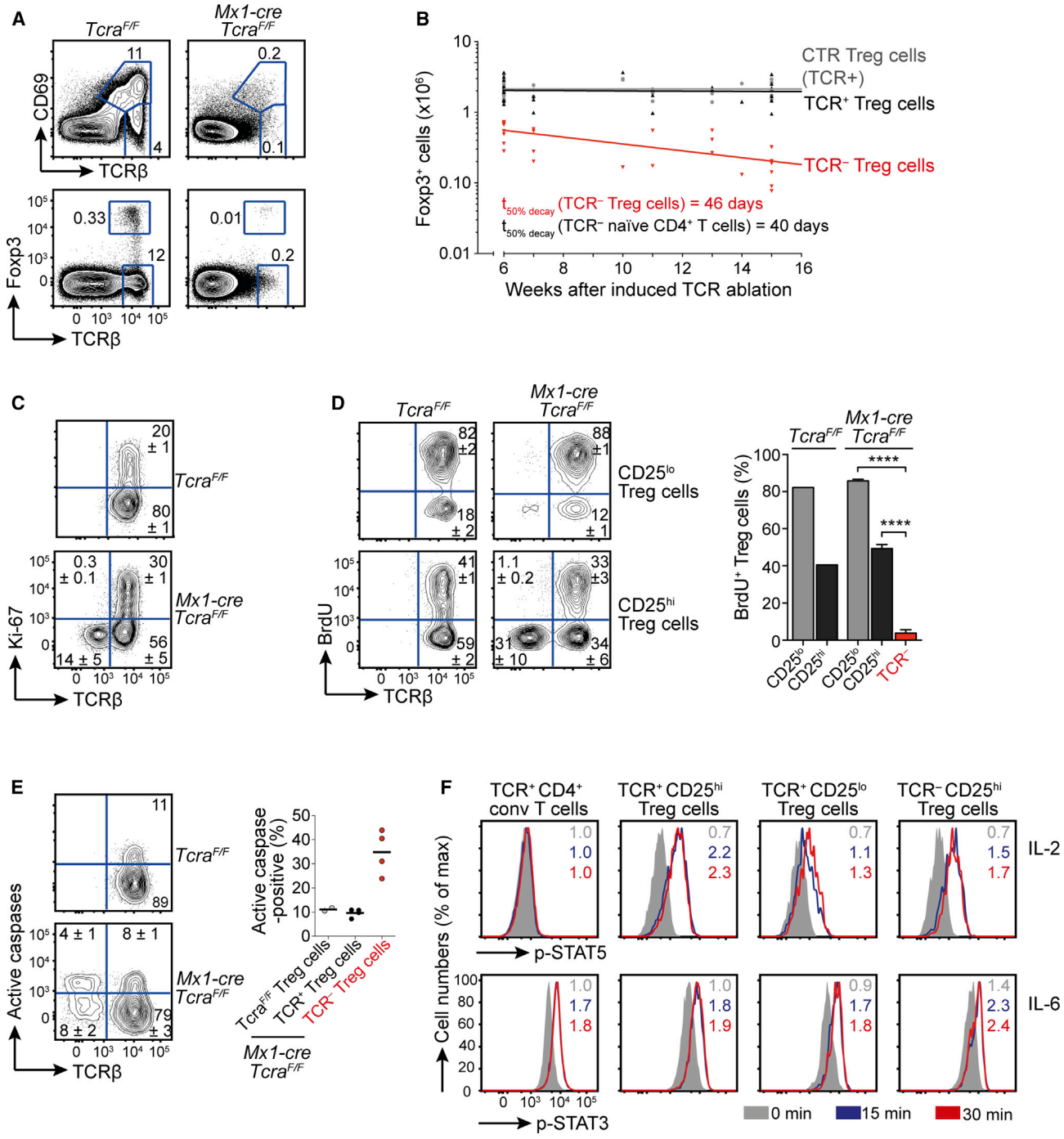

Figure 4. Regulatory T Cell Homeostasis Is Impaired upon TCR Ablation

(A) Expression of CD69 and Foxp3 plotted against TCRβ on total thymocytes, 6 weeks after poly(I:C) injection. Plots are representative of five independent experiments.

(B) Number of splenic Foxp3$^+$ Treg cells from in total 24 control (CTR) *Tcra*$^{F/F}$ mice, as well as number of TCR$^+$ and TCR$^-$ Treg cells from in total 23 *Mx1-cre Tcra*$^{F/F}$ mice from 14 independent experiments, at the indicated time after poly(I:C) injection. $t_{50\%\ decay}$ = time it takes until the population decayed to half of its size.

(C) Intracellular expression of Ki-67 in splenic Foxp3$^+$ Treg cells, 6 weeks after poly(I:C) injection. Numbers in representative plots indicate mean percentage ± SD of 4 mice per genotype and are representative for 3 independent experiments.

(D) BrdU was administered for 4 weeks via the drinking water, starting 2 weeks after poly(I:C) injection. Directly afterward, BrdU incorporation in CD25^{lo} and CD25^{hi} Foxp3$^+$ Treg cells was measured by flow cytometry. Numbers in representative plots indicate mean percentage ± SD of 2–4 mice per genotype. Bar chart depicts means + SD of one experiment with 2 *Tcra*$^{F/F}$, as well as 4 *Mx1-cre Tcra*$^{F/F}$ mice. ****p < 0.00001; one-way ANOVA.

(legend continued on next page)

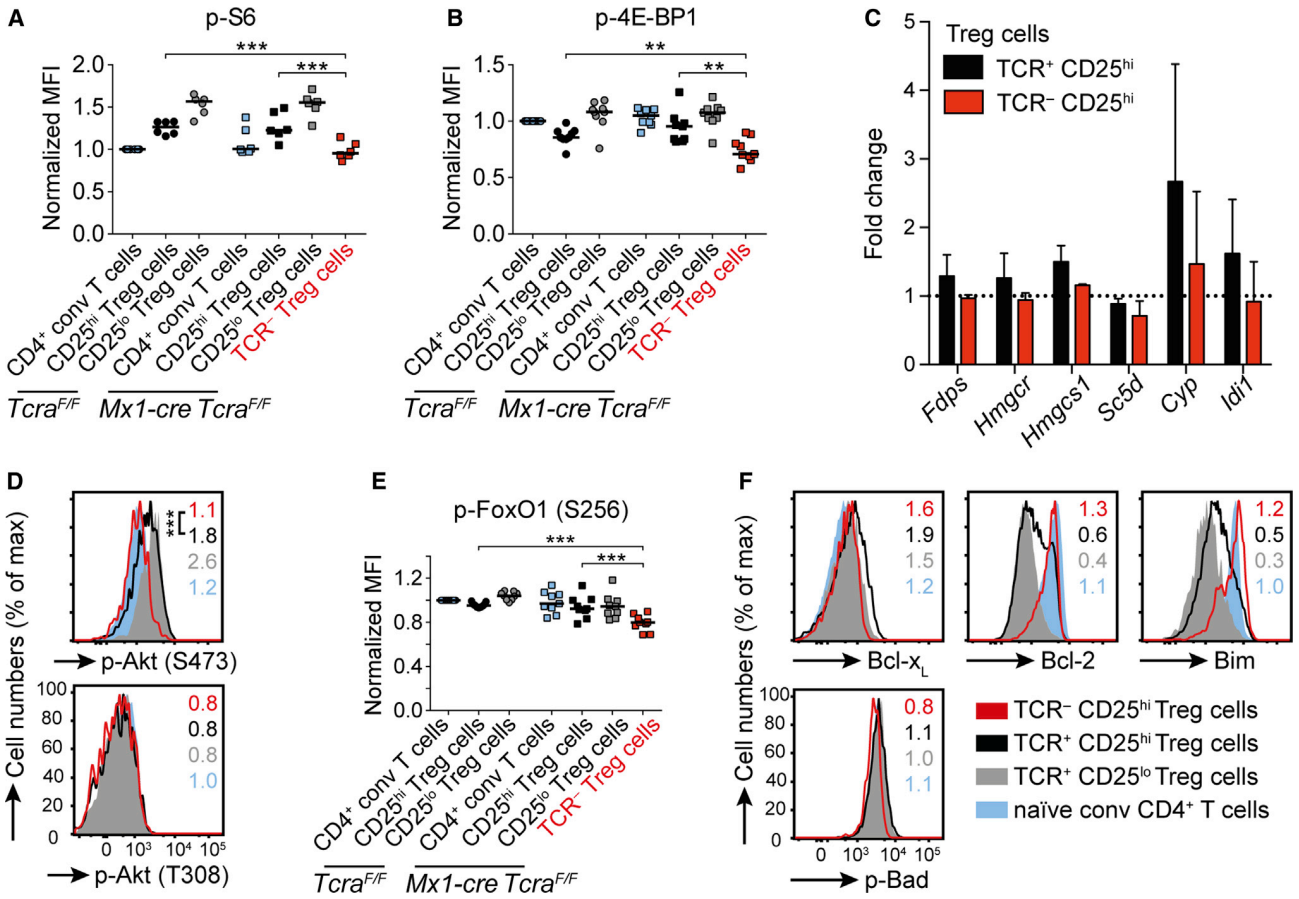

Figure 5. mTOR Signaling Pathways Are Attenuated in TCR-Deficient Treg Cells

(A, B, D, E, and F) Comparison of phosphorylation or expression of the respective proteins in the indicated splenic T cell subsets (Treg = Foxp3$^+$) 6 weeks after poly(I:C) injection. Numbers in representative histograms indicate means of the MFIs, normalized to Foxp3$^-$ CD4$^+$ CD44^{lo} T cells of *Tcra*$^{F/F}$ mice. Means were calculated from ≥ 5 mice per genotype from ≥ 2 independent experiments. Bars indicate medians. ***p < 0.001; **p < 0.01; one-way ANOVA.

(C) Differences in mRNA expression amounts of the indicated enzymes of the cholesterol biosynthesis pathway normalized to Ywhaz relative to Foxp3$^-$ CD4$^+$ conventional T cells (dotted line). Bars indicate means + SD from 3 samples (one mouse per sample for Foxp3$^-$ CD4$^+$ T cells and TCR$^+$ CD25^{hi} Foxp3$^+$ Treg cells and 3 mice pooled per sample for TCR$^-$ CD25^{hi} Foxp3$^+$ Treg cells). See also Figure S5.

these pathways still might be important to keep target genes in a poised state for rapid expression upon strong Treg cell stimulation.

TCR-Deficient Treg Cells Lose Most of Their Suppressive Protein Arsenal and Their Ability to Suppress T Cell Responses In Vivo

Various mechanisms are implicated in the suppressive ability of Treg cells (Josefowicz et al., 2012; Sakaguchi et al., 2008; Shevach, 2009). Among them are the consumption of the cytokine IL-2, the release of suppressive cytokines (IL-10, IL-35 [composed of p35 and Ebi3] and TGF-β) or toxic molecules (perforin, granzymes), and the modulation of the costimulatory abilities of antigen-presenting cells.

Gene-expression analysis of 10 1.5-fold or more regulated putative suppressor genes revealed that 8 were downregulated and 2 (Perforin and CD274) were upregulated in TCR-deficient Treg cells (Figures 6A and S6A). Verification of these and analysis of further candidates by flow cytometry and/or real-time PCR (Figures 6B and 6C) revealed that of the 20 putative suppressor genes tested, 59% (13) were significantly downregulated upon TCR ablation (Figures 6D and S6A): *Nt5e* (CD73), *Ctla4*, *Ebi3*, *Fgl2*, *Tnfrsf18* (GITR), *Il10*, *Il10r*, *Lag3*, *Tgfb1* (latency associated peptide, LAP), *Itgal* (LFA-1), *Nrp1*, *Pdcd1lg2* (PD-L2), and *Tigit*.

(E) Splenic Foxp3$^+$ Treg cells were stained in vitro for 1 hr for the presence of active caspases. Numbers indicate mean percentage ± SD of 2 *Tcra*$^{F/F}$ or 4 *Mx1-cre Tcra*$^{F/F}$ mice. Scatterplot shows the percentage of active caspase$^+$ Foxp3$^+$ Treg cells from 2 control *Tcra*$^{F/F}$ or from 4 *Mx1-cre Tcra*$^{F/F}$ mice. Bars indicate means.

(F) Comparison of STAT5 and STAT3 phosphorylation upon stimulation with IL-2 or IL-6 of the indicated T cell subsets from *Mx1-cre Tcra*$^{F/F}$ mice. Numbers in representative histograms indicate means of the MFIs, normalized to unstimulated Foxp3$^-$ CD4$^+$ CD25^{lo} TCR$^+$ T cells. Means were calculated from 6 mice from 2 independent experiments (p-STAT5) or from 3 mice (p-STAT3). See also Figure S4.

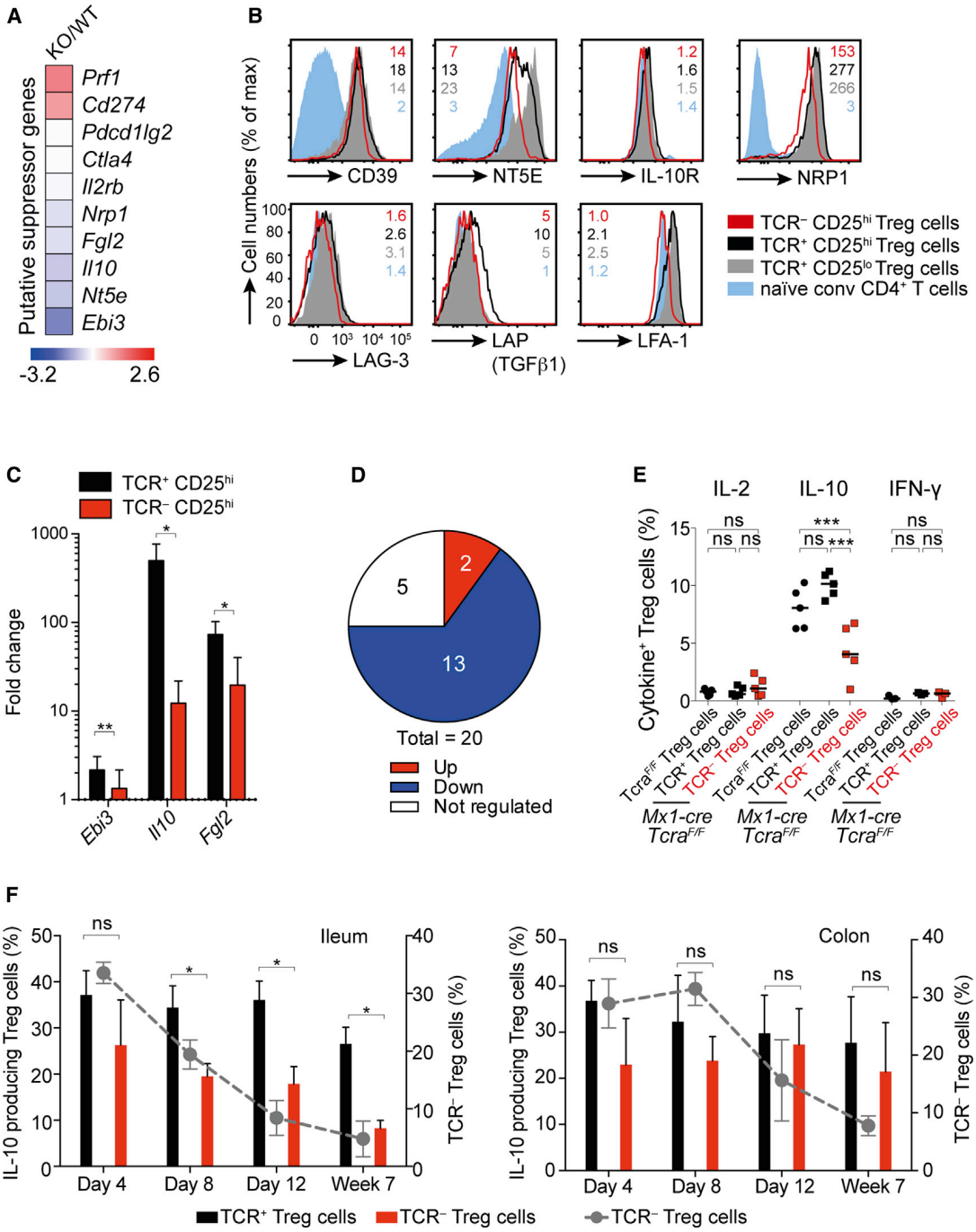

Figure 6. Regulatory T Cells Show Reduced Expression of Several Important Suppressive Molecules

(A) Heatmap showing mRNA expression of the indicated 1.5-fold regulated suppressive markers of TCR$^+$ versus TCR$^-$ Foxp3$^+$ Treg cells, 6 weeks after poly(I:C) injection, analyzed by Affymetrix microarray.

(B) Extracellular expression of the depicted markers of the indicated splenic T cell subsets (Treg = Foxp3$^+$), all from *Mx1-cre Tcra*$^{F/F}$ mice, 6 weeks after poly(I:C) injection. Numbers in representative histograms indicate means of the median fluorescence intensities (MFIs), normalized to Foxp3$^-$ CD4$^+$ CD44^{lo} naive T cells of *Tcra*$^{F/F}$ mice. Means were calculated from ≥ 5 mice per genotype from ≥ 2 independent experiments.

(C) Differences in mRNA expression amounts of the indicated suppressive markers normalized to Ywhaz relative to Foxp3$^-$ CD4$^+$ T cells (dotted line). Bars indicate means + SD from 3 samples (one mouse per replicate for Foxp3$^-$ CD4$^+$ T cells and CD25^{hi} Foxp3$^+$ TCR Treg cells and 3 mice pooled per replicate for TCR$^-$ CD25^{hi} Foxp3$^+$ Treg cells). **p < 0.01; *p < 0.05; t test.

(D) Regulation of 20 putative suppressive molecules in KO relative to WT Treg cells on the mRNA and/or protein amount (white, not regulated; red, upregulated, blue, downregulated).

(legend continued on next page)

In line with reduced *Il10* mRNA expression, a significantly smaller percentage of TCR$^-$ Treg cells produced IL-10 after PMA and Ionomycin activation in vitro in comparison to their TCR$^+$ counterparts (Figures 6E and S6B). Importantly, TCR-deficient Treg cells kept their anergic phenotype in respect to IL-2 (and interferon-γ [IFN-γ]) production upon activation (Figures 6E and S6B). After TCR ablation the proportion of TCR$^-$ Treg cells in the gut lamina propria decreased progressively (Figure 6F). In the ileum, a significantly smaller proportion of TCR$^-$ Treg cells produced IL-10 from day 8 onward. Conversely, in the colon, TCR$^-$ Treg cells largely maintained their ability to secrete IL-10 (Figures 6F and S6C). This indicates that the cytokine and/or costimulation milieu in the colon can at least partially substitute antigenic signals with regards to IL-10 production, but not to cellular homeostasis. We therefore conclude that, overall, the expression of suppressive genes by Treg cells largely depends on constant TCR signals, even though specific niches might maintain suppressive functions in absence of antigenic triggers.

To test the consequences of Treg cell TCR ablation in an in vivo setting, we employed CD4-CreER^{T2} animals (Sledzińska et al., 2013) because of the higher recombination efficiencies in mature T cells compared to *Mx1-cre* mice. Application of 3 or 5 mg tamoxifen for 5 consecutive days leads to loss of the TCR on around 70% of peripheral Treg cells (Figure S7A). We reconstituted T cell-deficient mice with naive T cells together with Treg cells isolated from either *Tcra*$^{F/F}$ control or CD4-CreER^{T2} *Tcra*$^{F/F}$ animals (Figure S7B). In the context of T cell deficiency, these cells rigorously expand. Three weeks after adoptive transfer, TCR ablation was induced through tamoxifen treatment (Figure 7A). Three days after cessation of tamoxifen feeding, we confirmed TCR ablation in 67% and 55% of CD4-CreER^{T2} *Tcra*$^{F/F}$ Treg cells present in the spleen and mesenteric lymph nodes, respectively (Figure S7C). The tamoxifen treatment induced a transient weight loss in all cohorts. However, while the control animals quickly recovered after cessation of tamoxifen feeding, we observed significantly reduced weight gain in animals in which we ablated the TCR on Treg cells (Figure 7B). Two of nine experimental animals developed diarrhea and signs of colitis with severe cellular infiltrations and associated inflammation (Figure S7D; data not shown). Furthermore, we noticed increased spleen and mesenteric lymph node weights, indicating ongoing inflammation, 24 days after TCR ablation on Treg cells (Figure 7C). This was partially due to infiltration of eosinophils, monocytes, and/or macrophages, as well as neutrophils in both organs (Figures 7D and S7E). At this time point, total Treg cell counts, of which 20% were TCR-deficient, were slightly increased in Treg cell TCR ablated animals, indicating a strong compensatory proliferation of TCR$^+$ Treg cells. The number of pTreg cells was not increased (Figure S7F). However, the initial yet transient presence of over 50% of TCR-deficient Treg cells was sufficient to disrupt normal immune homeostasis. Importantly, we also observed strongly increased numbers of CD4$^+$ T cells (Figure 7E), which showed an activated phenotype as indicated by increased CD69 expression (Figure 7F). Among the significantly expanded CD4$^+$ T cell subsets were T helper 17 (Th17) cells (Figure 7G) that are commonly connected to autoimmunity and inflammatory disease settings and are under strict control of regulatory T cells (Josefowicz et al., 2012). Reduced production of IL-10 also could contribute to disease development. In a similar experiment in *Rag2*$^{-/-}$ mice (Figures S7G–S7J), we did not observe differences in weight (data not shown), likely due to lower TCR ablation efficiencies (Figure S7H). However, TCR ablation exacerbated intestinal pathology (Figure S7I) and significantly increased numbers of splenocytes, including CD4$^+$ T cells (Figure S7J).

In order to test conditional Treg cell TCR ablation in an autoimmune disease setting with an unmanipulated effector T cell compartment, we used an experimental autoimmune encephalomyelitis (EAE) model (Figure 7H). Here, we transiently erased the Foxp3$^+$ Treg cell compartment by diphtheria toxin injections in DEREG mice and replenished the peripheral Treg cell niche with in vitro expanded control Treg cells (*Tcra*$^{F/F}$) or Treg cells with a tamoxifen-ablatable TCR (CD4-CreER^{T2} *Tcra*$^{F/F}$) (Figure S7K). Upon immunization with MOG$_{35–55}$ in complete Freund's adjuvant (CFA), we found that mice that received Treg cells whose TCR was ablated in vivo 6 days after immunization developed more severe EAE and behaved like mice who did not receive Treg cells after depletion of endogenous Treg cells (Figure 7I). The expansion of endogenous Treg cells, which is typical of the DEREG model, most likely masks the effects of TCR ablation at later time points after EAE induction. We obtained similar results when a higher number of Treg cells were transferred (Figures 7J and S7L and S7M).

Altogether, these results strongly support the notion that in the absence of continuous TCR signaling, Treg cells lose their ability to control normal immune homeostasis and to suppress autoimmune reactions.

DISCUSSION

Treg cells can be broadly separated into two different subsets in vivo. Naive, slowly cycling Treg cells and the effector subset, which is composed of highly proliferative cells characterized by a generally more activated state, likely due to recent autoantigen recognition. In line with this hypothesis, six weeks after TCR ablation we failed to detect TCR-deficient Treg cells expressing any of the characteristic activated or effector T cell markers, even though initial TCR ablation in these subsets was as efficient as in naive Treg cells. Our data thus clearly demonstrate that effector Treg cells cannot be generated or maintained in absence of TCR signals.

We propose that TCR-independent hypomethylation and Foxp3 expression in conjunction with other unaffected transcription factors largely ensure continued identity of TCR$^-$ Treg cells. Nevertheless, a large proportion of the Treg cell-defining gene expression, including Foxp3-regulated genes, depended on

(E) Percentages of splenic Foxp3$^+$ Treg cells expressing IL-2, IL-10, or IFN-γ upon in vitro activation with PMA and Ionomycin for 5 hr. Cells were extracted from mice and activated 6 weeks after poly(I:C) injection. Bars indicate medians. ***$p < 0.001$; ns, not significant; one-way ANOVA.

(F) Percentages of TCR$^-$ Treg cells of total Treg cells isolated from the gut lamina propria of *Mx1-cre Tcra*$^{F/F}$ mice at the indicated time points after poly(I:C) injection (right y axis). After stimulation with PMA and Ionomycin IL-10 production was assessed in TCR$^-$ CD25^{hi} and TCR$^+$ CD25^{hi} Foxp3$^+$ Treg cells (left y axis). Bars indicate means ± SD that were calculated from ≥ 3 mice per time point. *$p < 0.05$; ns, not significant; t test. See also Figure S6.

Please cite this article in press as: Vahl et al., Continuous T Cell Receptor Signals Maintain a Functional Regulatory T Cell Pool, Immunity (2014), http://dx.doi.org/10.1016/j.immuni.2014.10.012

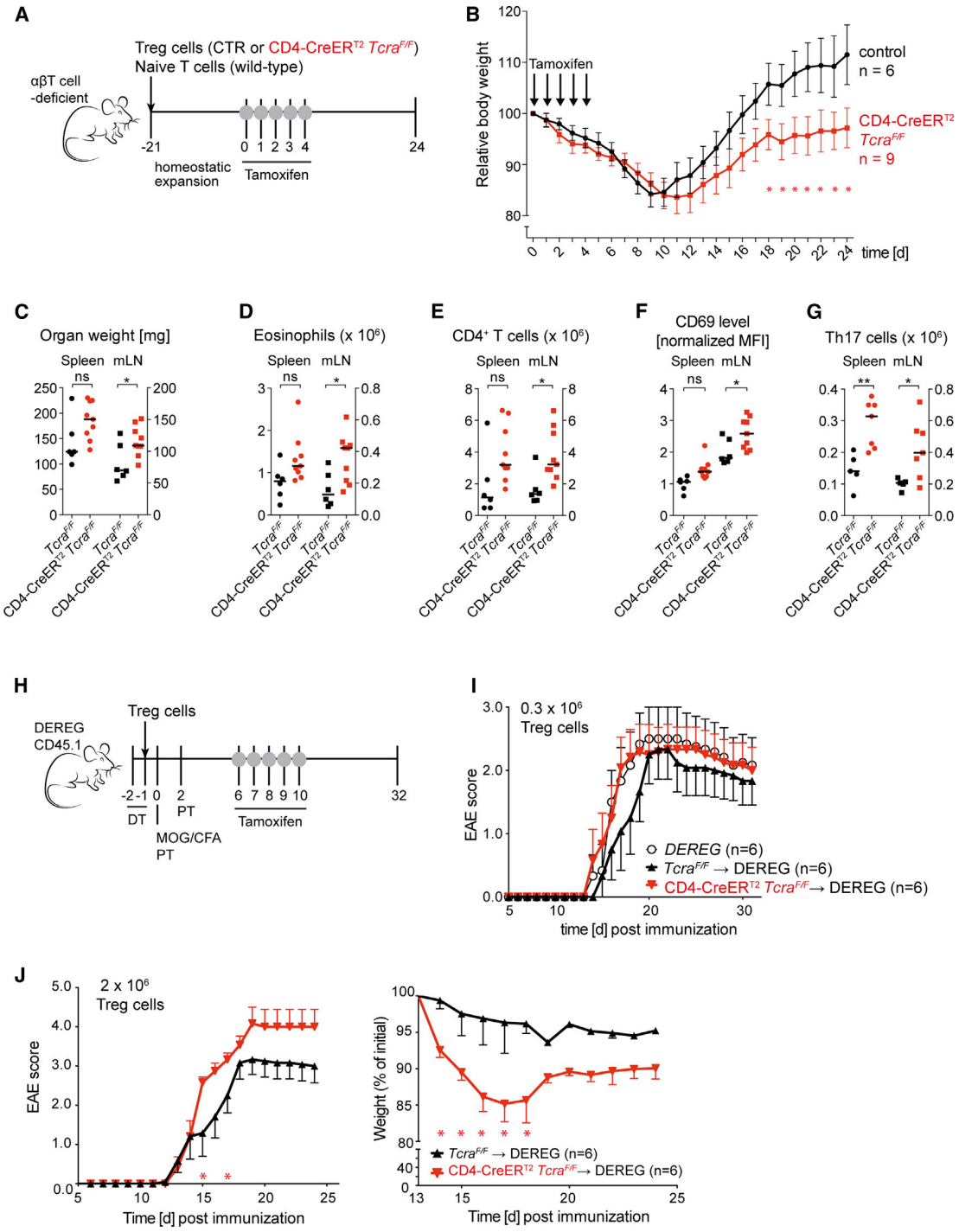

Figure 7. In Vivo TCR Ablation of Treg Cells Leads to Inflammation

(A–G) T cell-deficient *Tcra*$^{-/-}$ mice were reconstituted with Foxp3-I-eGFP$^-$ naive T cells together with CD4$^+$ CD25^{hi} Treg cells from either *Tcra*$^{F/F}$ control or from CD4-CreER^{T2} *Tcra*$^{F/F}$ mice. After 3 weeks of engraftment, TCR ablation was induced through tamoxifen feeding. Twenty-four days later, animals were sacrificed and analyzed.

(B) Body weight of the animals, normalized to the respective weight on the first day of tamoxifen treatment. Shown are means ± SEM; SEM are shown for visual clarity; *p < 0.05; t test.

(C) Weight of the indicated organs. Bars indicate medians. *p < 0.05; ns, not significant; one-way ANOVA.

(D, E, and G) Total cell numbers of (D) eosinophils (CD11c$^-$ CD11b$^+$ SiglecF$^+$ SSC-A^{hi}); (E) CD4$^+$ T cells (TCRβ$^+$ CD5$^+$); (G) Th17 T cells (Ror-γt$^+$ CD4$^+$ TCRβ$^+$ CD5$^+$). Bars indicate medians. **p < 0.01; *p < 0.05; ns, not significant; one-way ANOVA.

(legend continued on next page)

TCR signals to varying degrees. This might be explained by a differential dependence on strictly TCR controlled transcription factors such as Egr2, c-Maf, and c-Rel, and possibly also factors of the NFAT family. Surprisingly, target gene analysis pointed to IRF4 as a critical mediator of TCR-induced gene expression, although its protein amounts were only moderately affected by TCR loss. This indicated a critical role for TCR signals in controlling IRF4 activity in Treg cells, directly or through its transcriptional coregulators. We also found that loss of TCR signals correlated with a reduction of mTORC1 and mTORC2 activity in Treg cells to an amount comparable to naive $CD4^+$ T cells.

With respect to homeostatic maintenance, TCR^- Treg cells behaved identically to TCR^- naive $CD4^+$ T cells. In striking contrast to memory T and NKT cells (Polic et al., 2001; Vahl et al., 2013), TCR signals were indispensable for the proliferation of Treg cells under steady-state conditions in vivo. In the absence of thymic output, this nondividing pool of TCR-deficient Treg cells was reduced to half its size in 46 days, corresponding to a Treg cell loss of around 1.5% per day. Because directly ex vivo isolated TCR-deficient Treg cells were as viable as their TCR-proficient counterparts, this indicates that the decay of TCR-deficient Treg cells in vivo was not due to enhanced cell death but due to essentially abolished proliferation. The protein amounts of and balance between pro- (Bim) and anti-apoptotic (Bcl-2) proteins in TCR^- Treg cells resembled those found in naive $CD4^+$ T cells and were markedly different from TCR^+ Treg cells. Potential mechanisms for this phenomenon are attenuated AKT and mTORC2 signaling and/or other transcriptional regulation. Upon egress from the thymus, regulation of peripheral Treg cell homeostasis has been mainly attributed to cytokine signaling (Setoguchi et al., 2005). Conversely, we found that the homeostasis of TCR-deficient Treg cells was strongly impaired even though they expressed normal amounts of cytokine receptors for IL-2, IL-7, and IL-15 and signaled normally in response to IL-2 or IL-6 stimulation. Instead, our results suggest that constant TCR triggering constitutes an obligate prerequisite. It should be mentioned that in our experimental system, Cre-mediated TCR ablation in Treg cells is not complete, and therefore TCR-deficient Treg cells are competing with TCR-expressing cells. It is possible that the homeostatic defects of TCR-deficient Treg cells are confounded by this competition.

Loss of individual suppressive proteins in Treg cells does not match the dramatic phenotype of Foxp3-deficiency. Thus, depending on the type of immune response and the location in the body, several different suppression mechanisms are important. Still, it is not well understood how Treg cell TCR engagement is involved in suppression of target cells. At least in vitro, directly ex vivo isolated Treg cells are able to suppress without previous activation (Szymczak-Workman et al., 2009). It has been speculated that autoantigen recognition is key to maintain polyclonal Treg cells in an activated state, allowing them to control various different immune responses independently of TCR specificity (Shevach, 2009). Our data imply that TCR signals are absolutely required for the differentiation and maintenance of effector Treg subsets, which is critical for effective control of overshooting autoimmune or inflammatory responses in various disease contexts. Furthermore, in naive Treg cells, constant TCR triggers ensure high expression of most suppressive proteins. Treg cell TCR ablation in two in vivo models resulted in increased clinical effects, despite the fact that Treg cell TCR ablation remained incomplete at around 50%–70%. One possibility is that TCR^- Treg cells are unable to suppress but still occupy homeostatic niches and thereby impede the action of TCR^+ Treg cells.

In summary, our study demonstrates that Treg cells continuously receive biologically relevant signals through their autoreactive TCR and that these signals are essential for Treg cell homeostasis, signature gene expression, and especially for their suppressive functions. By ablating the TCR, we abolished MHCII recognition and (auto-)antigenic stimulation, and it is likely that both deficiencies contribute to varying degrees to the effects we observe. Future studies should aim at dissecting these individual contributions. In essence, our study solidifies the view of the Treg cell population as a constantly TCR-activated T cell subset whose activation is channeled into suppression through the actions of Foxp3.

EXPERIMENTAL PROCEDURES

Genetically Modified Mice

Mx1-cre (Kühn et al., 1995), $Tcra^F$ and $Tcra^-$ ($Tcra^{tm1Cgn}$; Polic et al., 2001), Foxp3-I-eGFP (Bettelli et al., 2006), CD4-$CreER^{T2}$ (Sledzińska et al., 2013), $Gt(ROSA)26Sor^{tm4(ACTB-tdTomato,-EGFP)Luo}/J$ (mT/mG; Muzumdar et al., 2007), and CD45.1-congenic DEREG (Lahl et al., 2007) mice were all kept on a C57BL/6 genetic background. Six- to eight-week-old *Mx1-cre* $Tcra^{F/F}$ or $Tcra^{F/F}$ mice were given a single dose (400 μg) of poly(I:C) (Amersham). All mice were analyzed 6 weeks later, unless otherwise indicated. Mice were housed in specific pathogen-free animal facilities of the MPIB and the Technische Universität München. All animal procedures were approved by the Regierung of Oberbayern.

Flow Cytometry

Single-cell suspensions were prepared and stained with the antibodies listed under Supplemental Experimental Procedures.

BrdU Incorporation

Mice were fed with 0.5 mg/mL BrdU (Sigma) in the drinking water for 4 consecutive weeks, and BrdU incorporation was measured with the BrdU Flow Kit (BD).

Cell Sorting and Gene-Expression Analysis

TCR^+ ($Foxp3^+$ $CD4^+$ $CD25^{hi}$ cells from $Tcra^{F/F}$ Foxp3-I-eGFP mice) and TCR^- ($Foxp3^+$ TCR^- $CD4^+$ $CD25^{hi}$ cells from *Mx1-cre* $Tcra^{F/F}$ Foxp3-I-eGFP mice) Treg cells were sorted 6 weeks after poly(I:C) injection with a FACSAria

(F) CD69 expression on $CD4^+$ T cells. Scatterplots show means of the MFIs, normalized to splenic $CD4^+$ T cells of control mice. *$p < 0.05$; ns, not significant; one-way ANOVA.

(H) Scheme of EAE experiment: DEREG mice were depleted of endogenous Treg cells by diphtheria toxin and then left unreconstituted (DEREG) or reconstituted with control ($Tcra^{F/F}$ → DEREG) or TCR ablatable $CD4^+$ $CD25^{hi}$ Treg cells (CD4-$CreER^{T2}$ $Tcra^{F/F}$ → DEREG) followed by induction of EAE.

(I and J) EAE experiment with 3×10^5 (I) or 2×10^6 (J) adoptively transferred $Tcra^{F/F}$ or CD4-$CreER^{T2}$ $Tcra^{F/F}$ $CD4^+$ $CD25^{hi}$ Treg cells or DEREG mice that were left unreconstituted. Mean clinical disease scores ± SEM of the indicated groups (n = 6) are shown on the left. SEM is shown for visual clarity. *$p < 0.05$; Mann-Whitney U test. Body weight, shown on the right, was normalized to the first measured weight of the respective animal; *$p < 0.05$; t test. See also Figure S7.

(BD). Cells from three to five mice were pooled for sorting one replicate, and four replicates for the controls as well as five replicates for the *Mx1-cre* $Tcra^{F/F}$ Foxp3-I-eGFP mice were generated. mRNA from 3–5 × 10^5 cells was purified with a RNeasy Micro kit (QIAGEN), amplified, labeled, and hybridized to Affymetrix M430 V2 microarrays (Geo: microarray data, GSE62532). Array normalization and expression value calculation was performed using DNA-Chip Analyzer (www.dchip.org). Heatmaps were generated with GenePattern Software. Gene set enrichment analysis (GSEA) was performed at http://www.broadinstitute.org/gsea/index.jsp. RNA from sorted cells was isolated (QIAGEN) and reverse transcribed (Promega) for qRT-PCR with Universal Probe Library probes and primers (Roche Diagnostics).

CpG Methylation Analysis by Bisulfite Sequencing

TCR^+ and TCR^- Treg cells were sorted 6 weeks and 15 weeks after poly(I:C) injection as for the gene expression analysis. Control tTreg and iTreg cells were generated, and the CpG methylation status was analyzed, as previously described (Ohkura et al., 2012).

In Vivo Suppression Assays

T cell-deficient $Tcra^{-/-}$ mice at the age of 6–8 weeks were reconstituted with 1 × 10^6 naive $CD4^+$ T cells (Foxp3-I-$eGFP^-$ $CD45RB^{hi}$ $CD25^-$) together with 0.25 × 10^6 Treg cells ($CD4^+$ $CD25^{hi}$ $CD45RB^{int}$ $CD38^{hi}$) from either CD4-$CreER^{T2}$ $Tcra^{F/F}$ or littermate control mice. Starting 3 weeks after cell transfer, mice were fed per os with 5 mg tamoxifen per day (Sigma) for 5 consecutive days, and their weight was monitored. Colon samples were fixed in 4% paraformaldehyde, embedded in paraffin, sectioned, and stained with hematoxylin and eosin. For the EAE model, endogenous DEREG CD45.1 Treg cells were depleted by injection of 500 ng diphtheria toxin (Calbiochem) on days −2 and −1 prior to immunization and substituted by 0.3 × 10^6 or 2 × 10^6 Treg cells obtained from either CD4-$CreER^{T2}$ $Tcra^{F/F}$ or littermate controls. EAE was induced by s.c. immunization with 200 μg of MOG35-55 (Auspep) in CFA containing 500 μg *M. tuberculosis* H37Ra (Difco) plus intravenous injection of 200 ng pertussis toxin (Sigma) on days 0 and 2 after immunization. Starting on day 5 postimmunization, mice were fed with tamoxifen (Hexal) in ClinOleic 20% (Baxter) for 5 consecutive days (0.15 mg/g ≈3 mg/mouse on day 5 and 0.10 mg/g ≈2 mg/mouse on the following days). Disease progress and severity were assessed as published (Korn et al., 2007).

Statistics

Statistical analysis of the results was performed by one-way ANOVA followed by Tukey's test, by Student's t test as indicated. p values are presented in figure legends where a statistically significant difference was found. EAE scores between groups were analyzed as disease burden per individual day with Mann-Whitney U test.

ACCESSION NUMBER

The GEO accession number for the microarray data reported in this paper is GSE62532.

SUPPLEMENTAL INFORMATION

Supplemental Information includes seven figures, two tables, and Supplemental Experimental Procedures and can be found with this article online at http://dx.doi.org/10.1016/j.immuni.2014.10.012.

AUTHOR CONTRIBUTIONS

J.C.V. and C.D. designed, performed, and analyzed most experiments and wrote the manuscript; K.H., S.H., J.C.F., J.N., N.O., D.R., T.B., B.P., L.K., T.K., A.S., and S.S. designed, performed, and analyzed experiments; H.M., S.S., M.Y.H., R.Z., A.S.-G., and K.K. analyzed experiments; M.S.-S. conceptualized the work, directed the study, analyzed data, and wrote the manuscript.

ACKNOWLEDGMENTS

This study was supported by the DFG through SFB 1054 TPA02 and an Emmy Noether grant to M.S.-S. J.C.V. and K.H. received PhD stipends from the Ernst Schering Foundation and the Boehringer Ingelheim Fonds, respectively. T.K. is supported by the DFG (Heisenberg, SFB 1054 TPB06, and SyNergy). We are grateful to R. Fässler for support. We thank J. Knogler, B. Habermehl, M. Schmickl, and A. Kawasaki for technical assistance.

Received: May 5, 2014
Accepted: October 22, 2014
Published: November 6, 2014

REFERENCES

Bensinger, S.J., Bandeira, A., Jordan, M.S., Caton, A.J., and Laufer, T.M. (2001). Major histocompatibility complex class II-positive cortical epithelium mediates the selection of CD4(+)25(+) immunoregulatory T cells. J. Exp. Med. *194*, 427–438.

Bettelli, E., Carrier, Y., Gao, W., Korn, T., Strom, T.B., Oukka, M., Weiner, H.L., and Kuchroo, V.K. (2006). Reciprocal developmental pathways for the generation of pathogenic effector TH17 and regulatory T cells. Nature *441*, 235–238.

Campbell, D.J., and Koch, M.A. (2011). Phenotypical and functional specialization of FOXP3+ regulatory T cells. Nat. Rev. Immunol. *11*, 119–130.

Chi, H. (2012). Regulation and function of mTOR signalling in T cell fate decisions. Nat. Rev. Immunol. *12*, 325–338.

Darrasse-Jèze, G., Deroubaix, S., Mouquet, H., Victora, G.D., Eisenreich, T., Yao, K.-H., Masilamani, R.F., Dustin, M.L., Rudensky, A., Liu, K., and Nussenzweig, M.C. (2009). Feedback control of regulatory T cell homeostasis by dendritic cells in vivo. J. Exp. Med. *206*, 1853–1862.

del Peso, L., González-García, M., Page, C., Herrera, R., and Nuñez, G. (1997). Interleukin-3-induced phosphorylation of BAD through the protein kinase Akt. Science *278*, 687–689.

Feuerer, M., Hill, J.A., Mathis, D., and Benoist, C. (2009). Foxp3+ regulatory T cells: differentiation, specification, subphenotypes. Nat. Immunol. *10*, 689–695.

Fisson, S., Darrasse-Jèze, G., Litvinova, E., Septier, F., Klatzmann, D., Liblau, R., and Salomon, B.L. (2003). Continuous activation of autoreactive CD4+ CD25+ regulatory T cells in the steady state. J. Exp. Med. *198*, 737–746.

Fontenot, J.D., Rasmussen, J.P., Williams, L.M., Dooley, J.L., Farr, A.G., and Rudensky, A.Y. (2005). Regulatory T cell lineage specification by the forkhead transcription factor foxp3. Immunity *22*, 329–341.

Fu, W., Ergun, A., Lu, T., Hill, J.A., Haxhinasto, S., Fassett, M.S., Gazit, R., Adoro, S., Glimcher, L., Chan, S., et al. (2012). A multiply redundant genetic switch 'locks in' the transcriptional signature of regulatory T cells. Nat. Immunol. *13*, 972–980.

Hedrick, S.M., Hess Michelini, R., Doedens, A.L., Goldrath, A.W., and Stone, E.L. (2012). FOXO transcription factors throughout T cell biology. Nat. Rev. Immunol. *12*, 649–661.

Huehn, J., Siegmund, K., Lehmann, J.C.U., Siewert, C., Haubold, U., Feuerer, M., Debes, G.F., Lauber, J., Frey, O., Przybylski, G.K., et al. (2004). Developmental stage, phenotype, and migration distinguish naive- and effector/memory-like CD4+ regulatory T cells. J. Exp. Med. *199*, 303–313.

Jorgensen, T.N., McKee, A., Wang, M., Kushnir, E., White, J., Refaeli, Y., Kappler, J.W., and Marrack, P. (2007). Bim and Bcl-2 mutually affect the expression of the other in T cells. J. Immunol. *179*, 3417–3424.

Josefowicz, S.Z., Lu, L.-F., and Rudensky, A.Y. (2012). Regulatory T cells: mechanisms of differentiation and function. Annu. Rev. Immunol. *30*, 531–564.

Kim, J.K., Klinger, M., Benjamin, J., Xiao, Y., Erle, D.J., Littman, D.R., and Killeen, N. (2009). Impact of the TCR signal on regulatory T cell homeostasis, function, and trafficking. PLoS ONE *4*, e6580.

Koonpaew, S., Shen, S., Flowers, L., and Zhang, W. (2006). LAT-mediated signaling in CD4+CD25+ regulatory T cell development. J. Exp. Med. *203*, 119–129.

Korn, T., Reddy, J., Gao, W., Bettelli, E., Awasthi, A., Petersen, T.R., Bäckström, B.T., Sobel, R.A., Wucherpfennig, K.W., Strom, T.B., et al. (2007). Myelin-specific regulatory T cells accumulate in the CNS but fail to control autoimmune inflammation. Nat. Med. *13*, 423–431.

Kühn, R., Schwenk, F., Aguet, M., and Rajewsky, K. (1995). Inducible gene targeting in mice. Science *269*, 1427–1429.

Lahl, K., Loddenkemper, C., Drouin, C., Freyer, J., Arnason, J., Eberl, G., Hamann, A., Wagner, H., Huehn, J., and Sparwasser, T. (2007). Selective depletion of Foxp3+ regulatory T cells induces a scurfy-like disease. J. Exp. Med. *204*, 57–63.

Moran, A.E., Holzapfel, K.L., Xing, Y., Cunningham, N.R., Maltzman, J.S., Punt, J., and Hogquist, K.A. (2011). T cell receptor signal strength in Treg and iNKT cell development demonstrated by a novel fluorescent reporter mouse. J. Exp. Med. *208*, 1279–1289.

Morikawa, H., Ohkura, N., Vandenbon, A., Itoh, M., Nagao-Sato, S., Kawaji, H., Lassmann, T., Carninci, P., Hayashizaki, Y., Forrest, A.R.R., et al.; FANTOM Consortium (2014). Differential roles of epigenetic changes and Foxp3 expression in regulatory T cell-specific transcriptional regulation. Proc. Natl. Acad. Sci. USA *111*, 5289–5294.

Muzumdar, M.D., Tasic, B., Miyamichi, K., Li, L., and Luo, L. (2007). A global double-fluorescent Cre reporter mouse. Genesis *45*, 593–605.

Ohkura, N., Hamaguchi, M., Morikawa, H., Sugimura, K., Tanaka, A., Ito, Y., Osaki, M., Tanaka, Y., Yamashita, R., Nakano, N., et al. (2012). T cell receptor stimulation-induced epigenetic changes and Foxp3 expression are independent and complementary events required for Treg cell development. Immunity *37*, 785–799.

Peng, S., Lalani, S., Leavenworth, J.W., Ho, I.-C., and Pauza, M.E. (2007). c-Maf interacts with c-Myb to down-regulate Bcl-2 expression and increase apoptosis in peripheral CD4 cells. Eur. J. Immunol. *37*, 2868–2880.

Polic, B., Kunkel, D., Scheffold, A., and Rajewsky, K. (2001). How alpha beta T cells deal with induced TCR alpha ablation. Proc. Natl. Acad. Sci. USA *98*, 8744–8749.

Rudra, D., deRoos, P., Chaudhry, A., Niec, R.E., Arvey, A., Samstein, R.M., Leslie, C., Shaffer, S.A., Goodlett, D.R., and Rudensky, A.Y. (2012). Transcription factor Foxp3 and its protein partners form a complex regulatory network. Nat. Immunol. *13*, 1010–1019.

Sakaguchi, S., Yamaguchi, T., Nomura, T., and Ono, M. (2008). Regulatory T cells and immune tolerance. Cell *133*, 775–787.

Setoguchi, R., Hori, S., Takahashi, T., and Sakaguchi, S. (2005). Homeostatic maintenance of natural Foxp3(+) CD25(+) CD4(+) regulatory T cells by interleukin (IL)-2 and induction of autoimmune disease by IL-2 neutralization. J. Exp. Med. *201*, 723–735.

Shevach, E.M. (2009). Mechanisms of foxp3+ T regulatory cell-mediated suppression. Immunity *30*, 636–645.

Siggs, O.M., Miosge, L.A., Yates, A.L., Kucharska, E.M., Sheahan, D., Brdicka, T., Weiss, A., Liston, A., and Goodnow, C.C. (2007). Opposing functions of the T cell receptor kinase ZAP-70 in immunity and tolerance differentially titrate in response to nucleotide substitutions. Immunity *27*, 912–926.

Sledzińska, A., Hemmers, S., Mair, F., Gorka, O., Ruland, J., Fairbairn, L., Nissler, A., Müller, W., Waisman, A., Becher, B., and Buch, T. (2013). TGF-β signalling is required for $CD4^+$ T cell homeostasis but dispensable for regulatory T cell function. PLoS Biol. *11*, e1001674.

Stephens, G.L., Andersson, J., and Shevach, E.M. (2007). Distinct subsets of FoxP3+ regulatory T cells participate in the control of immune responses. J. Immunol. *178*, 6901–6911.

Szymczak-Workman, A.L., Workman, C.J., and Vignali, D.A.A. (2009). Cutting edge: regulatory T cells do not require stimulation through their TCR to suppress. J Immunol *182*, 5188–5192.

Vahl, J.C., Heger, K., Knies, N., Hein, M.Y., Boon, L., Yagita, H., Polic, B., and Schmidt-Supprian, M. (2013). NKT cell-TCR expression activates conventional T cells in vivo, but is largely dispensable for mature NKT cell biology. PLoS Biol. *11*, e1001589.

Xing, Y., and Hogquist, K.A. (2012). T-cell tolerance: central and peripheral. Cold Spring Harb. Perspect. Biol. *4*, a007021–a007021.

Zeng, H., Yang, K., Cloer, C., Neale, G., Vogel, P., and Chi, H. (2013). mTORC1 couples immune signals and metabolic programming to establish T(reg)-cell function. Nature *499*, 485–490.

Immunity, Volume *41*

Supplemental Information

Continuous T Cell Receptor Signals Maintain a Functional Regulatory T Cell Pool

J. Christoph Vahl, Christoph Drees, Klaus Heger, Sylvia Heink, Julius C. Fischer, Jelena Nedjic, Naganari Ohkura, Hiromasa Morikawa, Hendrik Poeck, Sonja Schallenberg, David Rieß, Marco Y. Hein, Thorsten Buch, Bojan Polic, Anne Schönle, Robert Zeiser, Annette Schmitt-Gräff, Karsten Kretschmer, Ludger Klein, Thomas Korn, Shimon Sakaguchi, and Marc Schmidt-Supprian

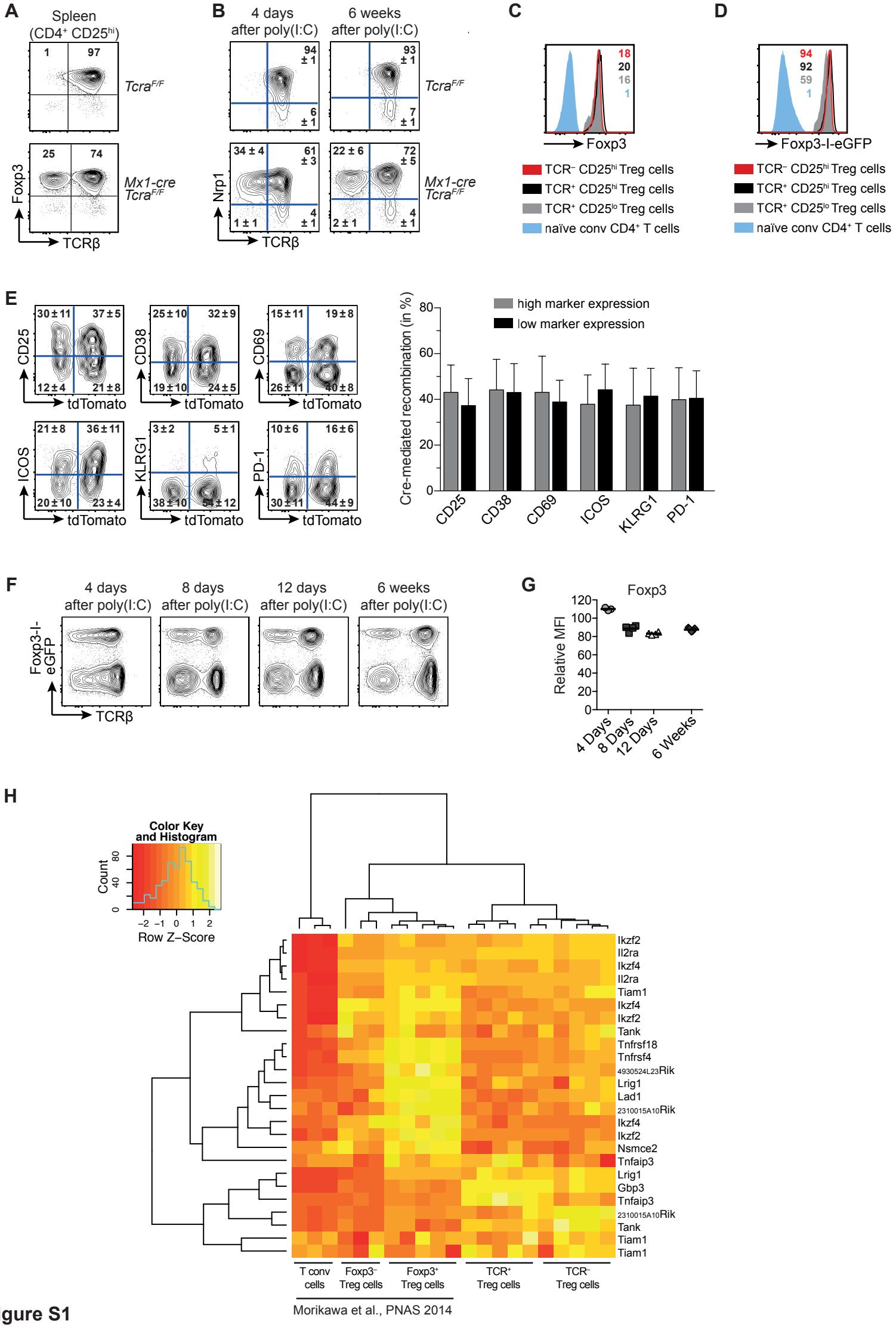
A
Spleen
(CD4+ CD25hi)
Tcra F/F
Mx1-cre Tcra F/F
Foxp3
TCRβ
B
4 days after poly(I:C)
6 weeks after poly(I:C)
Nrp1
C
Foxp3
TCR− CD25hi Treg cells
TCR+ CD25hi Treg cells
TCR+ CD25lo Treg cells
naïve conv CD4+ T cells
D
Foxp3-I-eGFP
E
CD25
CD38
CD69
ICOS
KLRG1
PD-1
tdTomato
high marker expression
low marker expression
Cre-mediated recombination (in %)
F
4 days after poly(I:C)
8 days after poly(I:C)
12 days after poly(I:C)
6 weeks after poly(I:C)
Foxp3-I-eGFP
G
Foxp3
Relative MFI
4 Days
8 Days
12 Days
6 Weeks
H
Color Key and Histogram
Count
Row Z–Score
Ikzf2
Il2ra
Ikzf4
Il2ra
Tiam1
Ikzf4
Ikzf2
Tank
Tnfrsf18
Tnfrsf4
4930524L23Rik
Lrig1
Lad1
2310015A10Rik
Ikzf4
Ikzf2
Nsmce2
Tnfaip3
Lrig1
Gbp3
Tnfaip3
2310015A10Rik
Tank
Tiam1
Tiam1
T conv cells
Foxp3− Treg cells
Foxp3+ Treg cells
TCR+ Treg cells
TCR− Treg cells
Morikawa et al., PNAS 2014

Figure S1

Figure S1, related to Figure 1. Expression of Foxp3 protein and of Treg cell-specifically hypomethylated genes remain stable despite TCR ablation

(A) Phenotype of TCR-deficient Treg cells. Surface TCRβ and intracellular Foxp3 expression of splenic $CD4^+$ $CD25^{hi}$ Treg cells from the indicated mice (which did not contain the Foxp3-I-eGFP knock-in) 2 wk after poly(I:C) injection. Plots are representative for at least 5 mice per genotype from 2 independent experiments.

(B) Extracellular Nrp1 expression on splenic Foxp3-I-$eGFP^+$ $CD25^{hi}$ Treg cells from the depicted animals, 4 d or 6 wk after poly(I:C) injection. Numbers in representative plots indicate mean percentage ± SD of at least 3 mice per genotype.

(C) Intracellular Foxp3 expression of the indicated splenic T cell subsets (Treg = $Foxp3^+$) 6 wk after poly(I:C) injection. Median fluorescence intensities (MFIs) were normalized to $CD25^{hi}$ Treg cells of *Tcra*$^{F/F}$ animals, then set to 1 for $CD4^+$ conventional T cells. Numbers in representative histogram indicate means of MFIs. Means were calculated from 14 mice from at least 4 independent experiments.

(D) Foxp3-I-eGFP expression of the indicated splenic T cell subsets 6 wk after poly(I:C) injection. Median fluorescence intensities (MFIs) were normalized to $CD25^{hi}$ Treg cells of *Tcra*$^{F/F}$ animals, then set to 1 for $CD4^+$ conventional T cells. Numbers in representative histogram indicate means of MFIs. Means were calculated from 16 mice from at least 5 independent experiments.

(E) Extracellular expression of the indicated markers on splenic $CD4^+$ $Foxp3^+$ Treg cells from *Mx1-cre* mT/mG mice 6 wk after poly(I:C) injection. Upon Cre-mediated recombination cells from these reporter mice switch from expressing membrane-bound Tomato (tdTomato, mT) to membrane-bound GFP (mG). Numbers in representative plots indicate mean percentage ± SD of 4 mice. Bar charts indicate mean percentage + SD of tdTomato-negative (mGFP-positive) cells among cells expressing high (grey) or low (black) amounts of the respective marker.

(F) GFP expressed from the Foxp3-I-eGFP knock-in allele is plotted against TCRβ expression on splenic $CD4^+$ $CD5^+$ T cells at the indicated time points after poly(I:C) injection. Each Dot plot is representative for at least 3 mice per time point.

(G) Ratio of intracellular Foxp3 expression of $TCR^–$ vs. TCR^+ Treg cells ($CD4^+$ $CD5^+$ $Foxp3^+$) cells from *Mx1-cre Tcra*$^{F/F}$ animals at the indicated time points after poly(I:C) injection. Median fluorescence intensities (MFIs) were normalized to TCR^+ Treg cells and plotted as % values. Bars depict means of MFIs.

(H) Shown are the expression profiles of genes associated with Treg cell-specific DNA demethylated regions whose expression is up-regulated in Treg cells compared with conventional T cells (Morikawa et al., 2014). The mRNA expression of splenic TCR^{+} $CD25^{hi}$ Treg cells from 4 $Tcra^{F/F}$ control preparations (pooled from 3 – 5 mice per preparation) and TCR^{-} $CD25^{hi}$ Treg cells from 5 *Mx1-cre* $Tcra^{F/F}$ preparations (pooled from 3 – 5 mice per preparation), 6 wk after poly(I:C) injection, was analyzed by Affymetrix microarray. These gene expression profiles were compared with previously described profiles of conventional T cells (T conv), *Foxp3*-null Treg cells ($Foxp3^{-}$ Treg cells) and Treg cells ($Foxp3^{+}$ Tregs) and (expression values taken from (Samstein et al., 2012)).

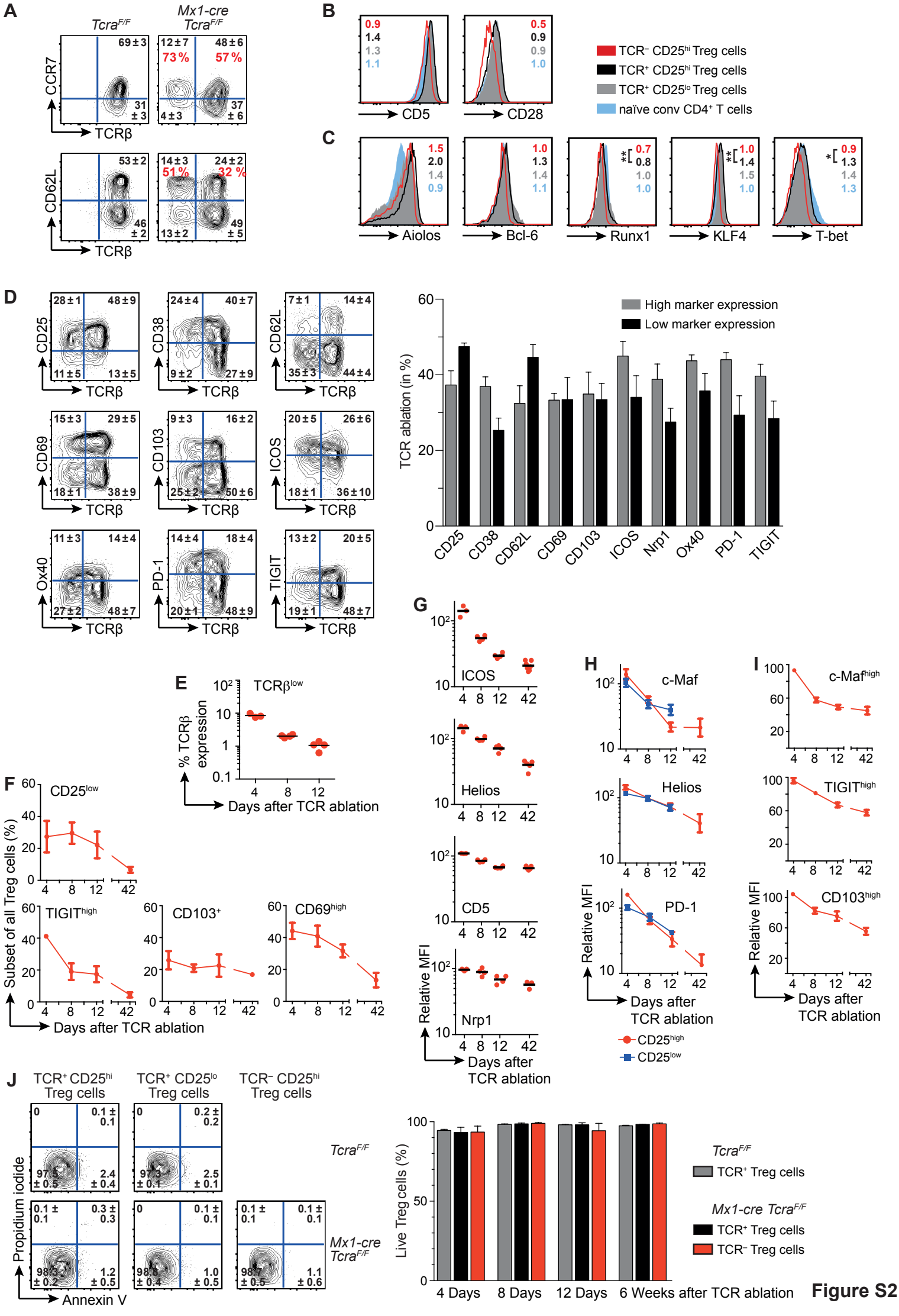
A
Tcra F/F
Mx1-cre Tcra F/F
CCR7
TCRβ
CD62L
B
CD5
CD28
TCR⁻ CD25hi Treg cells
TCR⁺ CD25hi Treg cells
TCR⁺ CD25lo Treg cells
naïve conv CD4⁺ T cells
C
Aiolos
Bcl-6
Runx1
KLF4
T-bet
D
CD25
CD38
CD62L
CD69
CD103
ICOS
Ox40
PD-1
TIGIT
High marker expression
Low marker expression
TCR ablation (in %)
E
TCRβlow
% TCRβ expression
Days after TCR ablation
F
CD25low
TIGIThigh
CD103+
CD69high
Subset of all Treg cells (%)
Days after TCR ablation
G
ICOS
Helios
CD5
Nrp1
Relative MFI
Days after TCR ablation
H
c-Maf
Helios
PD-1
Relative MFI
Days after TCR ablation
CD25high
CD25low
I
c-Maf high
TIGIT high
CD103 high
Relative MFI
Days after TCR ablation
J
TCR⁺ CD25hi Treg cells
TCR⁺ CD25lo Treg cells
TCR⁻ CD25hi Treg cells
Tcra F/F
Mx1-cre Tcra F/F
Propidium iodide
Annexin V
Live Treg cells (%)
TCR⁺ Treg cells
TCR⁻ Treg cells
4 Days
8 Days
12 Days
6 Weeks after TCR ablation

Figure S2

Figure S2, related to Figure 2. Marker expression of TCR-deficient Treg cells

(A) Extracellular expression of CCR7 or CD62L on splenic Foxp3-I-eGFP^{+} CD25^{hi} Treg cells from the depicted animals, 6 wk after poly(I:C) injection-induced TCR ablation. Black numbers in representative plots indicate mean percentage ± SD of at least 6 mice per genotype from at least 2 independent experiments. Red numbers indicate mean percentage among TCR^{+} or TCR$^{–}$ Treg cells, respectively.

(B and C) Extracellular (B) or intracellular (C) expression of the depicted markers of the indicated splenic T cell subsets (Treg = Foxp3^{+}), all from *Mx1-cre Tcra$^{F/F}$* animals 6 wk after poly(I:C) injection. Numbers in representative histograms indicate means of MFIs, normalized to Foxp3$^{–}$ CD4^{+} CD44^{lo} naïve conventional T cells of *Tcra$^{F/F}$* animals. Means were calculated from at least 5 mice per genotype from at least 2 independent experiments. ***, P < 0.001; **, P < 0.01; *, P < 0.05; one-way ANOVA.

(D) Extracellular expression of the indicated markers on splenic GFP^{+} CD4^{+} CD5^{+} Treg cells from *Mx1-cre Tcra$^{F/F}$* Foxp3-I-eGFP animals 4 d after poly(I:C) injection induced TCR ablation. Numbers in representative plots indicate mean percentage ± SD of 3 mice. Bar charts indicate mean percentage +SD of TCR$^{–}$ Treg cells (Foxp3-I-eGFP^{+} CD4^{+} CD5^{+}) among cells expressing high (grey) or low (black) amounts of the respective marker.

(E-I) Decay of the indicated Treg cell lineage-specifying proteins after TCR ablation. At the indicated time points *Mx1-cre Tcra$^{F/F}$* splenocytes were isolated, stained and gated on CD4^{+} CD5^{+} Foxp3^{+} Treg cells. Data for day 42 correspond to data shown in Figure 2.

(E) Decay of TCRβ surface expression on TCR$^{lo\ or\ deficient}$ Treg cells at the indicated time-points after TCR ablation. TCRβ surface levels on Foxp3^{+} TCRβ$^{lo\ or\ deficient}$ Treg cells were calculated relative to TCRβ^{+} Foxp3^{+} Treg cells in the same mice, whose TCRβ surface levels were set to 100 for each time-point. Antibody staining of TCRβ on B cells was subtracted as background staining.

(F) Percentage of TCR$^{–}$ Foxp3^{+} Treg cells expressing the indicated levels of the respective cell surface proteins at different time points after induced TCR ablation. Data indicates mean percentage ± SD of at least 3 mice per time point.

(G) Ratios of median fluorescent intensities (MFI) shown in %: MFI of TCR-deficient divided by MFI of TCR^{+} Foxp3^{+} Treg cells x 100. Depicted are values for individual mice (at least 3 per time point) and bars indicate means.

(H) Ratios of median fluorescent intensities (MFI) shown in % separately for $CD25^{hi}$ (red) and $CD25^{lo}$ (blue) $Foxp3^+$ Treg subsets: MFI of TCR-deficient relative divided by MFI of TCR^+ Treg cells x 100. Depicted are means ± SD for at least 3 per time point. Meaningful amounts of $CD25^{lo}$ TCR^- Treg cells could not be identified at day 42.

(I) Ratios of median fluorescent intensities (MFI) shown in %, gated on cells with high levels of the depicted protein: relative MFI of indicated protein on TCR-deficient divided by MFI on TCR^+ $Foxp3^+$ Treg cells x 100. Depicted are values for individual mice (at least 3 per time point) and means. This analysis shows that cells expressing high amounts of these proteins down-regulate them over time (parallel to their disappearance over time). Even though the proportion of $CD103^+$ TCR-deficient Treg cells remains constant over 12 days (see F), surface levels of CD103 in this subset decrease.

(J) Propidium iodide and Annexin V stainings of indicated TCR^+ and TCR^- Treg cell subsets 6 wk after poly(I:C) injection induced TCR ablation. Black numbers represent mean percentages ± SD of at least 3 animals per genotype. Bar charts indicates percentage of live (propidium $iodide^-$, Annexin V^-) Treg cells of total Treg cells (Foxp3-I-eGFP$^+$ CD4$^+$ CD5$^+$) at indicated time points after poly(I:C) injection. Bar charts show mean percentage + SD of at least 3 mice per time point per genotype.

A

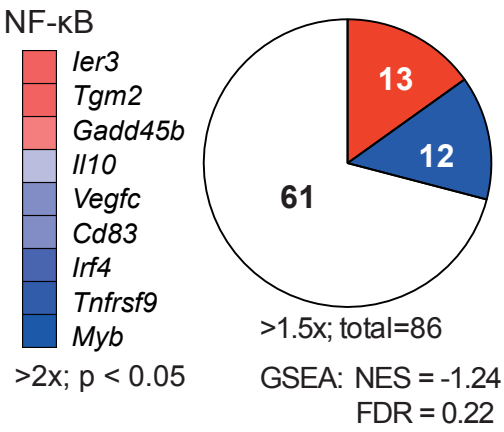

B

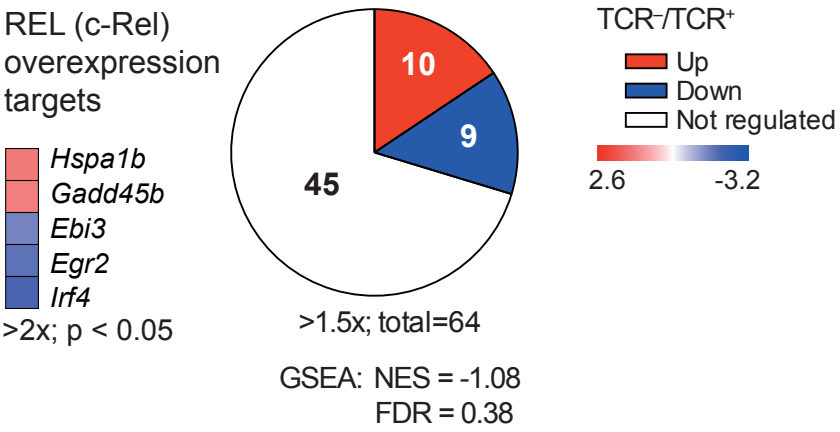

C

Gene set		SIZE	ES	NES	NOM p-val	FDR q-val	FWER p-val	RANK AT MAX
C2 cgp v4.0 (3402 gene sets)	Rank							
ZHAN_MULTIPLE_MYELOMA_CD2_DN	1	30	-0.61	-2.03	0.00	0.07	0.03	836
BILD_E2F3_ONCOGENIC_SIGNATURE	2	119	-0.50	-1.99	0.00	0.06	0.05	1571
YANG_BCL3_TARGETS_UP	3	185	-0.44	-1.91	0.00	0.07	0.10	1165
RAY_TUMORIGENESIS_BY_ERBB2_CDC25A_UP	4	55	-0.66	-1.91	0.00	0.07	0.10	1162
ISSAEVA_MLL2_TARGETS	5	26	-0.60	-1.90	0.00	0.06	0.10	639
GAVIN_FOXP3_TARGETS_CLUSTER_P4	6	72	-0.62	-1.89	0.00	0.06	0.10	1032
C3 TFT v4.0 (615 gene sets)	Rank							
V$EGR3_01	1	44	-0.58	-1.87	0.00	0.05	0.03	1486
V$EGR2_01	2	91	-0.44	-1.76	0.00	0.10	0.08	833
V$MYOGNF1_01	3	23	-0.59	-1.75	0.00	0.07	0.08	2116
V$E2F_Q3_01	4	144	-0.47	-1.73	0.00	0.07	0.10	1359
C7 Imm sig v4.0 (1910 gene sets)	Rank							
GSE17974_CTRL_VS_ACT_IL4_AND_ANTI_IL12_6H_CD4_TCELL_DN	1	110	-0.53	-1.95	0.00	0.01	0.00	917
GSE9650_EXHAUSTED_VS_MEMORY_CD8_TCELL_UP	2	104	-0.59	-1.93	0.00	0.01	0.01	1476
GSE7852_TREG_VS_TCONV_THYMUS_UP	3	137	-0.68	-1.88	0.00	0.01	0.02	1417
GSE30083_SP2_VS_SP3_THYMOCYTE_UP	4	95	-0.61	-1.86	0.00	0.01	0.03	1113
GSE30962_ACUTE_VS_CHRONIC_LCMV_SECONDARY_INF_CD8_TCELL_DN	5	137	-0.65	-1.86	0.00	0.02	0.05	1078
GSE7852_TREG_VS_TCONV_LN_UP	6	149	-0.69	-1.84	0.00	0.03	0.05	1514
GSE1460_DP_THYMOCYTE_VS_NAIVE_CD4_TCELL_ADULT_BLOOD_UP	7	117	-0.55	-1.84	0.00	0.02	0.05	1850
GSE17580_TREG_VS_TEFF_UP	8	138	-0.61	-1.84	0.00	0.02	0.05	1725
GSE30962_ACUTE_VS_CHRONIC_LCMV_PRIMARY_INF_CD8_TCELL_DN	9	139	-0.71	-1.82	0.00	0.02	0.06	1525
GSE20366_CD103_POS_VS_NEG_TREG_KLRG1NEG_DN	10	116	-0.54	-1.81	0.00	0.02	0.07	1535
GSE20366_TREG_VS_TCONV_UP	11	98	-0.68	-1.81	0.00	0.02	0.07	1881
GSE13738_RESTING_VS_BYSTANDER_ACTIVATED_CD4_TCELL_DN	12	144	-0.46	-1.80	0.00	0.02	0.07	1093
GSE24142_DN2_VS_DN3_THYMOCYTE_ADULT_UP	13	100	-0.51	-1.80	0.00	0.02	0.07	1213
GSE20366_TREG_VS_NAIVE_CD4_TCELL_HOMEOSTATIC_CONVERSION_UP	14	128	-0.55	-1.78	0.00	0.03	0.10	1651
GSE30083_SP1_VS_SP2_THYMOCYTE_DN	15	84	-0.45	-1.78	0.00	0.03	0.10	1217
GSE7852_TREG_VS_TCONV_UP	16	143	-0.74	-1.77	0.00	0.03	0.10	1469
GSE7460_TCONV_VS_TREG_THYMUS_DN	17	139	-0.66	-1.77	0.00	0.03	0.10	1535

Figure S3

Figure S3, related to Figure 3. Effects of TCR ablation on gene expression

(A and B) Changes in the expression of NF-κB (A) and c-Rel (B) target genes. Pie charts show the number of detected target genes within the respective category (white: not regulated, red: ≥ 1.5-fold up-regulated in KO relative to WT Treg cells; blue: ≤ 67% of the expression in TCR^+ Treg cells). Heatmaps depict TCR-deficient divided by TCR^+ fold-change values (Log_2-transformed, ≥ 2-fold) of significantly regulated genes ($p<0.05$, t test).

(C) Analysis reports of gene set enrichment analyses (http://www.broadinstitute.org/gsea/index.jsp) of gene expression data from TCR-deficient and TCR-expressing $CD25^+$ $Foxp3^+$ Treg cells. Results are ranked by normalized enrichment score (NES) and shown for family wise error rate FWER ≤ 1 (which all also had a FDR ≤ 1). The following gene set collections analyses are shown: C2 chemical and genetic perturbations (cgp v4.0, 3402 gene sets); C3 transcription factor targets (TFT v4.0, 615 gene sets); C7 immunologic signatures (imm sig v4.0, 1910 gene sets). Highlighted in red are gene sets mentioned in the manuscript.

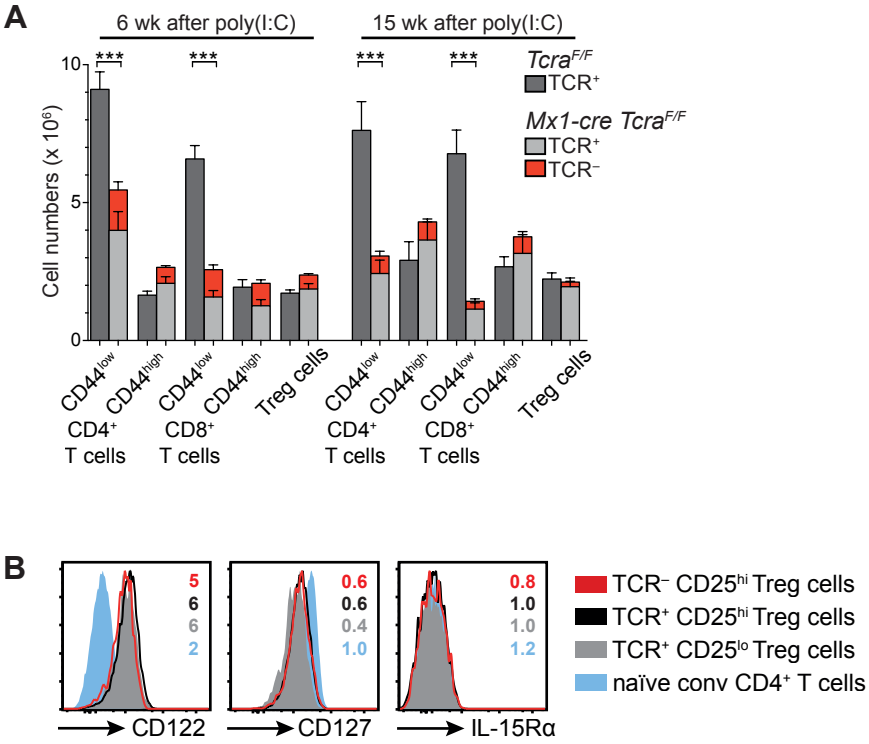
A
6 wk after poly(I:C)
15 wk after poly(I:C)
***
***
***
***
Tcra^F/F
TCR+
Mx1-cre Tcra^F/F
TCR+
TCR–
Cell numbers (x 10^6)
10
5
0
CD44low
CD44high
CD44low
CD44high
Treg cells
CD44low
CD44high
CD44low
CD44high
Treg cells
CD4+ T cells
CD8+ T cells
CD4+ T cells
CD8+ T cells

B
5
6
6
2
0.6
0.6
0.4
1.0
0.8
1.0
1.0
1.2
CD122
CD127
IL-15Rα
TCR– CD25hi Treg cells
TCR+ CD25hi Treg cells
TCR+ CD25lo Treg cells
naïve conv CD4+ T cells

Figure S4

Figure S4, related to Figure 4. Treg cell homeostasis in absence of TCR input

(A) Total splenic cell counts of Foxp3^{-} CD4^{+} and CD8^{+}, naïve (CD44^{lo}) and memory or effector (CD44^{hi}), as well as Foxp3^{+} Treg cells, of the depicted animals, 6 wk or 15 wk after poly(I:C) injection. Data represents means and + SD of three independent experiments with at least 6 mice per genotype and time point. ***, $P < 0.001$; one-way ANOVA.

(B) Extracellular expression of the respective cytokine receptor subunits on splenic Foxp3-I-eGFP^{+} Treg cells of the depicted animals, 6 wk after poly(I:C) injection. Numbers in representative histograms indicate means of the median fluorescence intensities (MFIs), normalized to CD4^{+} CD44^{lo} naïve conventional T cells of *Tcra*$^{F/F}$ animals. Means were calculated from at least 5 mice per genotype from at least 2 independent experiments.

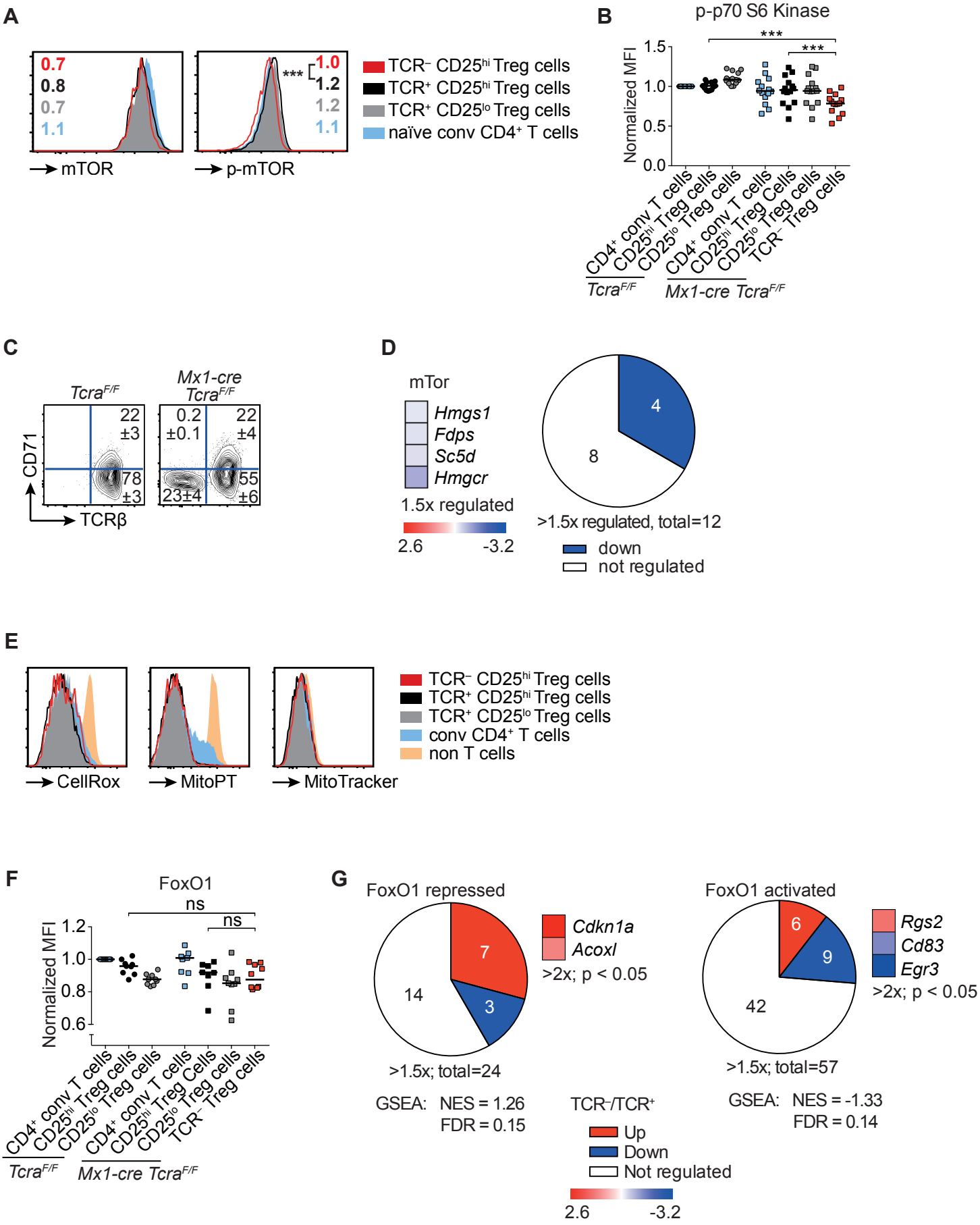
A
0.7
0.8
0.7
1.1
mTOR
***
1.0
1.2
1.2
1.1
p-mTOR
TCR⁻ CD25hi Treg cells
TCR⁺ CD25hi Treg cells
TCR⁺ CD25lo Treg cells
naïve conv CD4⁺ T cells
B
p-p70 S6 Kinase
Normalized MFI
1.5
1.0
0.5
0.0
***
***
CD4⁺ conv T cells
CD25hi Treg cells
CD25lo Treg cells
CD4⁺ conv T cells
CD25hi Treg Cells
CD25lo Treg cells
TCR⁻ Treg cells
TcraF/F
Mx1-cre TcraF/F
C
TcraF/F
Mx1-cre TcraF/F
CD71
TCRβ
22 ±3
78 ±3
0.2 ±0.1
23±4
22 ±4
55 ±6
D
mTor
Hmgs1
Fdps
Sc5d
Hmgcr
1.5x regulated
2.6
-3.2
4
8
>1.5x regulated, total=12
down
not regulated
E
CellRox
MitoPT
MitoTracker
TCR⁻ CD25hi Treg cells
TCR⁺ CD25hi Treg cells
TCR⁺ CD25lo Treg cells
conv CD4⁺ T cells
non T cells
F
FoxO1
ns
ns
Normalized MFI
1.2
1.0
0.8
0.6
CD4⁺ conv T cells
CD25hi Treg cells
CD25lo Treg cells
CD4⁺ conv T cells
CD25hi Treg Cells
CD25lo Treg cells
TCR⁻ Treg cells
TcraF/F
Mx1-cre TcraF/F
G
FoxO1 repressed
7
3
14
Cdkn1a
Acoxl
>2x; p < 0.05
>1.5x; total=24
GSEA: NES = 1.26
FDR = 0.15
FoxO1 activated
6
9
42
Rgs2
Cd83
Egr3
>2x; p < 0.05
>1.5x; total=57
GSEA: NES = -1.33
FDR = 0.14
TCR⁻/TCR⁺
Up
Down
Not regulated
2.6
-3.2

Figure S5

Figure S5, related to Figure 5. TCR ablation affects mTOR signals

(A, B, and F) Comparison of phosphorylation or expression of the respective proteins in the indicated splenic T cell subsets of the indicated animals, 6 wk after poly(I:C) injection. Numbers in representative histograms indicate means of the median fluorescence intensities (MFIs), normalized to Foxp3^{-} CD4^{+} CD44^{lo} naïve conventional T cells of *Tcra*$^{F/F}$ control mice. Means were calculated from at least 5 mice per genotype from at least 2 independent experiments. Bars indicate medians. ***, $P < 0.001$; one-way ANOVA.

(C) Extracellular expression of CD71 on splenic Foxp3-I-eGFP^{+} Treg cells of the depicted animals, 6 wk after poly(I:C) injection. Numbers in representative plots indicate mean percentage ± SD of 3 mice per genotype.

(D and G) Heatmaps depict TCR-deficient divided by TCR^{+} fold-change values of significantly regulated genes of the cholesterol biosynthesis (D) or FoxO1 (G) pathways. The mRNA expression of splenic TCR^{+} CD25^{hi} Foxp3^{+} Treg cells from 4 *Tcra*$^{F/F}$ control replicates (TCR^{+}) and TCR^{-} CD25^{hi} Foxp3^{+} Treg cells from 5 *Mx1-cre Tcra*$^{F/F}$ replicates (TCR-deficient), 6 wk after poly(I:C) injection, was compared by Affymetrix microarray. Each replicate was pooled from 3 – 5 mice. Pie charts show the number of detected genes within the respective category (white: not regulated, red: ≥ 1.5-fold up-regulated in KO relative to WT Treg cells; blue: ≤ 67% of the expression in TCR^{+} Treg cells).

(E) Mitochondrial reactive oxygen species production (CellRox), membrane potential (MitoPT) and mass (MitoTracker) were analyzed by flow cytometry. Plots are representative for at least 6 mice per genotype from at least 3 independent experiments.

A

	Gene	Array	RT-PCR	FACS
down	*Ebi3*	3.4	22.7	
	Nt5e/CD73	2.2		2
	Il10	2.2	40.8	2.3
	Fgl2	1.9	3.7	
	Nrp1	1.9		1.7
	Gzmb	1.7		
	Il2rb	1.6		1.2
	Ctla4	1.6		2.7
	Pdcd1lg2	1.5		
	Entpd1/CD39	1.2		1.3
	Itgal	1.2		2.1
	Tgfb1	1.2		
	Tnfrsf18/GITR	1.2		1.8
	Tgfb1/LAP			2.2
	Il10ra			1.5
	Tigit			14
	Lag3			1.6
up	*Hmox1*	1.2		
	Pdcd1lg1/CD274	1.5		
	Prf1	1.9		

B

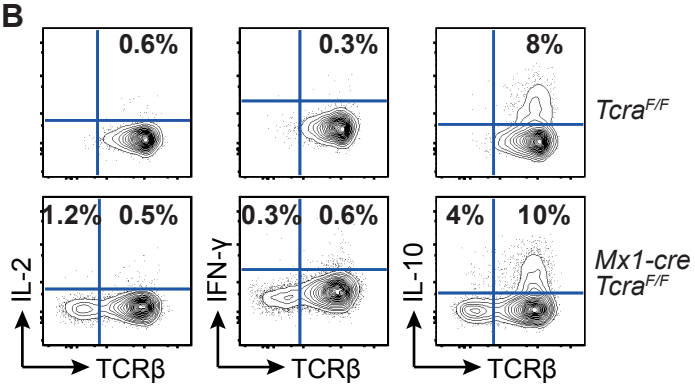

C

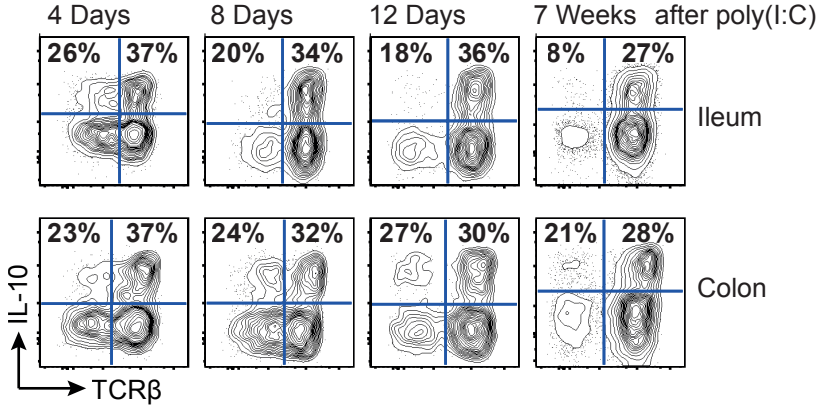

Figure S6

Figure S6, related to Figure 6. Effects of TCR ablation on Treg cell suppressor function

(A) Overview showing the expression changes of 20 suppressive markers of TCR^+ vs. TCR^- Treg cells, 6 w after poly(I:C) injection, analyzed by Affymetrix microarray, flow cytometry or qRT-PCR (blue, significantly down-regulated; red, significantly up-regulated at $P < 0.05$; t test corrected for multiple testing where necessary).

(B) Intracellular IL-2, IL-10 and IFN-γ expression of splenic Foxp3-I-$eGFP^+$ Treg cells, activated *in vitro* with PMA and Ionomycin for 5 h. Cells were extracted from mice and activated 6 wk after poly(I:C) injection. Numbers indicate mean percentages of TCR^+ or TCR^- Treg cells expressing the respective cytokine. Data are representative for at least 4 animals per genotype.

(C) Intracellular IL-10 expression of $CD4^+$ Foxp3-I-$eGFP^+$ Treg cells after activation *in vitro* with PMA and Ionomycin for 1 h. Cells were isolated from the lamina propria of the ileum or colon of *Mx1-cre* $Tcra^{F/F}$ animals at the indicated time points after poly(I:C) injection. Numbers indicate mean percentages of TCR^+ $CD25^{hi}$ or TCR^- $CD25^{hi}$ Treg cells expressing the respective cytokine. Data are representative for at least 3 animals per time point.

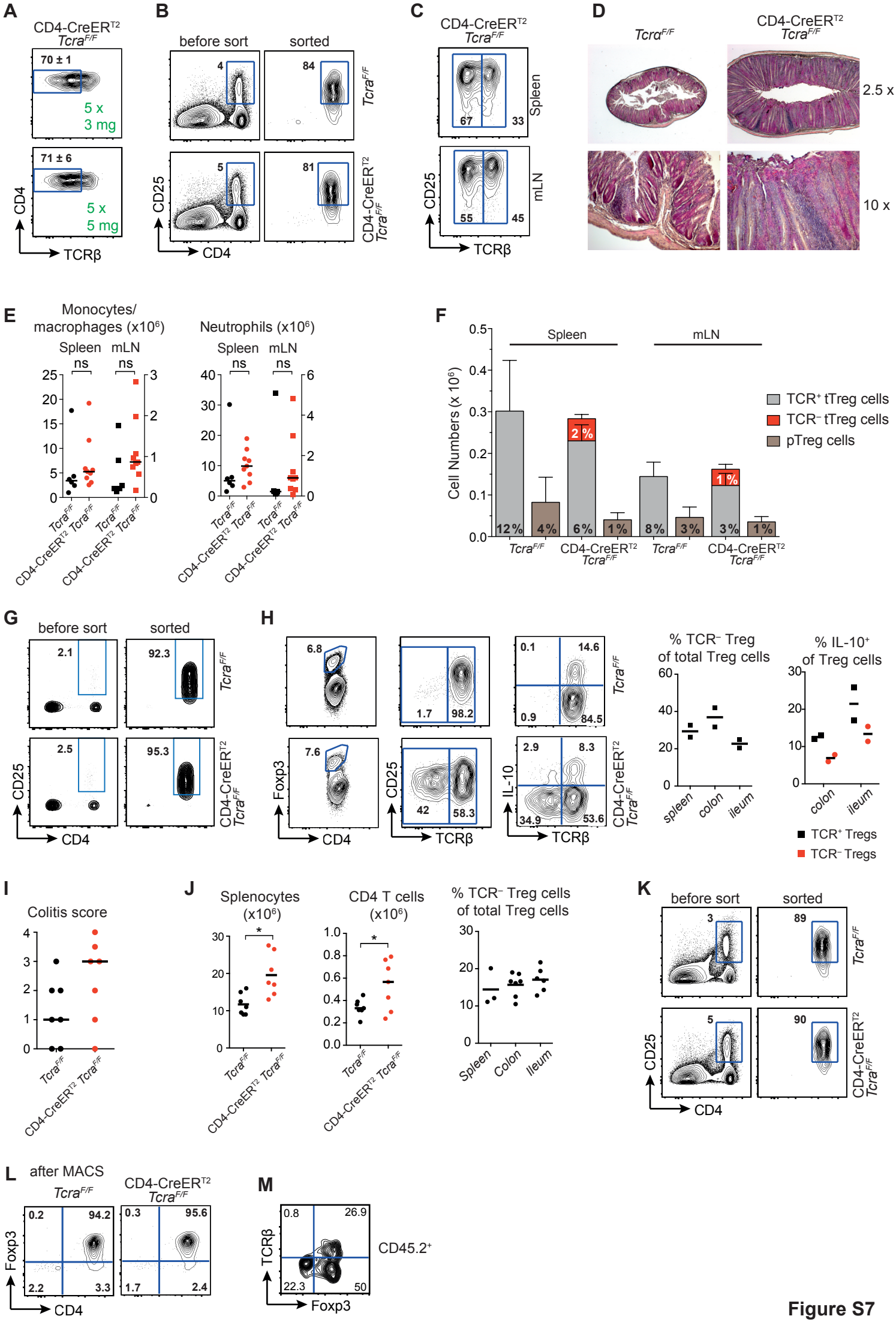
A
CD4-CreER^{T2} Tcra$^{F/F}$
70 ± 1
5 x 3 mg
71 ± 6
5 x 5 mg
CD4
TCRβ
B
before sort
sorted
4
84
Tcra$^{F/F}$
5
81
CD4-CreER^{T2} Tcra$^{F/F}$
CD25
CD4
C
CD4-CreER^{T2} Tcra$^{F/F}$
67
33
Spleen
55
45
mLN
CD25
TCRβ
D
Tcra$^{F/F}$
CD4-CreER^{T2} Tcra$^{F/F}$
2.5 x
10 x
E
Monocytes/ macrophages (x10^6)
Neutrophils (x10^6)
Spleen
mLN
ns
Tcra$^{F/F}$
CD4-CreER^{T2} Tcra$^{F/F}$
F
Spleen
mLN
Cell Numbers (x 10^6)
TCR$^+$ tTreg cells
TCR$^-$ tTreg cells
pTreg cells
12%
4%
6%
2%
1%
8%
3%
3%
1%
Tcra$^{F/F}$
CD4-CreER^{T2} Tcra$^{F/F}$
G
before sort
sorted
2.1
92.3
Tcra$^{F/F}$
2.5
95.3
CD4-CreER^{T2} Tcra$^{F/F}$
CD25
CD4
H
6.8
1.7
98.2
0.1
14.6
0.9
84.5
Tcra$^{F/F}$
7.6
Foxp3
CD4
42
58.3
CD25
TCRβ
2.9
8.3
34.9
53.6
IL-10
TCRβ
CD4-CreER^{T2} Tcra$^{F/F}$
% TCR$^-$ Treg of total Treg cells
spleen
colon
ileum
% IL-10$^+$ of Treg cells
colon
ileum
TCR$^+$ Tregs
TCR$^-$ Tregs
I
Colitis score
Tcra$^{F/F}$
CD4-CreER^{T2} Tcra$^{F/F}$
J
Splenocytes (x10^6)
CD4 T cells (x10^6)
*
Tcra$^{F/F}$
CD4-CreER^{T2} Tcra$^{F/F}$
% TCR$^-$ Treg cells of total Treg cells
Spleen
Colon
Ileum
K
before sort
sorted
3
89
Tcra$^{F/F}$
5
90
CD4-CreER^{T2} Tcra$^{F/F}$
CD25
CD4
L
after MACS
Tcra$^{F/F}$
CD4-CreER^{T2} Tcra$^{F/F}$
0.2
94.2
2.2
3.3
0.3
95.6
1.7
2.4
Foxp3
CD4
M
0.8
26.9
22.3
50
TCRβ
Foxp3
CD45.2$^+$

Figure S7

Figure S7, related to Figure 7. TCR ablation affects Treg cell function *in vivo*

(A) TCR ablation efficiency in Treg cells 2 d after a 5 d cycle of 3 mg/day or 5 mg/day tamoxifen administration. Representative plots of Treg cells ($CD4^+$ $CD5^+$ $CD25^+$) isolated from spleens of CD4-$CreER^{T2}$ $Tcra^{F/F}$ animals two days after administration of the indicated tamoxifen dose. This gating scheme was chosen as we purified $CD4^+$ $CD5^+$ $CD25^+$ Treg cells (> 94% $Foxp3^+$) for the *in vivo* suppression experiments. Black numbers represent mean percentage ± SD of TCR-deficient Treg cells.

(B-F) T cell-deficient animals (TCRα knockout) were reconstituted with naïve T cells ($Foxp3^–$) sorted from Foxp3-I-eGFP mice together with sorted Treg cells from either $Tcra^{F/F}$ control or from CD4-$CreER^{T2}$ $Tcra^{F/F}$ animals. After 3 wk of engraftment, $CreER^{T2}$ translocation was induced through 5 d of 5 mg/day tamoxifen feeding.

(B) Treg cell purification for the homeostasis model. Frequency of $CD4^+$ $CD25^+$ cells from the indicated animals before and after sorting with a FACSAria III (BD).

(C) Plots show percentages of $TCR^–$ $Foxp3^+$ Treg cells isolated from spleen and mesenteric lymph nodes 7 d after the last tamoxifen dose (one CD4-$CreER^{T2}$ $Tcra^{F/F}$ mouse). TCR ablation occurs equally in $CD25^{hi}$ and $CD25^{lo}$ Treg cells.

(D-F) At day 24 d animals were sacrificed and analyzed. Haematoxylin and eosin stained colon samples of the indicated genotypes are shown in (D) with the indicated magnification. $Tcra^{F/F}$, representative of 2 mice; CD4-$CreER^{T2}$ $Tcra^{F/F}$, representative of 3 mice.

(E) Total cell numbers of monocytes/macrophages ($CD11b^+$ $Gr1^{int}$ $SiglecF^–$); neutrophils ($CD11b^+$ $Gr1^{hi}$ $SiglecF^–$). Bars indicate medians. ns = not significant; one-way ANOVA.

(F) Total cell numbers of Treg cells. Since naïve T cells were purified from Foxp3-I-eGFP reporter mice, pTreg cells could be identified by Foxp3-I-eGFP expression. The number of tTreg cells was calculated by deducting the number of pTreg cells from the number of total $Foxp3^+$ Treg cells. Percentage indicates the proportion of Treg cells of the total $CD4^+$ T cell pool in the respective animals.

(G-J) $Rag2^{–/–}$ mice were reconstituted with 0.5 x 10^6 FACS-purified $CD4^+$ $CD45RB^{hi}$ $CD25^–$ naïve T cells together with 0.2 x 10^6 FACS-purified $CD4^+$ $CD25^{hi}$ $CD45RB^{int}$ $CD38^{hi}$ Treg cells from either $Tcra^{F/F}$ control or from CD4-$CreER^{T2}$ $Tcra^{F/F}$ animals. After 3 wk of engraftment, Cre expression was induced through two 5 d cycles of 3 mg/day tamoxifen feeding interrupted by a 7 day rest period.

(G) Representative plots of FACS purified Treg cells from indicated genotypes before and after sorting with a FACSAria III. Plots are representative of 8 (*Tcra*$^{F/F}$) and 9 (CD4-CreER^{T2} *Tcra*$^{F/F}$) animals.

(H) Representative plots show Treg cells isolated from the colon and ileum lamina propria and spleens of *Rag2*$^{-/-}$ mice reconstituted with CD4-CreER^{T2} *Tcra*$^{F/F}$ or control *Tcra*$^{F/F}$ Treg cells 2 days after the first 5 day of 3mg/day tamoxifen cycle. Lamina propria lymphocytes were either directly stained *ex vivo* or restimulated with PMA and Ionomycin for 1 h for the assessment of IL-10 production by flow cytometry. Percentages of Foxp3^{+} Treg cells amongst CD4 T cells and TCR^{-} Treg cells amongst total Treg cells (no stimulation) and IL-10^{+} Treg cells (restimulation with PMA and Ionomycin) are shown in dot plots. Scatter plots show the proportion of TCR-deficient Treg cells and of IL-10 producing Treg cells in the indicated organs.

(I) Colitis scores of *Rag2*$^{-/-}$ animals 27 d after start of tamoxifen treatment with either *Tcra*$^{F/F}$ or CD4-CreER^{T2} *Tcra*$^{F/F}$ Treg cells (n=7 per group). Bars indicate medians.

(J) Total cell numbers of splenocytes and CD4^{+} T cells from indicated genotypes 27 d after start of tamoxifen treatment. Shown are values for individual mice of the indicted genotypes and medians. *, $P < 0.05$; t test. Additionally, percentages and mean percentages of TCR^{-} Treg cells from spleen and lamina propria of ileum and colon are shown in scatter plots.

(K, L) Treg cell purification for the EAE experiments. Frequency of CD4^{+} Foxp3^{+} cells of total cells from the indicated animals after (K) CD4^{+} CD25^{hi} CD45RB^{int} CD38^{hi} cell sorting on a FACSAria III (BD; experiment shown in Fig. 7I) and after (L) MACS purification (Miltenyi Biotec, CD4^{+} CD25^{+} Regulatory T cell Isolation Kit, mouse; experiment shown in Fig. 7J). Shown are representative plots of 5 animals per group.

(M) Percentage of TCR^{-} Treg cells (CD45.2^{+} CD5^{+} CD4^{+} Foxp3^{+}) among total transferred CD45.2^{+} cells, isolated from pooled spleen and lymph nodes of DEREG mice 16 d after tamoxifen administration.

Table S1, related to Figure 3. Gene expression changes in TCR-deficient Treg cells

Excel sheets of Affymetrix data, lists of 2- and 3-fold regulated probe sets and lists of 2- and 3-fold regulated genes.

Table S2, related to Figure 3. Gene lists used to query gene expression data

Results from gene set enrichment analyses (GSEA). Curated gene lists: Putative Suppressors (genes implicated in Treg cell-mediated suppression), taken from (Fontenot et al., 2005; Josefowicz et al., 2012); Treg Signature (genes defining Treg cell lineage), taken from (Hill et al., 2007); Foxp3 Up (genes positively regulated by Foxp3), Foxp3 down (genes repressed by Foxp3), both taken from (Zheng et al., 2007); Egr2 (target genes of Egr2), taken from (Zheng et al., 2013); c-Rel over (Gene affected by c-Rel overexpression), c-Rel ko (gene affected by c-Rel knockout), both taken from (Bunting et al., 2007); NFAT (NFAT target genes), collected from (Diehn et al., 2002; Hermann-Kleiter and Baier, 2010; Hogan et al., 2003; Macián et al., 2001; Robbs et al., 2008; Yang and Chow, 2003); IRF4 (IRF4 target genes) collected from (Cretney et al., 2011; Zheng et al., 2009); mTOR (genes regulated through the mTOR pathway) taken from (Zeng et al., 2013); GATA3 Foxp3 (genes regulated by the GATA3 and Foxp3 complex), taken from (Rudra et al., 2012); NF-kB (NF-κB target genes), taken from (Hopewell et al., 2013); Cbfb (genes differentially regulated in Cbfb-deficient Treg cells), taken from (Kitoh et al., 2009); FoxO1 up (genes regulated in Treg cells expressing Foxo1AAA), Foxo1 down (genes regulated in Treg cells lacking Foxo1) taken from (Ouyang et al., 2012); ERAD (ER-associated degradation), UPR (unfolded protein response), both taken from Quiagen PCR array PAMM-089Z.

SUPPLEMENTAL EXPERIMENTAL PROCEDURES

Flow Cytometry

Single-cell suspensions were prepared and stained with monoclonal antibodies: 4-1BB (17B5), Aiolos (8B2), Bcl-2 (10C4), Bcl-6 (BCL-DWN), CCR7 (4B12), CD103 (2E7), CD122 (TM-b1), CD126 (D7715A7), CD127 (A7R34), CD25 (PC61.5), CD28 (37.51), CD200 (OX90), CD38 (90), CD39 (24DMS1), CD4 (RM4-5), CD44 (IM7), CD45RB (C363.16A), CD5 (53-7.3), CD62L (MEL-14), CD69 (H1.2-F3), CD71 (R17217), CD73 (eBioTY/11.8), CD8α (53-6.7), CD83 (Michel-17), c-Maf (sym0F1), c-Rel (1RELAH5), CTLA-4 (UC10-4B9), Egr2 (erongr2), Eomes (Dan11mag), Eos (ESB7C2), Fas (15A7), FasL (MFL3), FolR4 (eBio12A5), Foxp3 (FJK-16s), GARP (YGIC86), GATA-3 (TWAJ), GITR (DTA-1), Helios (22F6), ICAM-1 (YN1/1.7.4), ICOS (7E.17G9), IFN-γ (XMG1.2), IL-2 (JES6-5H4), IL-10 (JES3-16E3), IL-15Rα (DNT15Ra), IL-17A (17B7), IRF4 (3E4), ITGAL (M17/4), Ki-67 (SolA15), KLRG-1 (2F1), LAG-3 (eBioC9B7W), LAP (TW7-16B4), Ly6C (HK1.4), Nur77 (12.14), Ox40 (Ox86), PD-1 (J43), Ror-γt (AFKJS-9), Runx1 (RXDMC), T-bet (eBio4B10), TIGIT (GIGD7) and TCRβ (H57-597) (all from eBioscience). CD49b (HMa2) and IL-10R (1B1.3a) were both from BioLegend, Nrp1 (AF566) was from R&D Systems, Bcl-xL (7B2.5) from Southern Biotech and Bim (#Y36) from Epitomics.

For intracellular transcription factor stainings, cells were fixed and permeabilized with the Foxp3 staining kit (eBioscience). For intracellular cytokine stainings, cells were activated for 4 h with 50 nM phorbol-12-myristat-13-acetat (PMA; Sigma) and 500 nM ionomycin (Merck Millipore), and monensin (eBioscience) was added for the last 3 h of culture. For lamina propria lymphocytes intracellular cytokine stainings, cells were activated for 1 h with 80 nM PMA and 1 µM ionomycin. Afterwards, cells were fixed and permeabilized with the Cytofix/Cytoperm kit (BD).

To detect active caspases, cells were stained for 1 h with the CaspGLOW Red Active Caspase Kit (BioVision) as recommended by the manufacturer.

For staining phosphorylated signaling proteins, lymphocytes were extracted in serum-free buffer. After surface staining, cells were fixed with the PhosFlow Lyse/Fix Buffer and permeabilized with the PhosFlow Perm Buffer III (both from BD). Afterwards, cells were stained intracellularly with antibodies against p-4E-BP1 (236B4), p-Bad (40A9), FoxO1 (L27), p-FoxO1 (#9461), mTOR (#5048, 7C10), p-mTOR (#5536, D9C2), p-p70 S6K (#9204, T421) and p-S6 (#4851, D57.2.2E), all

from Cell Signaling, and p-AKT(T308, J1-223.371), p-AKT(S473, M89-61), p-STAT3 (pS727) and p-STAT5 (pY694) from BD. For secondary stainings, we used anti-rabbit-Alexa647 from Invitrogen. For analysis of STAT3 and STAT5 phosphorylation, cells were stimulated with IL-6 (20 ng/mL, R&D systems) for 15 and 30 min or IL-2 (10 ng/mL, Chiron Proleukin) for 5 and 15 min respectively.

To measure mitochondrial parameters, cells were stained with the CellRox, Mitotracker (both from Invitrogen) and TMRM (ImmunoChemistry Technologies) kits following manufacturer's instructions. Samples were acquired on a FACSCantoII (BD) machine, and analyzed with FlowJo software (Treestar).

To evaluate the relative expression of regulatory T cell marker genes, the median fluorescence intensities (MFI) of at least five mice per genotypes were calculated with FlowJo, and the MFI for the $CD4^+$ naïve conventional ($CD44^{lo}$ $Foxp3^-$ $TCR\beta^+$) T cells of *Tcra*$^{F/F}$ control mice was set to 1 for each set. For Foxp3, MFIs were normalized to those of $CD25^{hi}$ control Treg cells.

Heatmaps were generated using perseus (MaxQuant software).

Colitis Scoring

Colitis scoring was performed essentially as in (Cox et al., 2012); colitis severity was scored on a scale from 0-5, with 0 representing a normal colon and 5 severe colitis.

Isolation of Lamina Propria Lymphocytes

Isolation of lamina propria lymphocytes was performed as previously described (Jankovic et al., 2013). Shortly, Peyer's patches were excised from ileum (defined as distal 1/3 of small intestine) and intestines flushed with $PBS^{-Ca/-Mg}$. 1 cm pieces of longitudinally opened intestines were washed and incubated with HBSS containing 2 mM EDTA, 10 mM Hepes, 10 % FCS, 1 % P/S, and 1 mM DTT. After incubation on a shaker (250 rpm) at 37°C for 15 min, supernatant was separated via filters (100 µm BD Falcon Cell Strainers). Next, intestines were incubated in $PBS^{+Ca/+Mg}$ supplemented with FCS (10%), Collagenase II (200 u/mL; Worthington), and DNase I (0.1 mg/mL; Roche) on a shaker at 37°C. Cells in suspension were then purified on a 40/80% Percoll gradient (Biochrom). For restimulation and FACS analysis cells were washed two times in RPMI complete medium.

In vitro expansion of Treg cells

MACS purified Treg cells were cultured in a concentration of 0.5 x 10^6 cells/mL in 96 well format and in complete RPMI medium (10% FCS) supplemented with 1 ng/mL PMA, 200 ng/mL ionomycin and 200 U/mL IL-2.

SUPPLEMENTAL REFERENCES

Bunting, K., Rao, S., Hardy, K., Woltring, D., Denyer, G.S., Wang, J., Gerondakis, S., and Shannon, M.F. (2007). Genome-wide analysis of gene expression in T cells to identify targets of the NF-kappa B transcription factor c-Rel. J Immunol *178*, 7097–7109.

Cox, J.H., Kljavin, N.M., Ota, N., Leonard, J., Roose-Girma, M., Diehl, L., Ouyang, W., and Ghilardi, N. (2012). Opposing consequences of IL-23 signaling mediated by innate and adaptive cells in chemically induced colitis in mice. Mucosal Immunol *5*, 99–109.

Cretney, E., Xin, A., Shi, W., Minnich, M., Masson, F., Miasari, M., Belz, G.T., Smyth, G.K., Busslinger, M., Nutt, S.L., et al. (2011). The transcription factors Blimp-1 and IRF4 jointly control the differentiation and function of effector regulatory T cells. Nat Immunol *12*, 304–311.

Diehn, M., Alizadeh, A.A., Rando, O.J., Liu, C.L., Stankunas, K., Botstein, D., Crabtree, G.R., and Brown, P.O. (2002). Genomic expression programs and the integration of the CD28 costimulatory signal in T cell activation. Proc Natl Acad Sci USA *99*, 11796–11801.

Fontenot, J.D., Rasmussen, J.P., Gavin, M.A., and Rudensky, A.Y. (2005). A function for interleukin 2 in Foxp3-expressing regulatory T cells. Nat Immunol *6*, 1142–1151.

Hermann-Kleiter, N., and Baier, G. (2010). NFAT pulls the strings during CD4+ T helper cell effector functions. Blood *115*, 2989–2997.

Hill, J.A., Feuerer, M., Tash, K., Haxhinasto, S., Perez, J., Melamed, R., Mathis, D., and Benoist, C. (2007). Foxp3 Transcription-Factor-Dependent and -Independent Regulation of the Regulatory T Cell Transcriptional Signature. Immunity *27*, 786–800.

Hogan, P.G., Chen, L., Nardone, J., and Rao, A. (2003). Transcriptional regulation by calcium, calcineurin, and NFAT. Genes Dev *17*, 2205–2232.

Hopewell, E.L., Zhao, W., Fulp, W.J., Bronk, C.C., Lopez, A.S., Massengill, M., Antonia, S., Celis, E., Haura, E.B., Enkemann, S.A., et al. (2013). Lung tumor NF-κB signaling promotes T cell-mediated immune surveillance. J Clin Invest *123*, 2509–2522.

Jankovic, D., Ganesan, J., Bscheider, M., Stickel, N., Weber, F.C., Guarda, G., Follo, M., Pfeifer, D., Tardivel, A., Ludigs, K., et al. (2013). The Nlrp3 inflammasome regulates acute graft-versus-host disease. J Exp Med *210*, 1899–1910.

Josefowicz, S.Z., Lu, L.-F., and Rudensky, A.Y. (2012). Regulatory T cells: mechanisms of differentiation and function. Annu Rev Immunol *30*, 531–564.

Kitoh, A., Ono, M., Naoe, Y., Ohkura, N., Yamaguchi, T., Yaguchi, H., Kitabayashi, I., Tsukada, T., Nomura, T., Miyachi, Y., et al. (2009). Indispensable role of the Runx1-Cbfbeta transcription complex for in vivo-suppressive function of FoxP3+ regulatory T cells. Immunity *31*, 609–620.

Macián, F., López-Rodríguez, C., and Rao, A. (2001). Partners in transcription: NFAT

and AP-1. Oncogene *20*, 2476–2489.

Morikawa, H., Ohkura, N., Vandenbon, A., Itoh, M., Nagao-Sato, S., Kawaji, H., Lassmann, T., Carninci, P., Hayashizaki, Y., Forrest, A.R.R., et al. (2014). Differential roles of epigenetic changes and Foxp3 expression in regulatory T cell-specific transcriptional regulation. Proc Natl Acad Sci USA *111*, 5289–5294.

Ouyang, W., Liao, W., Luo, C.T., Yin, N., Huse, M., Kim, M.V., Peng, M., Chan, P., Ma, Q., Mo, Y., et al. (2012). Novel Foxo1-dependent transcriptional programs control T(reg) cell function. Nature *491*, 554–559.

Robbs, B.K., Cruz, A.L.S., Werneck, M.B.F., Mognol, G.P., and Viola, J.P.B. (2008). Dual roles for NFAT transcription factor genes as oncogenes and tumor suppressors. Molecular and Cellular Biology *28*, 7168–7181.

Rudra, D., Deroos, P., Chaudhry, A., Niec, R.E., Arvey, A., Samstein, R.M., Leslie, C., Shaffer, S.A., Goodlett, D.R., and Rudensky, A.Y. (2012). Transcription factor Foxp3 and its protein partners form a complex regulatory network. Nat Immunol *13*, 1010–1019.

Samstein, R.M., Arvey, A., Josefowicz, S.Z., Peng, X., Reynolds, A., Sandstrom, R., Neph, S., Sabo, P., Kim, J.M., Liao, W., et al. (2012). Foxp3 exploits a pre-existent enhancer landscape for regulatory T cell lineage specification. Cell *151*, 153–166.

Yang, T.T.C., and Chow, C.-W. (2003). Transcription cooperation by NFAT.C/EBP composite enhancer complex. J Biol Chem *278*, 15874–15885.

Zeng, H., Yang, K., Cloer, C., Neale, G., Vogel, P., and Chi, H. (2013). mTORC1 couples immune signals and metabolic programming to establish T(reg)-cell function. Nature *499*, 485–490.

Zheng, Y., Zha, Y., Spaapen, R.M., Mathew, R., Barr, K., Bendelac, A., and Gajewski, T.F. (2013). Egr2-dependent gene expression profiling and ChIP-Seq reveal novel biologic targets in T cell anergy. Mol Immunol *55*, 283–291.

Zheng, Y., Chaudhry, A., Kas, A., Deroos, P., Kim, J.M., Chu, T.-T., Corcoran, L., Treuting, P., Klein, U., and Rudensky, A.Y. (2009). Regulatory T-cell suppressor program co-opts transcription factor IRF4 to control T(H)2 responses. Nature *458*, 351–356.

Zheng, Y., Josefowicz, S.Z., Kas, A., Chu, T.-T., Gavin, M.A., and Rudensky, A.Y. (2007). Genome-wide analysis of Foxp3 target genes in developing and mature regulatory T cells. Nature *445*, 936–940.

Editorial

TCR signals fuel T_{reg} cells

Christoph Drees, J. Christoph Vahl and Marc Schmidt-Supprian

Regulatory T (T_{reg}) cells safeguard against autoimmunity and overshooting inflammation. During their development in the thymus, T_{reg} cells are selected by stronger autoantigenic T cell receptor (TCR) signals than conventional T cells. These TCR signals are critically important for the initiation of two key lineage defining events, namely induction of the transcription factor Foxp3 and hypomethylation of a specific gene set. Recent studies shed light on the role of continuous (autoreactive) TCR signals for identity, homeostasis and functions of mature T_{reg} cells.

Induced TCR ablation on mature T_{reg} cells only minimally reduces Foxp3 expression [1, 2] and does not affect hypomethylation patterns [1]. Stable Foxp3 expression was also observed in T_{reg} cells lacking the TCR signal transduction proteins Lck [3] or SLP-76 [4] and upon ablation of the co-stimulatory receptor CD28 [5]. Fittingly, mature T_{reg} cells, expressing a TCR but deprived of peripheral autoantigenic stimulation due to lack of MHC II on hematopoietic cells, still express Foxp3 [6]. Therefore, once a core T_{reg} cell identity has been established in the thymus, it is maintained independently of peripheral TCR signals.

In contrast, the T_{reg} cell surface phenotype and their signature gene expression were strongly affected by the various means of inhibiting TCR signals [1-3, 6]. However, the peripheral T_{reg} cell pool is heterogeneous in that it consists of naïve and various subsets of effector-like T_{reg} cells. Induced TCR ablation showed that, at least under homeostatic conditions in healthy mice, effector-like T_{reg} cells strictly depend on TCR signals for their generation and/or maintenance. Attempts to distinguish between naïve and effector-like T_{reg} cells based on CD62L/CD44 [2] or CD25 [1] expression revealed that both require TCR signals to maintain their characteristic surface phenotype and gene expression, independently of their homeostasis. Interestingly, apart from reduced levels of TCR-activated transcription factors such as Egr2 and c-Rel and their respective target genes, loss of TCR signals strongly affects IRF4-controlled genes. The concept that DNA hypomethylation ensures the expression of key T_{reg} cell genes is supported by the reduced, but still robust expression of CTLA-4, GITR and Eos of TCR-deficient T_{reg} cells [1].

Both induced TCR and co-stimulatory CD28 ablation cause a decline in T_{reg} cells in the absence of thymic T cell production, which goes hand in hand with completely abrogated [1] or reduced [5] homeostatic proliferation, respectively. This is not due to reduced responsiveness to homeostatic cytokines, such as IL-2. Interestingly, T_{reg} cells deprived of MHC II contact proliferate well in response to anti-CD3 stimulation [6] and TCR-deficient T_{reg} cells divide when stimulated with TCR-bypassing PMA/Ionomycin [2], indicating that these cells do not become anergic to proliferation-inducing signals. The protein levels of Bcl-2 and Bim are two-fold upregulated in T_{reg} cells upon TCR loss, to the same levels as in naïve CD4 T cells [1]. However, none of the studies reported a significant difference in survival between TCR signaling impaired and normal T_{reg} cells *in vivo*, and BrdU pulse-chase experiments suggest impaired turn-over/proliferation, but normal survival of Lck-deficient T_{reg} cells [3]. Collectively, these experiments show that TCR signal-induced proliferation forms an essential homeostatic requirement for all T_{reg} cell subsets.

T_{reg} cells suppress immune responses through the release of inhibitory cytokines, competition for IL-2, access to and functional modulation of antigen presenting cells and direct cytotoxic killing. TCR-deficient T_{reg} cells show reduced expression of inhibitory and cytotoxic molecules including IL-10 and Granzyme B. In addition, the expression of proteins through which T_{reg} cells regulate the functions of antigen presenting cells, such as CTLA-4, NT5E/CD73, LFA-1 and NRP1, is significantly reduced [1, 2, 6]. TCR signaling impaired T_{reg} cells fail to efficiently suppress T cell activation and proliferation *in vitro* [3-6]. Conversely, augmenting TCR signaling by ablating the DAG-metabolizing kinase DGKζ enhances the *in vitro* suppression capacity [4]. Importantly, T_{reg} cells require constant TCR signals to sustain their suppressive abilities *in vivo*: MHC II contact-deprived T_{reg} cells fail to control naïve T cell expansion upon co-transfer [6], TCR-deficient T_{reg} cells cannot control effector T cell differentiation/proliferation and cytokine production *in situ* [2] and induced TCR ablation limits T_{reg} cell-mediated control of colitis and EAE [1]. Therefore, TCR signals continuously arm T_{reg} cells for suppression, in addition to their role in their homeostasis.

Expression height of Ly-6C, which is strongly elevated in Lck-deficient [3] and TCR-deficient [1] T_{reg} cells, appears to differentiate T_{reg} cells receiving strong TCR signals (Ly-6C-) from those that do not (Ly-6C+) [7]. Purified Ly-6C- and Ly-6C+ T_{reg} cells differed dramatically in phenotype, gene expression and their ability to suppress *in vitro* and *in vivo*. Accordingly, effector T_{reg} cells are exclusively Ly-6C-. However, on average half

of the TCR-deficient T_{reg} cells lacked Ly-6C (Vahl et al., unpublished), showing that not all Ly-6C- T_{reg} cells result from continuous TCR triggering. Modern multiparameter flow cytometry should help to further unravel the dynamic complexities of T_{reg} cell subsets.

In summary, we conclude that while TCR signals are dispensable for maintaining the core T_{reg} cell identity, they are continuously fueling their homeostasis, effector differentiation and suppressive functions.

Marc Schmidt-Supprian: Hematology and Oncology, Klinikum rechts der Isar, Technische Universität München, Munich, Germany

***Correspondence to**: Marc Schmidt-Supprian, **email** suppri-an@gmail.com*

Keywords: Immunology and Microbiology Section, Immune response, Immunity

***Received**: July 01, 2015*

***Published**: July 12, 2015*

REFERENCES

1. Vahl JC et al. Immunity 2014; 41:722-36.
2. Levine AG et al. Nat Immunol 2014; 15:1070-8.
3. Kim JK et al. PLoS ONE 2009; 4:e6580.
4. Schmidt AM et al. The Journal of Immunology 2015; 194:4362-70.
5. Gogishvili T et al. Eur J Immunol 2012; 43:188-93.
6. Delpoux A et al. Eur J Immunol 2012; 42:1237-49.
7. Delpoux A et al. The Journal of Immunology 2014; 193:5914-23.